



**Excited-state intramolecular proton-transfer (ESIPT)-
inspired solid state emitters**

Journal:	<i>Chemical Society Reviews</i>
Manuscript ID	CS-SYN-07-2015-000543.R3
Article Type:	Review Article
Date Submitted by the Author:	08-Oct-2015
Complete List of Authors:	Padalkar, Vikas; Kyoto University, Department of Molecular Engineering Seki, Shu; Kyoto University, Department of Molecular Engineering



Excited-State Intramolecular Proton-Transfer (ESIPT)-Inspired Solid State Emitters

Received 00th July 2015,
Accepted 00th October 2015

Vikas S. Padalkar,^{a*} and Shu Seki^{a*}

DOI: 10.1039/x0xx00000x

www.rsc.org/chemsocrev

Solid state emitters based on excited state intramolecular proton transfer (ESIPT) have been attracting considerable interest since past few years in the field of optoelectronic devices because of their desirable unique photophysical properties. The photophysical properties of the solid state ESIPT fluorophores determine their possible applicability in functional materials. Less fluorescence quantum efficiencies and short fluorescence lifetime in solid state are the shortcomings of the existing ESIPT solid state emitters. Designing of ESIPT chromophores with high fluorescence quantum efficiencies and long fluorescence lifetime in the solid state is a challenging issue because of unclear mechanism of solid state emitters in the excited state. Reported designed strategies, detailed photophysical properties, and their applications will help in assisting researchers to overcome existing challenges in designing novel solid state ESIPT fluorophores for promising applications. This review highlights recently developed solid state ESIPT emitters with focus on molecular design strategies and their photophysical properties, reported in the last five years.

1. Introduction

Excited state intramolecular proton transfer (ESIPT) [All abbreviations are summarized in abbreviation section before references section] is a photochemical process that produces a tautomer with a different electronic structure from the original excited form¹. It is a four-level photo-cycle ($E \rightarrow E^* \rightarrow K^* \rightarrow K$) scheme implemented by enol (E) \rightarrow keto (K) photo-tautomerisation process¹⁻³ **Figure 1**. The ESIPT phenomenon was reported first for salicylic acid by Waller in 1950s⁴. After the discovery of ESIPT, many researchers studied the fundamental photophysics, proton transfer dynamics, picosecond kinetics, vibronically resolved spectroscopic study, kinetics and thermodynamics at singlet state, femtosecond and time-resolved study of ESIPT fluorophores^{3,5-9}.

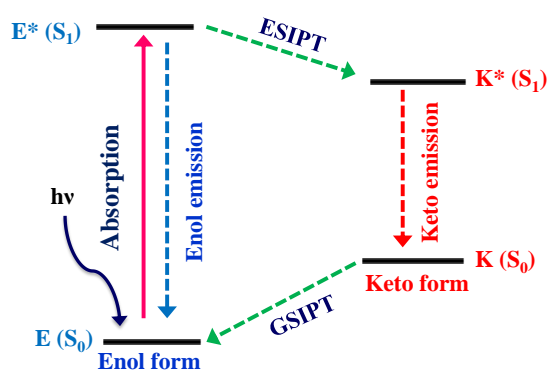


Figure 1 Four level ESIPT process

^a Department of Molecular Engineering, Graduate School of Engineering, Kyoto University, Nishikyo-ku, Kyoto, 615-8510, Japan
Email: vikaspadalkar@gmail.com (V.S.P), seki@moleng.kyoto-u.ac.jp (S.S).

Recently, Park et al³, Wang et al⁹, Zhao et al², and Chuo et al^{8,10}, critically reviewed the photophysical properties, synthetic strategies and potential applications of the ESIPT fluorophores.



Vikas Padalkar

Vikas Padalkar completed his graduation (2005) and post-graduation (2007) from University of Pune, and received his Ph. D degree in Chemistry from University of Mumbai (2011). Prior to obtaining his doctorate degree he has worked with Merck Pharmaceuticals Mumbai. He has worked as a post-doctoral research fellow at Institute of Chemical Technology, Mumbai (2011– March 2014) on project “Stand-off detection of explosives based on immunochemical techniques”. He joined Osaka University in April, 2014 (Professor Seki Laboratory) as JSPS post-doctoral research fellow and currently, he is continuing his JSPS-research with Professor Shu Seki in Kyoto University, Japan. His research interests include development of fluorescent organic materials for functional applications.



Shu Seki

Shu Seki graduated from the University of Tokyo in 1993, and received his Ph. D degree in 2001 from Osaka University. He joined the Argonne National Laboratory, USA, in 1993, and the Delft University of Technology in 2001. He was a full Professor of Applied Chemistry, Graduate School of Engineering, Osaka University, Japan (2009–2015). Since April 2015, he has been appointed as full professor in Department of Molecular Engineering, Kyoto University, Japan. His research is primarily focused on the physical chemistry of condensed matter, functional organic materials and nanomaterials.

The remarkable properties of the ESIPT fluorophores are large Stokes shift (~ 200 nm)³, dual emission³, ultrafast process^{11,12}, and spectral sensitivity to the surrounding medium¹³. The pre-requisite for ESIPT is the presence of intramolecular hydrogen bond (H-bond) between proton donor ($-\text{OH}$ and $-\text{NH}_2$) and proton acceptor ($=\text{N}-$ and $-\text{C}=\text{O}$) groups in close proximity to each other in a molecule^{2,3,9,10,14–16}. ESIPT is extremely fast ($k_{\text{ESIPT}} > 10^{12} \text{ s}^{-1}$) and is able to proceed even in rigid glass at very low temperature¹¹. The rate of ESIPT processes depends on donor/acceptor groups and the surrounding medium¹⁷. Broad, tunable and dual emissions are attractive properties of ESIPT chromophores that covers the whole visible domain which can result in the production of white light^{18,19}. Most of the ESIPT chromophores show dual emission, short wavelength emission due to excited state enol form (E^*) (normal emission) and the longer one due to excited state keto form (K^*) (ESIPT emission) through a four-level photocycle^{3,8,9}. In addition, this process generates different transient species^{3,8,9}. Due to transient changes involved in ESIPT process, ESIPT emission gets easily affected by its micro-environment, leading to change in the fluorescence properties²⁰. The spectral properties of the ESIPT fluorophores depend on hydrogen bonding, rotamerisation process, acidity/basicity of the surrounding medium, and substituents present on donor and acceptor units^{2,3,8,10}. The fluorescence properties of the ESIPT fluorophores are tunable by changing these parameters^{2,3,8}.

Up till now, most studied ESIPT fluorophores have been derivatives of 2-(2'-hydroxyphenyl)benzimidazole (HBI)^{21–26}, 2-(2'-hydroxyphenyl)benzoxazole (HBO)^{27–30} and 2-(2'-hydroxyphenyl)benzothiazole (HBT)^{20,28,31–36}. Along with HBIs, HBOs, and HBTs, derivatives of quinoline^{37–39}, benzophenones⁴⁰, flavones^{41–43}, anthraquinones^{44,45}, benzotriazoles⁴⁶, thiodiazoles⁴⁷, salicylidene aniline⁴⁸, quinoxalines⁴⁹, benzazoles¹², chromones⁵⁰, coumarins^{51,52}, and naphthalimides^{34,53} have been reported for ESIPT study. Besides, a novel class of imidazo[1,2-a]pyridines showing ESIPT was recently reported by Araki et al.,^{54–57}. Because of unique photophysical properties, ESIPT fluorophores have been applied in various fields, such as molecular logic gates⁵⁸, newer arenas of biotechnology^{9,59}, fluorescence imaging^{60,61}, radiation scintillator^{41,62}, UV-absorber⁶³, and for fundamental photophysical dynamics studies⁶⁴. Reported ESIPT molecules are highly emissive in solution but weakly emissive in the solid state^{2,3,9}. Recently, solid state emitters with high fluorescence quantum efficiencies have attracted wide attention in the field of optoelectronic devices and laser applications^{65–69}. ESIPT chromophores which are highly emissive in rigid media but non-emissive (or weakly emissive) in solution are more appropriate fluorophores for optoelectronics devices^{66,69–71}.

Till date, many articles describing synthesis methods, extensive photophysics and applications of ESIPT in solution have been reported, however ESIPT inspired solid state emitters have not been explored to a large extent. In this review article, the solid state ESIPT emitters and their photophysical properties, applications, and designed strategies have been critically summarized. First, the fundamentals of solid state emitters have been briefly summarized by considering their molecular design strategies. Secondly, a short summary has been made of those solid state ESIPT emitters which were reported before 2011 and which are highlighted by Park et al.³. Thirdly, the innovative concepts of

solid state emitters reported in last five years have been discussed³. In the last part, the conclusion and prospects for developing novel solid state emitters for high-tech applications have been summarized.

2. Scope and Limitations

In this article, a critical review of the recent literature relevant to solid state emitters based on ESIPT mechanism has been presented. The strategies for molecular design, absorption, emission properties, quantum efficiencies, fluorescence lifetime, and applicability of the ESIPT solid state emitters have been summarized and discussed. The structure-photophysics relation and application of the ESIPT fluorophores have been highlighted with the help of representative examples.

More than 4018 research articles related to ESIPT have been published by researchers since 1950s. Synthesis methods and photophysical properties of the ESIPT chromophores in solution have been well summarized in literature in the form of review articles^{2,3,8,9,64}. In 2011, Park et al. summarized some strategies to achieve solid state emission for ESIPT chromophores by discussing representative examples³. Afterward many new strategies and solid state ESIPT chromophores have been developed but not yet summarized to assist researchers in overcoming existing shortcomings in the practical implementation of ESIPT systems into actual optoelectronic devices. In order to have recent updates on strategies for designing novel ESIPT solid state emitters and considering our research background in the field of ESIPT^{24,27,28,31,32,37,72–75}, here we have critically reviewed the papers which were published in these 5 years. In this review, we have mainly focused on solid state emitters and their properties in the solid-state. References such as patents, abstracts, and summaries of the conference presentations are not included in this review.

3. Solid state ESIPT emitters

Most of the reported organic chromophores are highly emissive in solution with high fluorescence quantum efficiencies, but weakly emissive (or non-fluorescent) in rigid medium due to aggregation-caused quenching mechanism (ACQ)⁷⁶. To achieve solid state emission, it is necessary to suppress the other radiationless deactivation pathways which occur at the excited state. Different strategies^{3,70,77–80} were exploited to obtain solid state emissions for various type of ESIPT chromophores such as (i) controlling mode of molecular packing (ii) aggregation-induced emission (AIE) (iii) aggregation-induced enhanced emission (AIEE) (iv) restriction of intramolecular rotation (RIR) etc. In addition to above mentioned strategies for solid state emission, various new strategies have been reported by researchers recently. It is well known that ESIPT chromophores emit with multiple band with a high Stokes shift which covers a broad range of spectrum^{2,3,8}. In most of the ESIPT chromophores, fluorescence quantum efficiencies of the large Stokes shifted ESIPT emission (K^*) are generally low due to non-radiative deactivation pathways occurring at K^* state^{2,3,8}. ESIPT chromophores which emit at red region with very high fluorescence quantum efficiencies in solid state are attracting considerable attention in functional materials. Approaches such as dendrimer encapsulation, aggregation-induced emission (AIE), aggregation-induced enhanced emission (AIEE), restriction of

intramolecular rotation (RIR), polymer doping, and restriction of twisted intramolecular charge transfer (RTICT) mechanisms have been considered responsible for solid state emission and enhancement of quantum efficiencies. Various strategies of ESIPT emission in solvent versus solid state (crystalline state/ polymorphic form/ supported rigid medium) emission have been summarized below.

1. Hydrogen bonding: Intramolecular H-bonding is key factor for efficient ESIPT process because the proton transfer process takes place through characteristics four-level photocycle (5- or 6-membered cyclic transition state)^{3,8,9}. In polar solvents, in addition to intramolecular H-bonding, the possibility of intermolecular H-bonding between acidic proton of chromophores (hydroxy/amino groups of ESIPT chromophore) and solvents molecules²⁰. Polar solvents (alcohols) acting only as hydrogen bond acceptors can hamper the ESIPT process by formation of intermolecular hydrogen bonding with solvent molecules, which result in suppression of keto (K*) emission⁸¹. In solid state, hampering of ESIPT process through intermolecular H-bonding with solvents molecules is omitted which causes enhancement of K* emission in solid state.
2. Restriction of twisted intramolecular charge transfer: Twisted intramolecular charge transfer (TICT) process in the excited keto state (K*) after ESIPT, is one of the pathway for fluorescence quenching of ESIPT fluorescence in solution^{82,83}. TICT is significantly influenced by the geometrical properties of intramolecular H-bond associated with the basic atom (–N=) of ring structure⁸⁴. TICT and strength of intramolecular H-bond are co-operative in the Keto (K*) state of ESIPT molecules, which determines the emission properties³. TICT deactivation is prominent in solution, which causes suppression of keto (K*) emission. However, in rigid media keto (K*) emission is significant because of restriction of TICT rotation (rigidochromism)^{3,85}.
3. Restriction of intramolecular rotation: Restriction of intramolecular rotation (RIR) is also a key factor in enhancement of fluorescence quantum efficiencies in solution and rigid media of ESIPT fluorophores^{3,26,86,87}. RIR effectively suppresses the non-radiative pathways via vibronic and rotational relaxation. RIR is more efficient in solid state in comparison to solvent due to physical constraint in the solid state (restriction of free rotations)^{3,26,86,87}. RIR process helps in maintaining suitable geometry for intramolecular H-bonds as well as in suppressing the non-radiative pathways by mean of intermolecular vibronic relaxation (except few cases)^{3,26,86,87}.
4. Restriction of *cis-trans* isomerization: *Cis-trans* isomerization of the ESIPT keto form deactivates the excited state which causes fluorescence quenching in solution^{84,88–90}. However, in rigid media *cis-trans* transformation of excited state keto form is restricted through tight molecular packing^{84,88–90}. This conformational restriction significantly blocks the non-radiative relaxation pathways and fascinates the radiative decay which results in enhancement of fluorescence in solid state^{84,88–90}.
5. Aggregation Effect: The limited vibrational/rotational relaxations are considered to be the origin of fluorescence emission in solid state over solution. Type of aggregation and characteristics of molecular stacking determines the fluorescence quantum efficiencies of ESIPT chromophores³. Generally, *J*-aggregation (slip-stacking/ head-to-tail interaction) enhances the fluorescence emission over *H*-aggregation (face-to-face interaction) for ESIPTs^{91,92}. The stacking of ESIPT fluorophores

depends on nature of group present on the ESIPT molecules. In common steric/bulky group's causes slip-stacking i.e. *J*-aggregation.

6. Torsion/ planarity of enol conformers: The stability of enol conformer depends on torsion between proton donor ring and acceptor ring^{93–95}. In solid state torsion/ twisting is less in comparison to solution because of physical constraint. In most of the cases torsion is coplanar in solid state, which is the origin for the enhancement of fluorescence in the crystalline state. However, in solution efficient radiationless decays process occur due to twisting motion^{93–95}. The torsion is dependent on molecular motion/ intermolecular interaction with neighbouring molecules/ packing-induced conformational fixation and/or alteration at a single molecular level. Mode of molecular packing determines the ESIPT emission.

Based on these approaches, recently developed ESIPT fluorophores, photophysical properties and their applications have been summarized in detail in the next section.

4. Recent progress in the solid state ESIPT emitters

In this section, recently developed strategies to suppress the deactivation pathways occurring at the excited state are summarized. Various fluorophores and approaches to improve fluorescence quantum efficiencies in solid state, which have been used by researchers, are highlighted below and details photophysical properties and applications are discussed in next section.

- a) White light generation from single molecule through RIR mechanism^{18,33,66,90,96,97}
- b) Aggregation-induced emission^{92,98–100}
- c) Aggregation-induced enhanced emission^{84,85}
- d) Polymer based ESIPT chromophores¹⁰¹
- e) ESIPT chromophores with polymorphic properties^{55,94,95,99,102–104}
- f) ESIPT-coupled aggregation-induced enhanced emission¹⁰⁵

These various approaches have been broadly classified into three main sections for simplicity

- i. Solid state ESIPT emitters through single molecule
- ii. Solid state ESIPT emitters based on polymorphic form (molecular packing)
- iii. Solid state ESIPT emitters through AIE / AIEE processes

The reported solid-state ESIPT fluorophores have been mainly used as organic light emitting diodes (OLEDs) / white light organic limiting diodes (WOLEDs). The various approaches for generation of white-light emission using ESIPT chromophores have been highlighted below and detailed discussion is covered in next section.

- a. White-light-emission (WLE) through single molecule dyad, consisting of two non interacting chromophores with ESIPT units⁸⁷: The two interactive chromophores having blue and orange-emitting ESIPT emission have been used for white-light generation. In this approach, the concept of frustrated energy transfer strategy between two units was used for generation of WLE. The generated white-light emission is the sum of emissions from the individual components. The WLE by this approach is independent of concentration.

- b. Mixture of proton-transfer and nonproton-transfer chromophores (ESIPT and non-ESIPT)¹⁹: ESIPT and non-ESIPT chromophores having similar UV-absorption properties but different luminescence properties have been used. Mixture of ESIPT chromophore with yellow emission and non-ESIPT chromophore with blue emission generates white light by simultaneous irradiation of UV light. The white luminescence composes of two independent emissions without involving energy transfer process. The use of compounds with similar molecular structures is more advantageous, because these compounds are expected to have similar physical properties.
- c. Mixture of three chromophores (two ESIPT and one non-ESIPT)¹⁷: White light generation by mixing three chromophores having yellow, red and blue emission. In this approach, proton transfer molecules with yellow and red emission and non-proton transfer molecules with blue emission have been used.
- d. Based on solvatochromism properties (solvent polarity and ability for forming H-bonds)⁶⁶: The emission properties of the ESIPT chromophores are sensitive towards microenvironment¹⁰⁶. This desired characteristic of ESIPT chromophores helps in tuning the fluorescence emission. Intra- and intermolecular H-bonding in ESIPT process generate different rotameric isomers/ transition species (cis-enol, cis-keto/ trans-keto/ deprotonated species etc) in non-polar, polar and polar-protic medium, which emits at different wavelength resulting in white light emission.
- e. Mixture of nanodots and ESIPT chromophore¹⁰⁷: Mixture of quantum dots (blue emission) and keto emission of ESIPT chromophore generates white-light emission. In this approach, emission tunability could be achieved simply by changing the relative amount of the two species.
- f. Tuning of acidic and basic centers of ESIPT chromophores¹⁰⁸: The emission properties of the ESIPT chromophores are dependent on electron nature and position of donor/ acceptor groups. White-light emission could be generated by tuning the position and strength of donor/ acceptors. These groups affect the acidity and basicity of donor and acceptor groups responsible for ESIPT due to mesomeric effect.
- g. Altering the surrounding medium (e.g. polymer matrices or rigid media)^{57,109}: Homogenous dispersion of two or more ESIPT chromophores (different Stokes shift) with different emission wavelength in a polymer matrix generates white light emission. Poly(*N*-vinylcarbazole) (PVK) as a blue-light emitting and hole-transporting polymer host material has been used for white light emitting electroluminescence. This approach is mainly based on principle of limited energy transfer between different ESIPT chromophores.
- h. Based on halochromism property of ESIPT chromophores¹⁰¹: ESIPT emission is highly sensitive towards acidic and basic medium. In acidic medium, protonation of imine nitrogen causes blue shift and in basic medium deprotonation of acidic hydrogen generates phenoxide ion which causes red shift. This helps in tuning the emission properties which generate white light emission by controlling acidity and basicity of medium.
- i. Controlling molecular packing of ESIPT chromophores (e.g. polymorphs)^{55,56}: The emission properties of the ESIPT chromophores are tunable by controlling the mode of

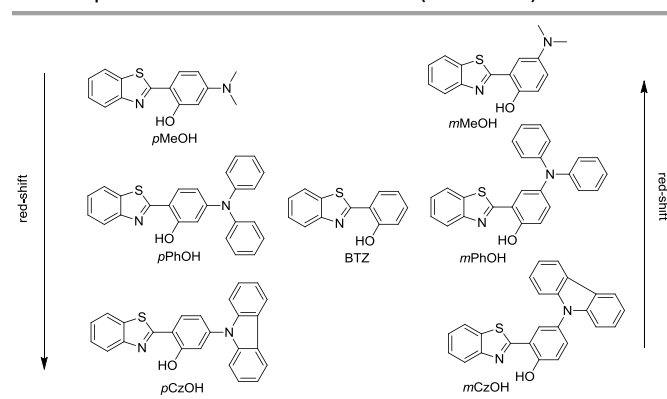
molecular packing. The difference in the modes of molecular packing affects the electron state of the proton transfer species and results in different luminescence color.

- j. AIE and AIEE processes generate white light emission of ESIPT chromophores¹⁰⁵: In aggregate state, blue or red shift of enol (E*) and keto (K*) emission or appearance of new emission bands result in white-light emission.
- k. Single ESIPT system by fine-tuning the energetics in the excited state¹⁸ (systematic balance between destruction of aromaticity and compensation of π -conjugation).
- l. Panchromatic emission⁹⁷ via modulating substitution pattern of ESIPT chromophores.

5. Solid state ESIPT emitters through single molecule

Generation of white light through mixture of two or more organic chromophores is very simple and more convenient over white light from single/ individual molecule. However it suffers from several limitations^{110,111}. Long term color stability, phase separation and differential aging are some of the limitations of white light generated from a mixture of chromophores. White light generation from single molecules^{112,113} would be more ideal, and it gives perfect color stability and easy reproducibility in the fabrication of white light organic light emitting diodes (WOLEDs). ESIPT is well known for dual emission or broad emission; these unique properties can be utilized for generation of white light by tuning microenvironment^{66,106}. ESIPT chromophores generally absorb in ultra-violet region and emit in visible region. Enol (E*) and keto (K*) emission cover the white light spectrum. Park et al., reviewed some ESIPT chromophores which generate white light and are emissive in the solid state³. In this section we have summarized solid state ESIPT emitters reported in last five years.

In early 2011, Wang and coworkers reported full color emitting organic materials based on 2-(2'-hydroxyphenyl) benzothiazole (BTZ) with superior ESIPT characteristics³³. Different BTZ chromophores were synthesized by modifying the 4- and 5- position of phenyl ring attached to thiazole ring with different substituted amino groups. Studied BTZ chromophores are summarized below (Scheme 1).



Scheme 1 Structure of BTZs

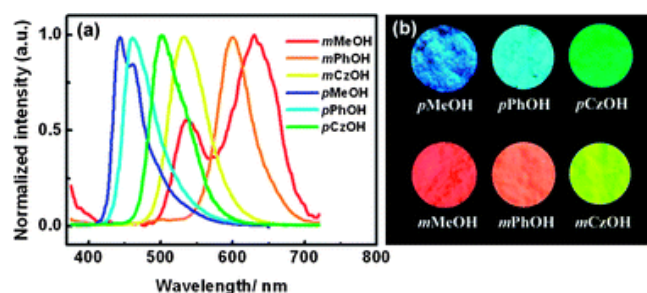


Figure 2 (a) solid state emission spectra of BTZ derivatives, (b) Photoluminescence image of BTZ derivatives. Reproduced with permission [33]. Copyright 2011 The Royal Society of Chemistry.

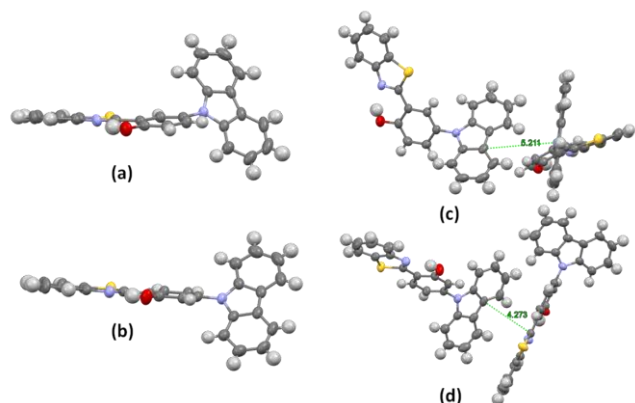


Figure 3 Single crystal of *m*-CzOH and *p*-CzOH (a) *m*-CzOH and (b) *p*-CzOH molecular structure with thermal ellipsoids drawn at the 50 % probability level; (c) *m*-CzOH and (d) *p*-CzOH intermolecular relationship. Reproduced from CIF file [33].

In BTZ chromophores, benzothiazole unit acts as an electron acceptor and substituted amino groups as an electron donor. The emission spectra and fluorescence quantum efficiencies of *m*-OH and *p*-OH BTZ chromophores were reported in solid state. In solid state, the emission spectra of *m*-substituted groups showed red shift in comparison to *p*-substituted amino group [*m*-MeOH ($\lambda_{em} = 630$ nm, $\Phi_{FL} = 5.65\%$), *m*-PhOH ($\lambda_{em} = 600$ nm, $\Phi_{FL} = 37.54\%$), *m*-CzOH ($\lambda_{em} = 532$ nm, $\Phi_{FL} = 66.86\%$), *p*-MeOH ($\lambda_{em} = 443$ nm, $\Phi_{FL} = 29.07\%$), *p*-PhOH ($\lambda_{em} = 461$ nm, $\Phi_{FL} = 30.16\%$), *p*-CzOH ($\lambda_{em} = 502$ nm, $\Phi_{FL} = 91.68\%$)]. In studied BTZ chromophores, the emission properties are dependent on position and nature of electron donor, *m*-OH type of BTZ showed blue shifted emission, while *p*-OH type of BTZ showed red shifted emission with increasing electron-donating ability of substituted amino group. The solid state emission spectra cover the entire visible light region and are highly emissive in the solid state **Figure 2**.

The single-crystal X-ray analysis showed that HBT unit of *m*-OH and *p*-OH type of chromophores exhibits planar nature **Figure 3** (suitable for ES IPT) with small dihedral angle between HBT and amino substituted groups. The absence of intermolecular interaction helps to suppress the non-radiative pathways resulting in solid state emission **Figure 3**. The high fluorescence quantum efficiencies were considered owing to favorable geometry for ES IPT and strong intra-molecular

hydrogen bonding instead of intermolecular interaction. This is the first report which describes extremely high quantum efficiencies reaching up to $\sim 92\%$ in their solid state for single ES IPT molecules.

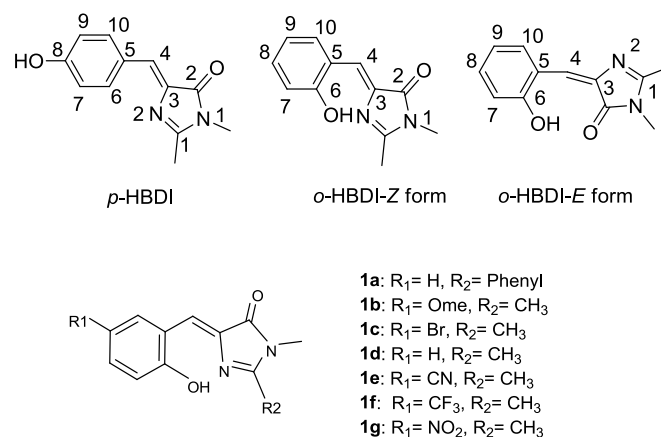
The electroluminescence (EL) devices were fabricated for each BTZ derivatives to evaluate EL characteristics. BTZ derivatives (*m*-OH and *p*-OH) were used as emitting materials for device fabrication.

4,4-Bis[*N*-(1-naphthyl)-*N*-phenyl-amino]biphenyl (NPB) was used as hole-transporting material, and 1,3,5-tri(1-phenyl-1H-benzo[*d*]imidazol-2-yl)phenyl (TPBI) as both electron-transporting and hole-blocking layer. *m*-CzOH showed good EL properties with device configuration [ITO/NPD (15) / *m*-CzOH (5 nm) / TBHI (75 nm) / LiF (0.5 nm) / Al (200 nm)] in comparison to other BTZ derivatives. The *m*-CzOH based device reached a maximum brightness of 7866 cd m^{-2} at 14.5 V and a maximum current efficiency of 2.80 cd A^{-1} at 6.5 V. Wang et al. concluded that device performance depends on thickness of emitting layer.

Recently, Chou and colleagues have reported the hydroxy analogues of green fluorescent protein (GFP) chromophore⁹⁰ (**Scheme 2**). GFP contains (*Z*)-4-(4-hydroxybenzylidene)-1,2-dimethyl-1H-imidazol-5(4H)-one (HBDI) chromophore in which emission properties are tunable by changing the substitution pattern at C (1) position. Synthesis, photophysical and luminescent properties of the seven *o*-hydroxy analogues of GFP which are solid state emitters have been summarized by Chou et al.

HBDI exhibits two possible conformers (*o*-HBDI-*Z* form and *o*-HBDI-*E* forms) due to exo-C(5)-C(4)-C(3) bonds. Compounds **1a–1g** exist mainly in *Z*-conformer in nonpolar solvents and solid state. This conformation leads to seven membered-ring-hydrogen bond, from which the ES IPT takes place, instead of eight-member-hydrogen bond transfer process via *E*-conformers. All studied compounds have the same core and differ in substitution at C(9) position.

The photophysical properties of *o*-HBDI-*Z* are dependent on substitution patterns as well as solvents. Electron donor groups at C(9) position of HBDI showed significant red shift in absorption and emission spectra in comparison to electron acceptor groups at C(9) of HBDI in solution and solid state.



Scheme 2 Hydroxy analogues of GFP

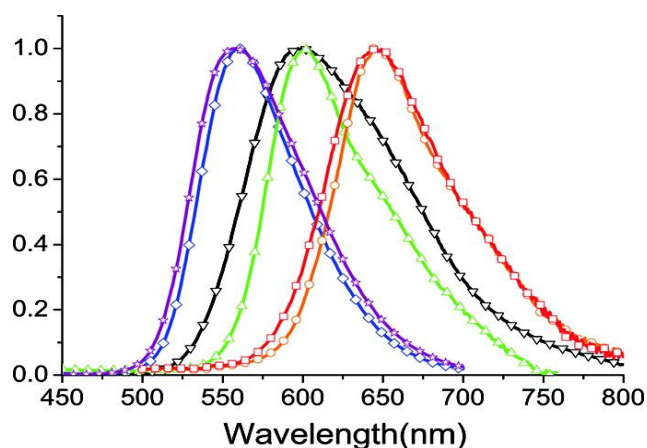


Figure 4 Solid state emission spectra of compounds **1a–1f** (**1a**–red, **1b**–orange, **1c**–green, **1d**–black, **1e**–blue, **1f**–purple). Reproduced with permission [90] Copyright 2011 American Chemical Society

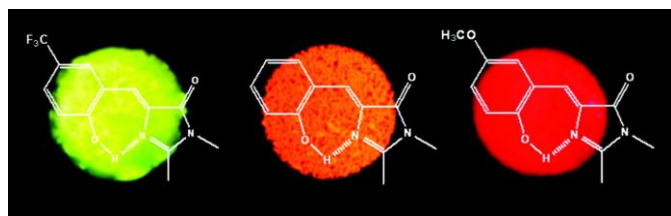


Figure 5 Solid–state fluorescence of compounds **1b**, **1d** and **1f**. Reproduced with permission [90]. Copyright 2011 American Chemical Society

In nonpolar solvent (cyclohexane), compounds showed red shifted emission over the polar solvent (acetonitrile) which indicates that ESIPT emission is more favorable in nonpolar solvent for studied compounds. In solid state, due to restriction of exo-C(5)–C(4)–C(3) bond rotation, intense tautomer emission (keto emission) with high quantum yields ($\Phi_{\text{FL}} = 9\text{--}90\%$) was observed for **1a–1g**. However, restriction of exo-C(5)–C(4)–C(3) bond rotation is not significant for compounds containing electron donor at C(9) position which causes lowering of quantum efficiencies (**1f**: $\Phi_{\text{FL}} = 85\%$, $\tau = 7.4$ ns; **1e**: $\Phi_{\text{FL}} = 84\%$, $\tau = 7.1$ ns; **1d**: $\Phi_{\text{FL}} = 40\%$, $\tau = 4.3$ ns; **1c**: $\Phi_{\text{FL}} = 59\%$, $\tau = 5.3$ ns; **1b**: $\Phi_{\text{FL}} = 19\%$, $\tau = 3.7$ ns; **1a**: $\Phi_{\text{FL}} = 9\%$, $\tau = 5.9$ ns). The significant enhancement of fluorescence quantum efficiency (10 fold; $\Phi_{\text{FL}} = 90\%$, $\tau = 10.2$ ns) was observed for electron acceptor nitro group in comparison to phenyl group at C (9) position. Tautomer emission (keto*) spectra of compounds in solid state cover the visible region **Figure 4**. Chromophores **1b**, **1d** and **1f** are highly emissive in solid state **Figure 5** in comparison with other studied analogue.

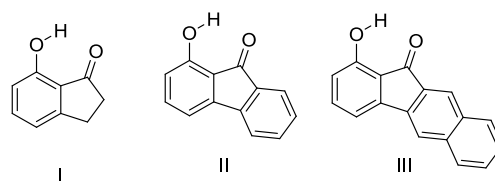
The applicability of *o*-HBDI-Z as emitters in electroluminescence was tested by fabricating OLED device. GFP analogue **1d** was used as emitting materials for device fabrication. 4,4'-*N,N*-Dicarbonyl-1,1'-biphenyl (CPB) was used as host, conducting polymer poly(ethylene dioxythiophene)/poly(styrene sulfonate) (PE-DOT : PSS) was used as the hole-injection layer, 4,4-bis[*N*-(1-naphthyl)-*N*-phenyl-amino]biphenyl (NPB), and 4,4',4''-tri(*N*-carbazolyl)triphenylamine (TCTA) were used as

hole-transport layers, 1,3,5-tri(1-phenyl-1H-benzo[*d*]imidazol-2-yl)phenyl (TPBI) was used as both electron-transporting and hole-blocking layer, LiF was used as electron-injection layer and Al as cathode. The device configuration was [ITO / PE-DOT: PSS (30 nm) / NPB (20 nm) / TCTA (5 nm) / CBP: **1d** (5 wt%, 25 nm) / TPBI (50 nm) / LiF (0.5 nm) / Al (100 nm)]. The device showed maximum brightness of 5790 cd m^{-2} at 17.5 V with CIE coordinates (0.55, 0.43) and maximum external efficiency 0.4 % at 0.82 cd A^{-1} and power efficiency 0.24 lm W^{-1} .

7-Hydroxy-1-indanone **I** based ESIPT molecules exhibiting good fluorescence quantum efficiencies in the crystalline form and in solution were reported by Chou group¹⁸ (**Scheme 3**). Two ESIPT molecules **II** and **III** showing dual emission were synthesized by chemical modification of 7-hydroxy-1-indanone at C(2)–C(3) positions.

Chromophores **I**, **II** and **III** contain hydroxyl group as proton donor and carbonyl as acceptor with suitable geometry for ESIPT process. Indene **I** showed long wavelength emission ($\lambda_{\text{ex}} = 315 \text{ nm}$, $\lambda_{\text{em}} = 530 \text{ nm}$; $\Delta\lambda = 13000 \text{ cm}^{-1}$; $\Phi_{\text{FL}} = 1.2\%$, $\tau = 1.0$ ns) in cyclohexane, while it is non-fluorescent in the solid state. Dual emissions were reported for **II** ($\lambda_{\text{em}} = 468 \text{ nm}$; $\Phi_{\text{FL}} = 1.9\%$; $\tau = 1.2$ ns and $\lambda_{\text{em}} = 535 \text{ nm}$; $\Phi_{\text{FL}} = 1.4\%$; $\tau = 1.2$ ns) and **III** ($\lambda_{\text{em}} = 450 \text{ nm}$; $\Phi_{\text{FL}} = 0.6\%$; $\tau = 0.67$ ns and $\lambda_{\text{em}} = 621 \text{ nm}$; $\Phi_{\text{FL}} = 2.0\%$; $\tau = 0.66$ ns) in cyclohexane. However, only **III** showed dual emission in solid state which is blue shifted emission ($\lambda_{\text{em}} = 453 \text{ nm}$ and 580 nm ; Overall $\Phi_{\text{FL}} = 10\%$) in comparison to emission in cyclohexane. The blue shift was assigned to π - π stacking in between the tetracyclic planes resulting in *H*-aggregation **Figure 6**.

In the solid state, dual emission of **III** covers entire white light spectrum with CIE (x, y) = (0.30, 0.27). The electroluminescent properties of indene **III** were investigated using a multi-layer OLED device structure with PE-DOT:PSS as hole-injection layer, NPB hole transport layer, TCTA was used to decrease the barrier between NPB and emitting layer. CBP was used as host for the emitter **III**. TPBI was used as both hole-blocking and electron-transporting layer. EL device was fabricated with ITO / PE-DOT:PSS-(30 nm) / NPB (15 nm) / TCTS (5 nm) / 5 wt% **III** doped CBP (25 nm) / TPBI (50 nm) / LiF (0.5 nm) / Al (100 nm) configuration. The maximum external quantum efficiency, current and power efficiency were 0.11%, 0.20 cd A^{-1} and 0.06 lm W^{-1} respectively with the CIE coordinates of (x, y) = (0.26, 0.35). The effect of voltage on EL spectra was also studied by authors. The EL spectra were constant when applied voltage was below 16 V (x, y) = (0.26, 0.35), however slight shift in CIE coordinates was observed at 20V (x, y) = (0.28, 0.40) **Figure 7**. This color shift was due to energy transfer from normal excited state to tautomer excited state at higher voltage. The EL spectra for devices incorporating **III** as dopant at different voltages are shown in **Figure 7**.



Scheme 3 7-Hydroxy-1-indanone based ESIPT molecules

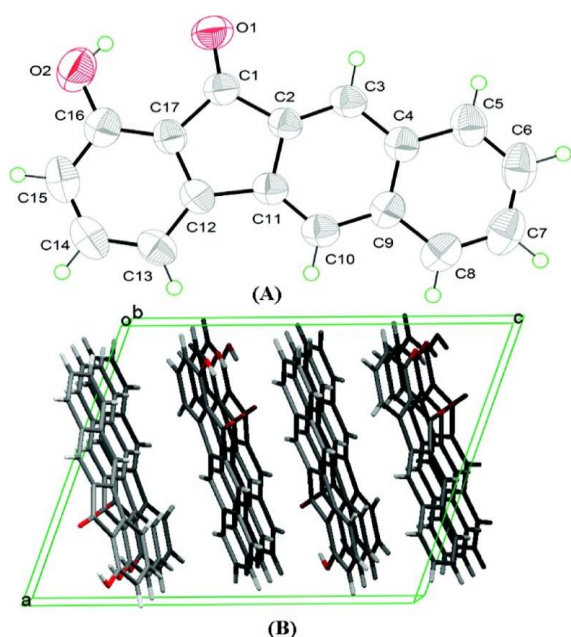


Figure 6 (A) Molecular structure of III with thermal ellipsoids drawn at the 50 % probability level. (B) Packing view of III, viewed along the *b* axis. Reproduced with permission [18]. Copyright 2011 American Chemical Society

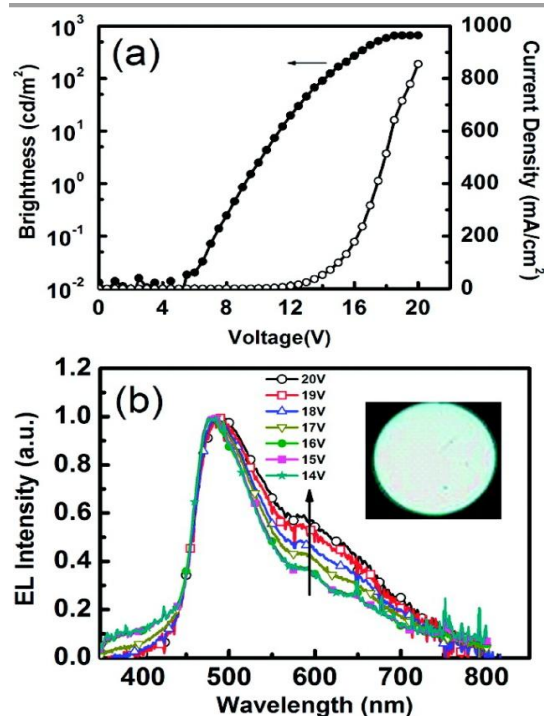
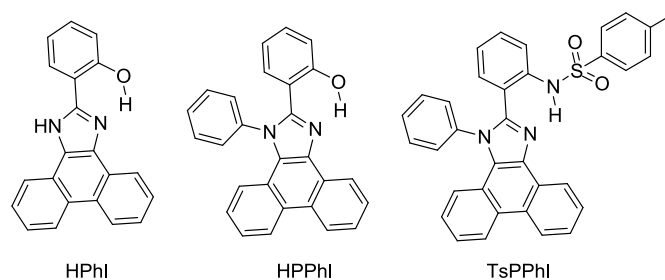


Figure 7 (a) Current density–voltage–luminance (*J–V–L*) characteristics. (b) EL spectra for devices incorporating III as dopant at different voltage. Inset: photo of the device in operation. Reproduced with permission [18]. Copyright 2011 American Chemical Society

Synthesis and optical properties of aryl and di-aryl substituted phenanthroimidazoles (**Scheme 4**) were reported by Manoj Kumar Nayak in 2012¹¹⁴. High fluorescence quantum efficiencies in solid state ($\Phi_{\text{FL}} = 39 - 68\%$) were reported for synthesized chromophores.



Scheme 4 Aryl and di-aryl substituted phenanthroimidazoles

In the design of the phenanthroimidazoles, twisted phenyl groups were purposefully incorporated on central imidazole nitrogen to explore the steric effect and bond rotation effect on the ESIPT process and photophysical properties. Similar types of chromophores, which are solid state emitters, were reported by Park et al. in 2005 for optoelectronic applications²⁶.

In solid state (film) high fluorescence quantum efficiencies ($\Phi_{\text{FL}} = 39-68\%$) were reported in comparison to quantum efficiencies ($\Phi_{\text{FL}} = 0.7-49\%$) in solution. From theoretical calculation using DFT, it was noted that 2-(1*H*-phenanthro[9,10-*d*]imidazol-2-yl)phenol (**HPhI**) is planar, while 2-(1-phenyl-1*H*-phenanthro[9,10-*d*]imidazol-2-yl)phenol (**HPPhI**) and 4-methyl-*N*-(2-(1-phenyl-1*H*-phenanthro[9,10-*d*]imidazol-2-yl)phenyl)benzenesulfonamide (**TsPPhI**) are non-planar.

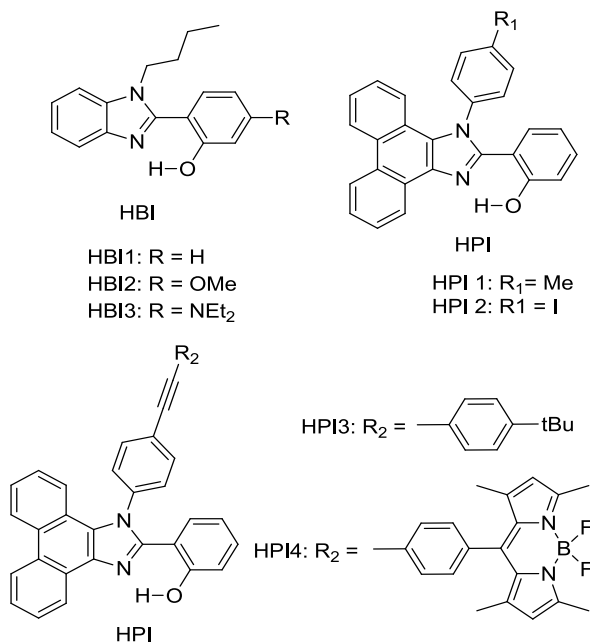
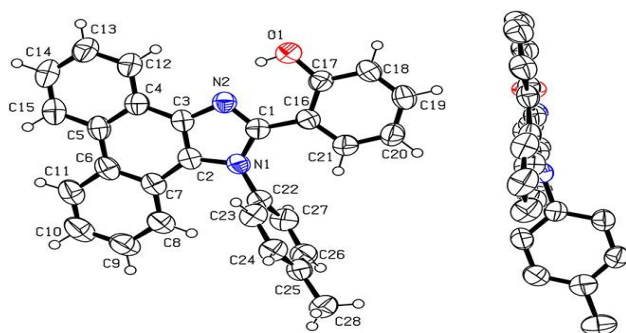
The torsion angles between imidazole and 2-phenyl ring are slightly twisted, whereas phenyl ring attached to imidazole nitrogen is almost perpendicular to the chromophore plane. This twisting causes prevention of direct $\pi-\pi$ stacking of chromophores and maintaining proper intermolecular distance for ESIPT, which effectively suppresses non-radiative decay. **TsPPhI** showed very high fluorescence quantum efficiency with bright emission in blue-green region at room temperature. This could be due to slip-stacked packing present in molecule instead of complete $\pi-\pi$ stacking. The free rotation occurring in solution for **HPPhI** and **TsPPhI** are restricted due to aggregation which results in enhancement of fluorescence efficiencies. Park et al., have already concluded that the incorporation of steric group on the ESIPT chromophore would improve the emission properties by suppressing other non-radiative pathways²⁶.

Subsequently, Ziessel et al. have reported *N*-alkylated-2-(2-hydroxyphenyl)benzimidazole (**HBI**) and *N*-arylated-9,10-phenanthroimidazole (**HPI**) ESIPT chromophores (**Scheme 5**) and their borate complexes²¹. Here we have considered only ESIPT chromophores instead of borate complexes. All studied compounds showed absorption in ultra-violet region with high absorption coefficient due to $\pi-\pi^*$ transition of polyaromatics and emission in near-visible or visible region. The fluorescence quantum efficiencies of the chromophores in the solid state were measured in KBr pellets. **HPI3** showed high quantum efficiency in comparison to other **HPI** and **HBI** chromophores (**Table 1**).

Table 1 Photophysical data of HPIs and HBIs

Comps	λ_{abs} (nm)	λ_{em} (nm)	$\Delta\lambda$ (nm)	Φ_{FL} (%)	τ (ns)
HPI4	370	473	5900	Nr	0.3
HPI3	374	474	5600	28	3.2
HPI1	379	473	5200	12	1.6
HBI3	371	447	4600	4	0.9
HBI2	333	465	8500	3	2.9
HBI1	372	415	2800	4	2.9

Nr: not reported

**Scheme 5** *N*-Alkylated-2-(2-hydroxyphenyl)benzimidazole (HBI) and *N*-arylated-9,10-phenanthroimidazoles (HPI) ES IPT chromophores**Figure 8** X-Ray single crystal data of HPI 1. Reproduced with permission [21]. Copyright 2013 American Chemical Society

From crystallographic analysis of HPI1, it was found that the phenol group is planar with HPI core, while aryl (tolyl) group is almost perpendicular to HPI core **Figure 8**. This planar nature with suitable bond distance and geometry enhances the ES IPT process. Aryl/ alkyl groups restrict the intramolecular rotation which helps to achieve solid state emission and enhancement of quantum efficiencies.

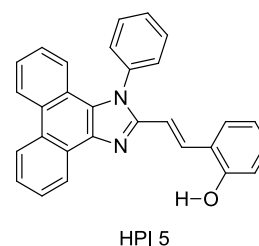
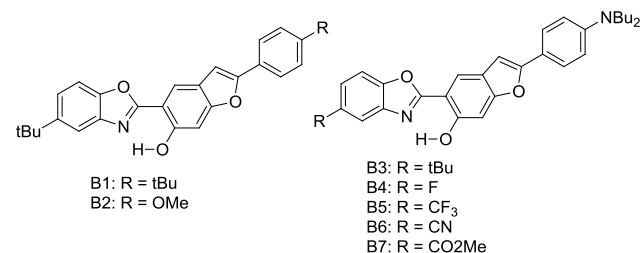
Thanikachalam and coworkers have reported HPI (**Scheme 6**) based solid state chromophore¹¹⁵ similar to HPI derivatives reported by Ziesel et al.²¹ and Park et al.²⁵.

In HPI5, ES IPT occurs through eight membered cyclic transition state, instead of common five and six membered proton transfer process. The chromophore showed 63% fluorescence quantum efficiency in solid film, which is higher than the fluorescence quantum efficiency in solvent (51%). The high fluorescence quantum efficiency in solid state was assigned to π - π staking and steric effect of phenyl groups in solid state.

Recently, white light emitters were reported by Ziesel group¹⁰⁸ by tuning the 2-(2'-hydroxybenzofuran)benzoxazole (HBBO) ES IPT unit (**Scheme 7**). Different electron donor (-NBu₂, -OMe and -tBu) and acceptor (-CF₃, -CN, -CO₂Me) groups were incorporated on fused hydroxybenzofuran system B1-B7 to achieve white light emission.

All chromophores showed similar absorption spectra in solution between 358 to 396 nm. The absorption spectra are weakly dependent on substitution pattern present on aromatic system. Intense single or dual emission bands located between 407 to 588 nm with quantum efficiencies up to 25 % were reported in different solvents. The fluorescence intensity of the compounds depends on electro-negativity of attracting groups present on hydroxybenzofuran core. The photophysical properties have been studied in solid state as dispersed in KBr matrices pallets and polymethyl methacrylate/polystyrene film. Dual emissions (E* and K*) were observed for B3-B7 chromophores in rigid media, which are identical to the emission spectra observed in solution for most of the chromophores **Figure 9**.

The fluorescence quantum efficiencies of the compounds in the solid state (Φ_{FL} = 8-54%), are much higher than that of solution (Φ_{FL} = 1-25%) and dependent on substitution pattern. The electron donor and acceptor groups increase or decrease the acidity and basicity of phenolic hydrogen and imidazole nitrogen, which helps to enhance the ES IPT process. In the case of B5 and B6, the proton transfer in the excited state is

**Scheme 6** Structure of HPI 5**Scheme 7** 2-(2'-Hydroxybenzofuran)benzoxazole (HBBO) ES IPT derivatives

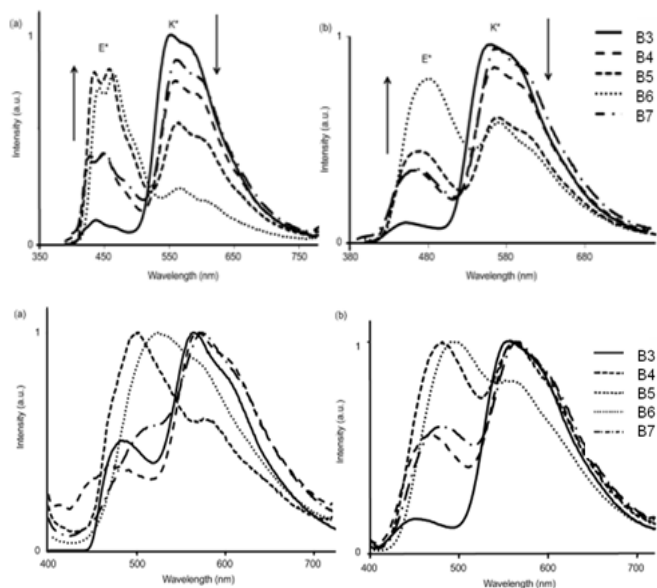


Figure 9 Emission spectra of **B3–B7** [top] (a) in cyclohexane (b) toluene [bottom] (a) in KBr pellets (b) PMMA–PS film]. Reproduced with permission [108]. Copyright 2014 Wiley-VCH Verlag GmbH & Co. KGaA, Weinheim.

more favorable among the series because of appropriate substitution pattern present on benzazole and benzafuran rings. Ziessel and coworkers concluded that in case of HBBO series chromophores, low fluorescence quantum efficiencies were observed in solution due to enhanced rate of non-radiative activation, while in solid state, the interaction with environment suppress the non-radiative process. As a consequence, enhancement in fluorescence quantum efficiencies with white light emission in solid state was observed.

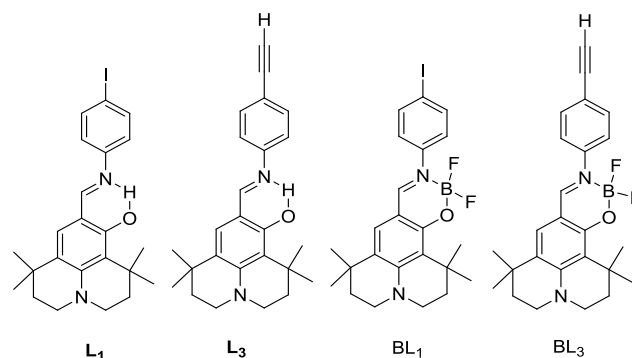
Simultaneously, panchromatic luminescence based on ESIPT julolidine chromophores **L₁** and **L₃** have been (Scheme 8) reported by Ziessel et al.⁹⁷. Chromophores exhibit panchromatic photoluminescence covering the whole visible region in organic solvents and solid state. The authors used julolidine as strong donor to achieve red shifted emission, as well as to favor chelation with metals. Four methyl groups were introduced on julolidine core to increase water solubility and to prevent concentration quenching in the solid state. ESIPT chromophores **L₁** and **L₃** were converted to boranil derivatives **BL₁** and **BL₃** by complexation with $\text{BF}_3 \cdot \text{Et}_2\text{O}$ to obtain high quantum efficiencies by harvesting ESIPT process. All compounds showed absorption at ~ 450 nm with very high extinction coefficient. The absorption properties are independent of solvent polarity. Chromophores **L₁** and **L₃** showed dual emission due to ESIPT process, E* emission ~ 470 nm and K* emission ~ 590 nm. The emission pattern of boranil is completely different than ESIPT ligands. After complexation blue shifted emissions were observed with significant enhancement of the fluorescence quantum efficiencies in solution (Table 2). The prototropic behavior of **L₁** and **L₃** was also studied in acetonitrile solvent. Absorption spectra showed red shift in acidic acetonitrile solution in comparison to pure acetonitrile solution. The disappearance of K* emission was observed for both ESIPT chromophores with appearance of new peak between E* and K* emission.

Table 2 Photophysical data of **L_n** and **BL_n**

Comps	Solvent	λ_{emE^*} (nm)	λ_{emK^*} (nm)	Φ_{FL} (%)	τ (ns)
L₁	Toluene	440	588	0.7	0.12
	DCM	468	596	0.5	0.13
	Methanol	462	586	0.3	0.07
L₃	Toluene	464	590	0.9	0.12
	DCM	478	602	0.7	0.14
	Methanol	466	592	0.4	0.08
BL₁	Toluene	467	Nr	52	1.1
	DCM	473	Nr	69	1.6
	Methanol	471	Nr	69	1.8
BL₃	Toluene	471	Nr	48	1.0
	DCM	477	Nr	71	1.6
	Methanol	472	Nr	72	1.7

Nr: Not reported

The panchromatic behavior of compounds was also studied in condensed medium and the results showed that in glossy medium compounds showed white light emission Figure 10. In solid state, **L₁** gave more balanced white light emission having color coordinates (x, y) = (0.34, 0.36) in comparison to **L₃** due to iodine atom present on phenyl ring. In short, white light emitters with high fluorescence quantum yields were synthesized by chemical modification of *p*-position of the phenyl ring.



Scheme 8: Julolidine based ESIPT chromophores and borate complexes

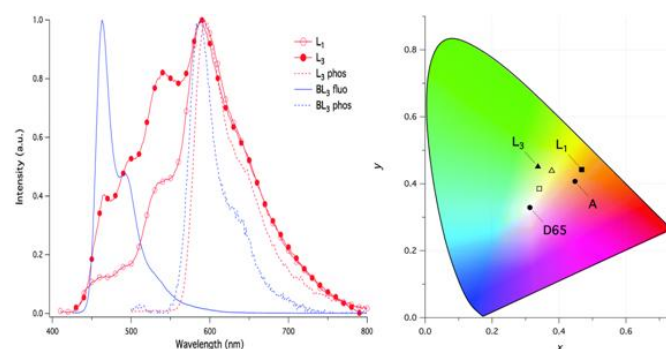
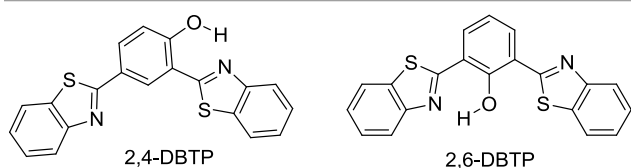


Figure 10 (Left) Normalized luminescence spectra of **L_n** and **BL_n** in $\text{CH}_3\text{OH}:\text{CH}_2\text{Cl}_2$ 1:1 glass; (Right) CIE coordinates of **L₁** and **L₃** in $\text{CH}_3\text{OH}:\text{CH}_2\text{Cl}_2$ 1:1 glass at 77K (filled symbol) and as powder film at rt (open symbol) and of the standard illuminates **A**(tungsten lamp) and **D65** (noon daylight). Reproduced with permission [97]. Copyright 2015 The Royal Society of Chemistry

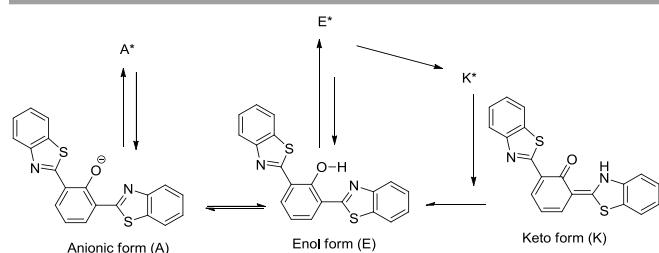
Review Article

Chem Soc Rev

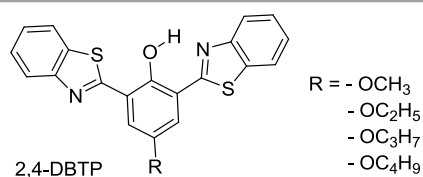
Blue–white–yellow color–tunable ESIPT chromophores (Scheme 9) sensitive towards the solvent polarity and emissive in solid state have been reported by Sakai et al.⁶⁶. 2,4–Dibenzothiazolylphenols (2,4–DBTP) and 2,6–dibenzothiazolylphenols (2,6–DBTP) chromophores were used for blue–white–yellow light generation. 2,4–DBTP ($\lambda_{\text{ex}} = 365$ nm, $\lambda_{\text{em}} = 570$ nm, $\Phi_{\text{FL}} = 68\%$) and 2,6–DBTP ($\lambda_{\text{ex}} = 365$ nm, $\lambda_{\text{em}} = 576$ nm, $\Phi_{\text{FL}} = 62\%$) showed bright yellow fluorescence in the solid state Figure 11. Similar blue shifted emissions were observed for 2,4–DBTP ($\lambda_{\text{ex}} = 378$ nm, $\lambda_{\text{em}} = 554$ nm, $\Phi_{\text{FL}} = 9\%$) and 2,6–DBTP in chloroform with significant decrease of fluorescence quantum efficiency. The emission bands at 570, 576 and 554 nm were assigned to K^* emission in solid state and in chloroform. The mixture of solvents (DMF and CHCl_3) was used for tuning the fluorescence properties of DBTPs. At the ratio of DMF: CHCl_3 as 1:1, 2,4–DBTP showed three emission bands covering entire range of visible light (generation of white light) Figure 11. In addition to K^* and E^* emission, new emission peak was observed between E^* and K^* and assigned to A^* emission (formation of anion) (Scheme 10). The absorption properties of 2,4–DBTP and 2,6–DBTP in mixture of solvents are identical. However, 2,6–DBTP was not found to be suitable for white light emission because of overlapping of K^* ($\lambda_{\text{em}} 565$ nm) and A^* ($\lambda_{\text{em}} 521$ nm) emissions. The fluorescence quantum efficiency of 2,4–DBTP were identical ($\Phi_{\text{FL}} = 68\%$) in crystalline state and in spin coated thin film, which indicates that 2,4–DBTP showed no interference with perylene matrices. The film of 2,4–DBTP and perylene–doped methylmethacrylate prepared in chloroform solvent emits white light Figure 12.



Scheme 9 Dibenzothiazolylphenols (2,4–DBTP and 2,6–DBTP) chromophores



Scheme 10 E^* , K^* and A^* emission pathway



Scheme 11 2–Dibenzothiazolylphenols

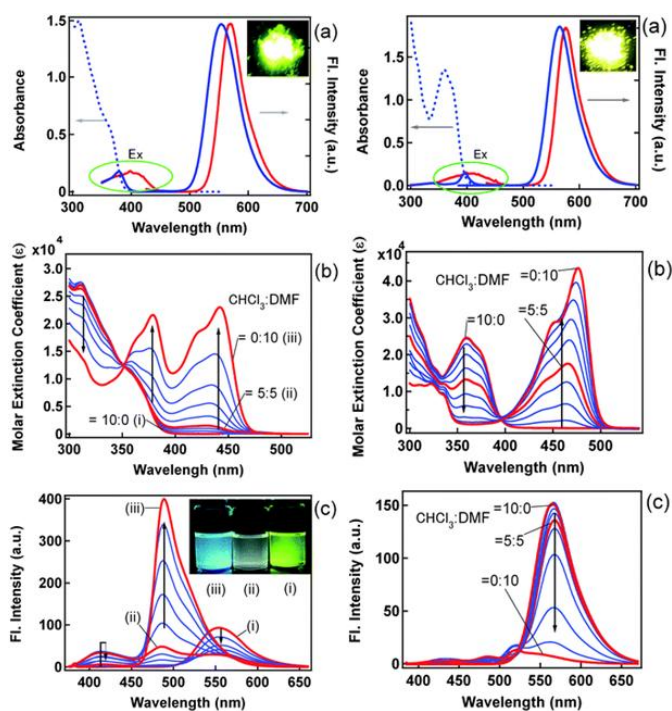


Figure 11 (a) Fluorescence and excitation spectra of 2,4–DBTP (left) 2,6–DBTP (right) in the solid state (red) and in chloroform (blue). (b) Absorption and (c) fluorescence spectral changes by changing the CHCl_3/DMF (v/v) ratio. Reproduced with permission [66]. Copyright 2013 The Royal Society of Chemistry.

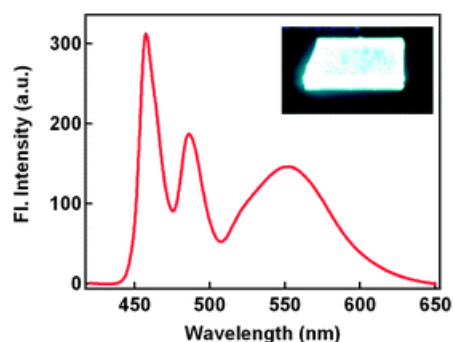


Figure 12 Fluorescence spectrum of the 2,4–DBTP and perylene co-doped PMMA film. Reproduced with permission [66]. Copyright 2013 The Royal Society of Chemistry

Simultaneously, Sakai et al. also reported solid state red emissive ESIPT chromophores based on 2,6–dibenzothiazolylphenols (2,6–DBTP) (Scheme 11) by introducing alkoxy group at 4–position¹⁰³. Four different alkoxy groups namely –OMe, –OEt, –OPr and –OBt were synthesized and their optical properties were studied.

2,6–DBTPs were fluorescent in solution as well as in solid state. The red shifted emission was observed for alkoxy substituted 2,6–DBTPs ($R = \text{Alkoxy}$: $\lambda_{\text{em}} = \sim 619$ nm, $R = \text{H}$: $\lambda_{\text{em}} = 565$). In chloroform 2,6–DBTPs showed identical fluorescence properties for all alkoxy derivatives. However, the fluorescence properties of the alkoxy derivatives were different in the solid state. In solid state, –OMe and –OEt showed red shifted emission, while –OPr and –OBt showed

blue shifted emission in comparison to emission in chloroform **Figure 13**. This indicates that the fluorescence properties of DBTPs in the solid-state significantly depend on length of alkyl group

The difference in solid state fluorescence properties were assigned to mode of molecular packing (*J*- and *H*-aggregation) described by X-ray single crystal data of -OMe and -OPr. In -OMe the *H*-bonded benzothiazole moieties involved in the ESIPT have slipped configuration (*J*-aggregation) **Figure 14**, while in -OPr crystal, its configuration is eclipsed (*H*-aggregation) **Figure 14**. The three planar π -units of -OMe and -OPr are almost in plane. In the case of -OMe the torsion angle between phenol and H bonded BT ($\theta = 3.7^\circ$) is little larger than -OPr ($\theta = 0.2^\circ$) which causes weaker hydrogen bonding in -OMe than -OPr. In ESIPT chromophores, it is well known that when the H-bond strength is strong, the fluorescence quantum yields will be high¹¹⁶. This supports the quantum yield trends of alkoxy derivatives (-OMe: $\lambda_{em} = 647$ nm, $\Phi_{FL} = 17\%$, -OEt: $\lambda_{em} = 633$ nm, $\Phi_{FL} = 32\%$, -OPr: $\lambda_{em} = 589$ nm, $\Phi_{FL} = 38\%$, -OBt: $\lambda_{em} = 592$ nm, $\Phi_{FL} = 44\%$ in spin coated polymer matrices). The high fluorescence quantum efficiencies and solid state fluorescence properties were supported by TD-DFT computations and the difference in solid state fluorescence was well explained by Davydov exciton coupling theory. In summary, alkoxy derivatives showed solid state emission with very high fluorescence quantum efficiencies even with absence of bulky group to prevent intermolecular interaction.

Among the studied alkoxy derivatives, -OEt derivative is best red non-doped red emitter in terms of color with moderate fluorescence quantum efficiency ($\lambda_{em} = 633$ nm, $\Phi_{FL} = 32\%$). The fluorescence properties of -OEt derivative are comparable with best fluorescent non-doped red emitters which are reported in literature. They all are large molecules and contain bulky groups in order to avoid twisting around the single bonds. Reported non-doped red emitters are diethynylbenzothiazole¹¹⁷ ($\lambda_{em} = 624$ nm, $\Phi_{FL} = 62\%$), perylene tetracarboxylic acid bisimide¹¹⁸ ($\lambda_{em} = 635$ nm, $\Phi_{FL} = 59\%$), spiribifluorene¹¹⁹ ($\lambda_{em} = 646$ nm, $\Phi_{FL} = 46\%$), 1,4-bis(alkenyl)-2,5-dipiperidinobenzene¹²⁰ ($\lambda_{em} = 641$ nm, $\Phi_{FL} = 34\%$) and mesitylboryl-substituted bithiophene¹²¹ ($\lambda_{em} = 657$ nm, $\Phi_{FL} = 30\%$).

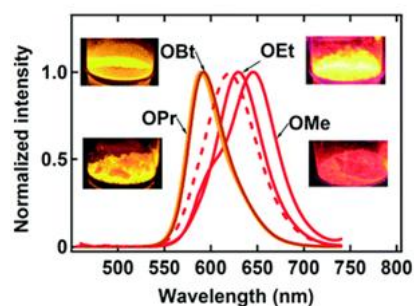


Figure 13 Fluorescence spectra of crystalline powder samples ($\lambda_{exc} = 400$ nm), the dotted line is the spectrum in chloroform (same for all alkoxy), all inset photographs under irradiation with a 365 nm UV lamp. Reproduced with permission [103]. Copyright 2014 The Royal Society of Chemistry

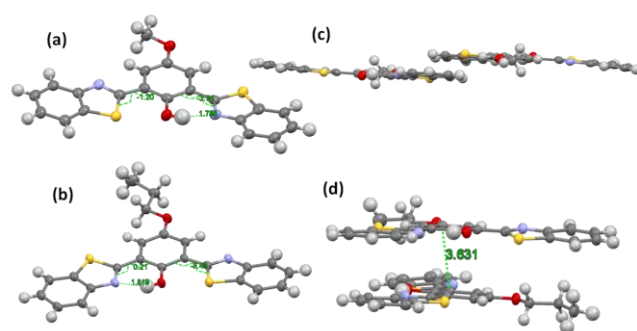
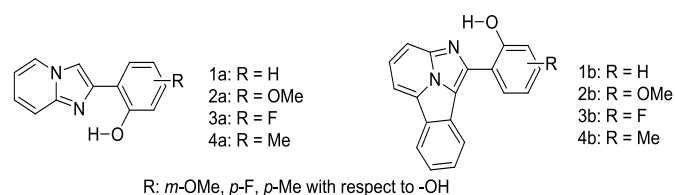


Figure 14 Molecular structure of (a) -OMe and (b) -OPr with 50 % probability; (c) packing of -OMe (d) packing of -OPr. Reproduced from CIF file [103]

Fused π -conjugated benzo[*a*]imidazo[5,1,2-*cd*]indolizine ESIPT fluorophores (**Scheme 12**) have been reported by Gryko et al.¹²². Benzo[*a*]imidazo[5,1,2-*cd*]indolizines derivatives were prepared from 2-(2'-hydroxy-phenyl)-imidazo[1,2-*a*]pyridines by cyclo-addition followed by dehydration reaction.

The effect of π -conjugation on ESIPT process was well studied by comparing photophysical properties of benzo[*a*]imidazo[5,1,2-*cd*]indolizines with structural analogues 2-(2'-hydroxy-phenyl)-imidazo[1,2-*a*]pyridines reported by Araki et al.^{94,95}.

In the solid state π -conjugated benzo[*a*]imidazo[5,1,2-*cd*]indolizines showed red shifted absorption and emission in comparison to corresponding imidazo[1,2-*a*]pyridines (**Table 3**). However, lowering of fluorescence quantum yields ($\Phi_{FL} = 18$ –26%) were observed for π -conjugated system. The absorption maxima of π -conjugated compounds **1b–4b** were bathochromically shifted by ~ 100 nm in comparison to corresponding imidazo[1,2-*a*]pyridines **1a–4a**. This red shift can be assigned to extended π -conjugations.



Scheme 12 π -Conjugated benzo[*a*]imidazo[5,1,2-*cd*]indolizine and 2-(2'-hydroxy-phenyl)-imidazo[1,2-*a*]pyridines ESIPT fluorophores.

Table 3 Photophysical data of **1a–4a** and **1b–4b**

Comps	λ_{abs} (nm)	λ_{em} (nm)	Φ_{FL} (%)	Comps	λ_{abs} (nm)	λ_{em} (nm)	Φ_{FL} (%)
1a	331	494	39	1b	410,435	612	26
2a	336	520	41	2b	416,443	568	24
3a	332	522	37	3b	410,435	626	18
4a	332	529	31	4b	414,439	626	21

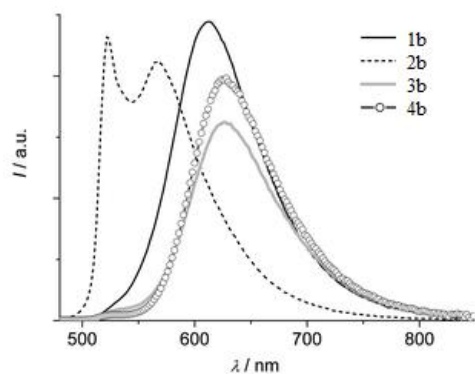


Figure 15. Emission spectra of compounds **1b–4b** in the solid state ($\lambda_{\text{exc}} = 440 \text{ nm}$). Reproduced with permission [122]. Copyright 2014 The Royal Society of Chemistry and the Centre National de la Recherche Scientifique

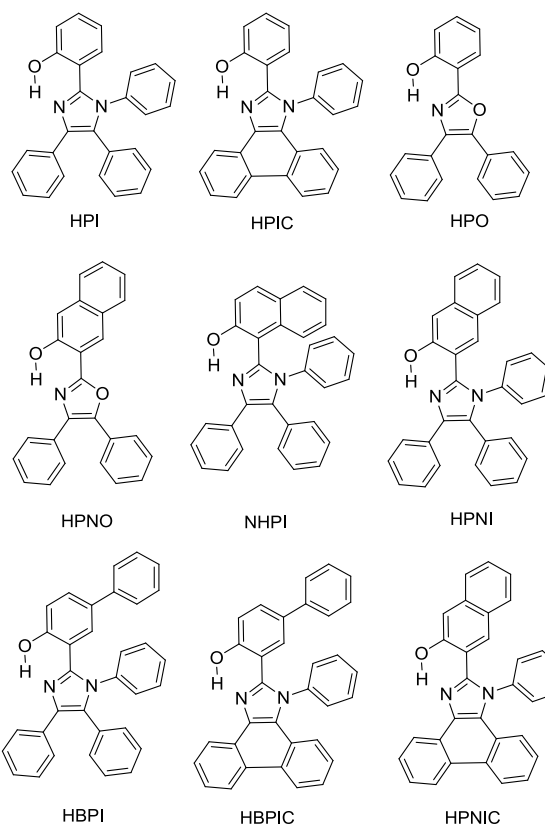
Except for compound **2b**, all compounds **1b** and **3b–4b** showed single broad emission which covers entire visible light. The blue shifted emission for **2b** may be due to electron donor methoxy group present on phenyl ring **Figure 15**.

Absorption and emission spectra of both series depend on solvent polarity. In polar aprotic solvent, the emission spectra consist of two bands which are characteristics of ESIPT, while in polar protic (methanol) solvent single hypsochromic emission, which corresponds to normal emission was observed for all the compounds. In nonpolar solvent, π -conjugated benzo[*a*]imidazo[5,1,2-*cd*]indolizines showed high fluorescence quantum efficiencies in comparison to imidazo[1,2-*a*]pyridines. Based on the results of Araki and coworkers for imidazo[1,2-*a*]pyridines derivatives, Gryko et al., concluded that π -conjugated imidazo pyridine maintained planar conformation in rigid media, because of restricted rotation of 2-hydroxyphenyl substituents. The lowering of quantum efficiencies of **1b–4b** in solid can be assigned to face-to-face stacking (intermolecular interaction) in comparison to imidazo[1,2-*a*]pyridines (slip-stacking).

Color tuning of imidazole based ESIPT chromophores by chemical alteration were reported by Park et al.²⁵. Nine different chromophores (**Scheme 13**) were synthesized and their photophysical properties were studied in solvents and on solid thin film.

The concept of nodal plane model^{44,123}, extension of effective conjugation^{25,124} and modification of heterocyclic rings¹⁷ were used for the development of color tunable chromophores. All these chromophores showed emission in visible region in chloroform and in solid state **Figure 16**.

In nodal plane (Nagaoka et al.) model¹²³, stabilization effect of aromatic ring at 2 position of imidazole ring can be predicated by considering the nodal pattern of wave function and delocalization of electrons in the excited state. In excited state extended conjugation along with nodal plane stabilizes the excited state keto and helps in lowering of K^* energy. In **NHPI** (1-(1,4,5-triphenyl-1*H*-imidazol-2-yl)phenol), **HPNI** (3-(1,4,5-triphenyl-1*H*-imidazol-2-yl)naphthalen-2-ol), **HPNIC** (3-(1-phenyl-1*H*-phenanthro[9,10-*d*]imidazol-2-yl)-naphthalen-2-ol) and **HPNO** (3-(4,5-diphenyloxazol-2-yl)-naphthalen-2-ol) contain extended conjugation at 2-position of imidazole (**Table 4**).



Scheme 13 Structures of *N*-aryl-HBI and HBO

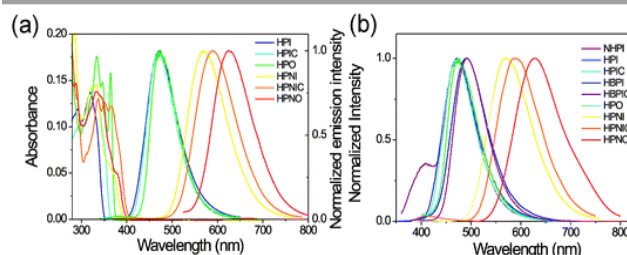


Figure 16 UV-Vis absorption and normalized photoluminescence spectra of synthesized molecules (a) chloroform (b) solid film in PMMA. Reproduced with permission [25]. Copyright 2012 PCCP Owner Societies.

HPNI, **HPNIC**, and **HPNO** showed long red shifted ESIPT emission due to stabilization of K^* through effective delocalization of electrons from aromatic naphthalene ring (**Table**). However, **NHPI** showed blue shifted K^* emission because, naphthalene ring lies out of the nodal plane. Park et al. used the strategy for extension of conjugation length to tune the fluorescence properties. In case of **HPIC** (2-(1-phenyl-1*H*-phenanthro[9,10-*d*]imidazol-2-yl)phenol), **HBPIC** (3-(1-phenyl-1*H*-phenanthro[9,10-*d*]imidazol-2-yl)-[1,1'-biphenyl]-4-ol), and **HPNIC**, extension of conjugation as well as planarity were achieved to obtain bathochromic shift (**Table 4**). In addition to above two strategies, electron donors and acceptors also affect the energies of the excited species. In **HPO** (2-(4,5-diphenyloxazol-2-yl)phenol) and **HPNO** (3-(4,5-diphenyloxazol-2-yl)naphthalen-2-ol) electron acceptor imidazole units were replaced by strong electron acceptor oxazole units to change the color properties.

Table 4 Photophysical data of imidazoles and oxazoles

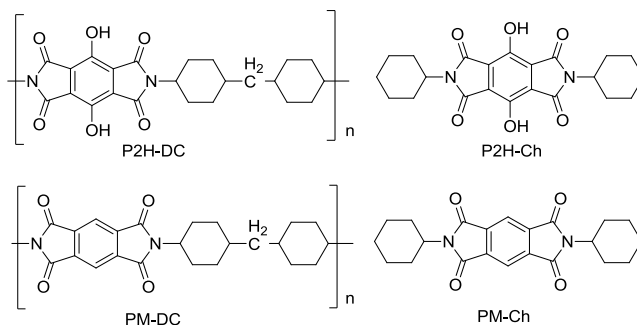
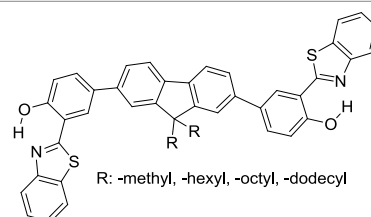
Comps	λ_{abs} (nm)	λ_{em} (nm)	$^a\Phi_{\text{FL}}$ (%)	$^b\Phi_{\text{FL}}$ (%)	τ (ns)
NHPI	343	475	2.6	15.8	0.2
HPNI	333	570	5.3	22	3.2
HPNIC	365	590	3.4	15	2.0
HPNO	333	630	0.6	4	0.8
NHPI	343	475	2.6	15	0.2
HPIC	364	470	17	34	1.3
HBPIC	368	495	29	56	2.7
HPO	333	475	13	19	1.4
HPI	318	470	15	35	1.7

$^a\Phi_{\text{FL}}$: Fluorescence quantum efficiency in chloroform; $^b\Phi_{\text{FL}}$: fluorescence quantum efficiency in polymer matrix (PMMA)

These three strategies help in tuning the fluorescence properties of compounds upon altering the energy gaps between HOMO and LUMO of enol and keto forms. To support these observations, theoretical calculations were reported by Park et al., HOMO and LUMO energies and band gap were evaluated computationally, by cyclic voltammetry technique and optical spectroscopy. These results conclude that strength of electron acceptor and donor, length of conjugation changes the energies of HOMO and LUMO which results in change in the color properties.

Recently, polyimide (**P2H-DC**) and imide (**P2H-Ch**) based ESIPT fluorophores (**Scheme 14**) exhibiting red fluorescence in solution and on solid thin film were reported by Ando et al.¹⁰¹. Polyimide **P2H-DC** and imide **P2H-Ch** contain hydroxy groups susceptible to ESIPT process, while polyimide **PM-DC** and imide **PM-Ch** are non-ESIPT chromophores. Photophysical properties of the ESIPT and non-ESIPT chromophores were studied purposefully, to study the importance of -OH group on color properties of imides. Initially, fluorescence properties of imides **PM-Ch** and **P2H-Ch** in chloroform were studied and results clearly indicate that hydroxy derivative **P2H-Ch** showed dual emission (E^* and K^*), while **PM-Ch** showed single normal emission. Photophysical properties of the polyimide were studied on solid thin film. The absorption properties of the **P2H-DC** ($\lambda_{\text{abs}} = 407$ nm) and **PM-DC** ($\lambda_{\text{abs}} = 317$ nm) were similar to monomers **P2H-Ch** ($\lambda_{\text{abs}} = 421$ nm) and **PM-Ch** ($\lambda_{\text{abs}} = 320$ nm). The colorless **PM-DC** film showed weak absorption at 317 nm, while **P2H-DC** film showed absorption peak at 407 nm along with shoulder peak at 418 nm. The emission properties of the **P2H-DC** ($\lambda_{\text{em}} = 642$ nm, $\Phi_{\text{FL}} = 10\%$) and **PM-DC** ($\lambda_{\text{em}} = 439$ nm) were completely different, but coincided well with emission bands of **P2H-Ch** (keto emission band in chloroform) and **PM-Ch**. This clearly indicates that red emission band of **P2H-DC** in solid state is corresponding to ESIPT emission with considerable enhancement of fluorescence quantum efficiency.

The effect of pH on absorption spectra of polyimide **P2H-DC** was studied by authors for pH range of 11–14. In basic media (pH = 11) new absorption peak appeared at 529 nm with gradual decrease of intensity of 407 nm peak. At pH 14 a new absorption band was observed at 630 nm with change of film color from yellow–red–deep blue. The appearance of new peaks was due to formation of mono and di-phenoxide ions in basic media even in the solid state.

**Scheme 14** Structures of ESIPT-polyimide and imide and non-ESIPT analogues**Scheme 15** Structures of fluorene-HBT ESIPT molecules

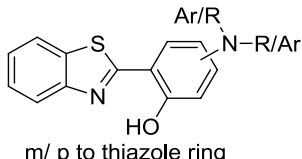
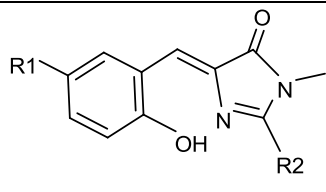
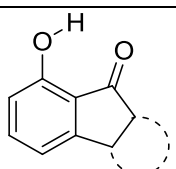
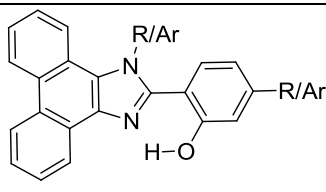
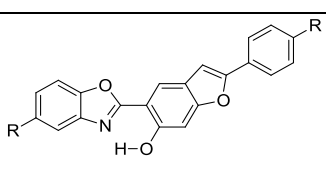
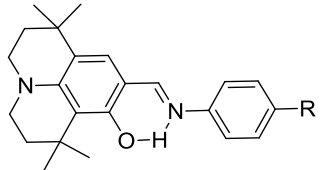
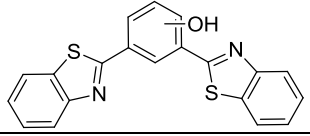
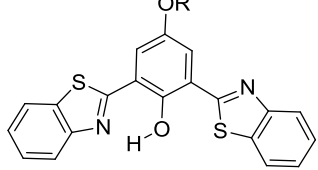
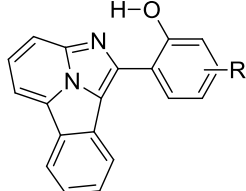
In summary, the polyimide was concluded to show red emission in solid state due to ESIPT process associated with halochromic properties.

Recently, highly emissive ESIPT solid state emitters based on fluorene-HBT motifs have reported by Padalkar et al.¹²⁵ (**Scheme 15**). Padalkar and co-workers synthesized different fluorescent compounds containing two HBT units attached to 7,7'-position and different alkyl groups at 9,9'-position on fluorene unit. Compounds absorb (~ 325 – 344) in UV region and emit (~ 405 – 552 nm) in the visible region. The absorption spectra of the compounds in solid state and in solution are almost identical. However, the emission spectra of compounds are different in different media. Compounds showed single emission in solid state, chloroform, toluene and DMF and multiple emissions in methanol and acetonitrile. The single emission in solid state is assigned to keto emission, and multiple emissions in methanol and acetonitrile are assigned to *cis*-enol, *cis*-keto, protonated *cis*-enol and phenoxide ions. The fluorescence quantum efficiencies of the compounds in solid state ($\Phi_{\text{FL}} = 54$ – 68%), are much higher than that of solution of different polarities ($\Phi_{\text{FL}} = 1$ – 11%). The fluorescence lifetime in solid state is between 3.48–5.21 ns, while it significantly less in chloroform (0.52–0.75 ns). The high fluorescence quantum efficiencies in solid state was assigned to slip-stacking and strong intramolecular hydrogen bonding which was confirmed by single X-ray crystal data as well as DFT computations by Padalkar et al.

A short summary of solid state ESIPT emitters as a single molecule is summarized in **Table 5**.

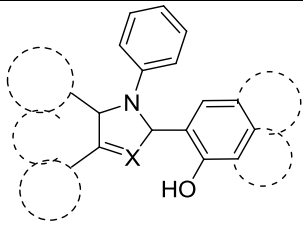
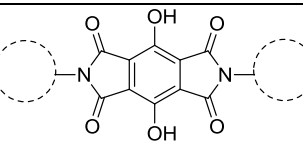
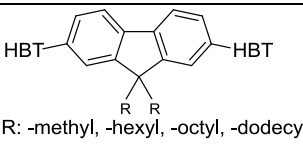
Recently, few more small molecules which are emissive in the solid state have been reported, but their detailed photophysical properties have not been explained by respective authors. The reported chromophores, which are derivatives of bis-imidazole¹²⁶, coumarin¹²⁷, benzothiazole-benzamide¹²⁸, benzothiazole hydroxy naphthalene-1-carbaldehyde¹²⁹, bis-benzothiazole¹³⁰ and *N*-salicylidine anilines¹³¹ are summarized below **Table 6**.

Table 5 Summary of solid state emitters through single molecules

ESIPTs Structure	Spectral and Photophysical data	Ref
 <p>m/ p to thiazole ring</p>	White light emission; Φ_{FL} = 5.65 – 91.68%; λ_{em} = 443 – 630 nm; λ_{Lem} = 460 – 648 nm; Planar structure; Intramolecular H-bonding interaction; FI. Depends on nature and position of amino substituted groups. Highest quantum efficiency reported till date for single small ESIPT molecule.	33
	White light emission; Φ_{FL} = 9.0 – 90%; λ_{em} = 560 – 649 nm, τ = 4.3 – 10.2 ns; Z-conformation; Seven membered ESIPT; RIR effect; FI. Properties depends on the electron donating/ withdrawing/ resonance properties of the substituents. Analogues of GFP chromophore. Radiationless quenching process can be reduced by substitution of bulky groups at C4 position.	90
	White light emission; Φ_{FL} = ~10%; λ_{em} = 435 – 580 nm, nearly planar structure; π - π stacking; H-aggregation; 5-fold enhancement of quantum efficiency in solid state; CIE (0.30, 0.27); π - π stacking can be minimized by introducing a bulky substituents on tetracyclic moiety.	18
	Φ_{FL} = 29–68%; λ_{em} = 375 – 480 nm; τ = 0.2 – 3.2 ns; slip-stacking; offset face-to-face stacking; Hydroxy phenyl ring is co-planar with imidazole, N-aryl ring perpendicular to imidazole ring, N-aryl rings suppress the non-radiative pathways or π - π stacking	25 114 115
	White light emission; Φ_{FL} = 8–54%; λ_{em} = 451 – 580 nm; CIE (0.34, 0.39); FI. depends on substitution patterns and position; electron-donating groups on benzofuranol side increases the pKa of compounds and acceptor on the benzoxazole decreases the basicity of cyclic amines. These combined effects provide broad dual-emission band.	108
	White light emission; panchromatic luminescence; dual emission; intramolecular H-interaction; λ_{em} = 465 – 590 nm; τ = 11.6 – 54.6 ns; CIE (0.34,0.38); Methyl groups helps for RIR; , FI. dependent on groups attached at p-position with respect to imine N; prototropic behaviour.	97
	White light emission; Blue-white-yellow emission; Φ_{FL} = 68%; λ_{em} = 570 nm (2,4-DBTP); Φ_{FL} = 62%; λ_{em} = 576 nm (2,6-DBTP); CIE (0.13 – 0.43 polymer film, 0.26–0.59 solution); generation of white light due to K*, E* and A* emission.	66
	Non-doped red emitters; Φ_{FL} = 17 – 44%; λ_{em} = 589 – 647 nm; CIE (0.57–0.65, 0.34–0.41); J- and H-Aggregation; Solid state emission depends on nature of alkoxy group; quantum efficiency is proportional to strength of intramolecular H-bond. Best non-doped red emitters reported till date (small molecule)	103
	Φ_{FL} = 18–27%; λ_{em} = 612 – 626 nm; 100 nm red shift for benzo[a]imidazo [5,1,2-cd]indolizines relative to corresponding imidazo[1,2-a]pyridines; Extending the length of conjugation causes red shift, but quenching in quantum efficiency (~half).	122

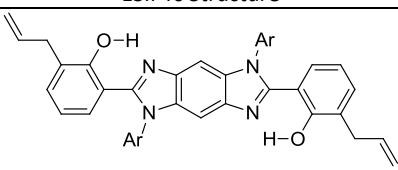
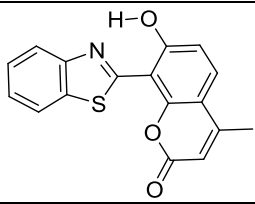
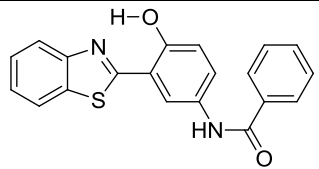
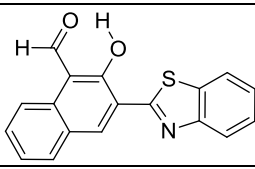
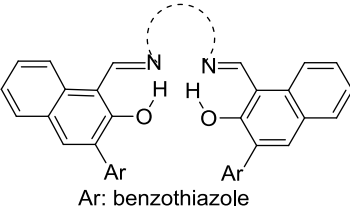
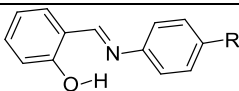
Φ_{FL} : Fluorescence quantum yields, λ_{Lem} : Luminescence emission, τ : Fluorescence lifetime, RIR: restriction of intramolecular rotation, CIE: CIE 1931 chromaticity diagram.

Table 5 (Continue) Summary of solid state emitters through single molecules

ESIPTs Structure	Spectral and Photophysical data	Ref
	Polymorph dependence emission; white emission; $\Phi_{FL} = 4 - 56\%$; $\lambda_{em} = 450 - 630 \text{ nm}$; $\tau = 0.2 - 2.77 \text{ ns}$; Color tuning: nodal plane approach, extension of conjugation, modification of heterocyclic ring and strength of electron donor and acceptor; intense FI. due to twisted phenyl ring.	25
	Red fluorescence; $\Phi_{FL} = 10\%$; $\lambda_{em} = 642 \text{ nm}$; pH dependent FI. properties; thermally stable $\sim 350 \text{ }^\circ\text{C}$; halochromism.	101
 R: -methyl, -hexyl, -octyl, -dodecyl	Yellow emitters, $\Phi_{FL} = \sim 68\%$; $\lambda_{em} = 544 - 552 \text{ nm}$; $\tau = 3.48 - 5.21 \text{ ns}$; slip-stacking, AIE, thermally stable $\sim 440 \text{ }^\circ\text{C}$; 10–60fold enhancement of quantum efficiency in solid state in comparison to solution.	125

Φ_{FL} : Fluorescence quantum yields, λ_{em} : Luminescence emission, τ : Fluorescence lifetime, RIR: restriction of intramolecular rotation, CIE: CIE 1931 chromaticity diagram, AIE: aggregation induced emission.

Table 6 Structures of solid state emitters (Photophysical data not discussed in detail)

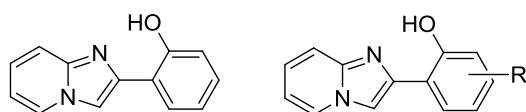
ESIPTs Structure	Spectral and Photophysical data	Ref
	Two-photon absorption; yellow-green emission; $\Phi_{FL} = 7 - 16\%$; $\lambda_{em} = 500 - 506 \text{ nm}$ (solvents); $2\lambda_{OPA} = 726 \text{ and } 772 \text{ nm}$ (dichloromethane); intramolecular H–interaction.	126
	Dual emission; S_1 and S_3 emission; $\Phi_{FL} = 4\%$; $\lambda_{em} = 363 \text{ and } 514 \text{ nm}$; $\tau = 8.7 \text{ and } 2.4 \text{ ns}$ (toluene); green-blue solid state emission; $\lambda_{em} = \sim 520 \text{ nm}$.	127
	Solid state emission; $\lambda_{em} = 550 \text{ nm}$.	128
	Multiple emission; $\lambda_{em} = \sim 500, 550 \text{ and } 650 \text{ nm}$; absorption and emission properties are solvent dependent; $\Phi_{FL} = 5 - 11\%$ (solvents). –OH and –CHO responsible for ESIPT.	129
 Ar: benzothiazole	Solid state emission; $\lambda_{em} = \sim 440, \sim 580, \text{ and } \sim 595 \text{ nm}$.	130
	Thermochromic; photochromic; $\lambda_{em} = \sim 500$; planar conformation; CH– π interaction; cis–trans isomerization; π – π stacking; close packed configuration.	131

6. Solid state ESIPT emitters based on polymorphic form (molecular packing)

Imidazo[1,2]pyridine is an important class of heterocyclic compounds widely used in medicinal field^{132,133}. Recently 2-(2'-hydroxyphenyl)imidazo[1,2]pyridine (**Scheme 16**) has attracted huge attention due to its unique photophysical properties⁵⁴⁻⁵⁷. These types of chromophores undergo excited state intramolecular proton transfer upon photoexcitation, which helps to enhance the fluorescence properties of the chromophores. The fluorescence properties of 2-(2'-hydroxyphenyl)imidazo[1,2]pyridine contain ESIPT unit which was first studied by Acuna and Douhal in 1996^{7,134,135}, and recently Gryko and Cyranski groups reported additional substituted ESIPT imidazo[1,2]pyridines¹²².

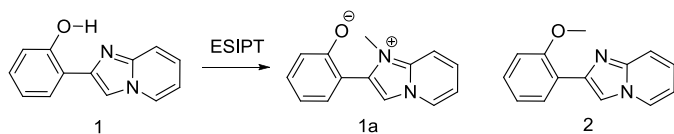
Extensive research on photophysical properties of 2-(2'-hydroxyphenyl)imidazo[1,2]pyridines in solution, crystalline state, in polymorph state, and in polymer matrices was performed by Araki and coworkers since 2008⁵⁴⁻⁵⁷. The various parameters such as polymer matrices, crystal structure, types of substituents, and molecular packing were studied to understand the ESIPT process of 2-(2'-hydroxyphenyl)imidazo[1,2]pyridines experimentally as well theoretically^{54-57,94,95}. In 2008, Araki and coworker reported effective mechanism for switching of organic solid state luminescence for 2-(2'-hydroxyphenyl)imidazo[1,2]pyridine⁵⁶. Two crystal polymorphs of different colors (blue-green (BG) and yellow (Y)) due to ESIPT phenomenon were studied in detail.

The emission maxima of compound **1** was reported in protic ethanol and compared with emission spectrum of compound **2**. Compound **1** showed weak fluorescence in blue region (E^* emission; $\lambda_{\text{ex}} = 332 \text{ nm}$, $\lambda_{\text{em}} = 377 \text{ nm}$, $\Phi_{\text{FL}} = 8\%$, $\tau = 2.63 \text{ ns}$ in THF) and large Stoke's shifted emission ($1a^*$ emission; $\lambda_{\text{ex}} = 602 \text{ nm}$, $\Phi_{\text{FL}} = 2\%$, $\tau = 0.5 \text{ ns}$ in THF) in orange region, while only blue emission (E^* emission; $\lambda_{\text{ex}} = 332 \text{ nm}$, $\lambda_{\text{em}} = 378 \text{ nm}$, $\Phi_{\text{FL}} = 11\%$, $\tau = 2.56 \text{ ns}$ in THF) was observed for compound **2**. This result clearly indicates that dual emissions in compound **1** were due to intramolecular hydrogen bonding. Blue emission is assigned to locally excited state and orange emission is the ESIPT emission from $1a^*$ (**Scheme 17**).



R = *o*-CH₃, *m*-OCH₃, *p*-Br, *m*-OH, *m*-*N,N*-diethyl respect to 2-OH

Scheme 16 2-(2'-Hydroxyphenyl)imidazo[1,2]pyridines

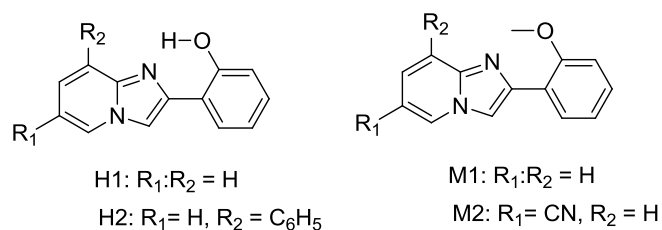


Scheme 17 Structure of compounds **1**, **1a** and **2**

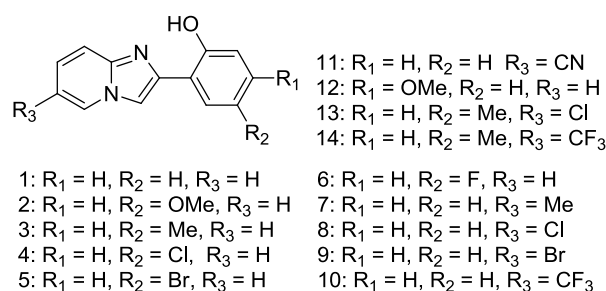
In frozen state compound **1** showed blue shifted ESIPT emission ($1a^*$ emission; $\lambda_{\text{ex}} = 521 \text{ nm}$, $\tau = 5.2 \text{ ns}$ in THF at 77K). Similar to frozen state, identical absorption and emission patterns were observed for compound **1** in amorphous ($\lambda_{\text{ex}} = 337 \text{ nm}$, $\lambda_{\text{em}} = 527 \text{ nm}$, $\Phi_{\text{FL}} = 39\%$, $\tau = 6.39$) and polymorphic forms (Polymorph-BG: $\lambda_{\text{ex}} = 339 \text{ nm}$, $\lambda_{\text{em}} = 496 \text{ nm}$, $\Phi_{\text{FL}} = 50\%$, $\tau = 5.91$; Polymorph-Y: $\lambda_{\text{ex}} = 337 \text{ nm}$, $\lambda_{\text{em}} = 529 \text{ nm}$, $\Phi_{\text{FL}} = 37\%$, $\tau = 5.84$) with little change in ESIPT emission. However significant enhancement in quantum efficiencies was observed in rigid media in comparison to dilute solution. The enhancement of quantum efficiencies and solid state emission was explained on the basis of molecular packing in amorphous and polymorphic forms. The dihedral angle between phenyl and imidazopyridine rings is close to zero for **BG** and **Y** polymorphs (Blue-green polymorph $\theta = 5.8^\circ$) (yellow polymorph $\theta = 1.3^\circ$), this indicates that both polymorphs are planar in nature. In polymorph -**Y** compound **1** is packed with co-planar conformation, while in **BG**-polymorph the conformation is a twisted one. This packing-induced small deviation of the molecular conformation may affect the ESIPT process. Molecular packing is a key factor for switching the color properties of the ESIPT imidazo[1,2]pyridines. In polymorph -**Y** and -**BG** the molecular packing of compound **1** is thermally controlled reproducible packing, which was confirmed from DSC and TGA data. Based on these results Araki et al., concluded that the luminescence properties of ESIPT imidazo[1,2]pyridine **1** are switchable in solid state with high quantum efficiencies.

After the discovery of polymorph dependent ESIPT luminescence for imidazo[1,2]pyridines, white light luminescence properties of the imidazo[1,2]pyridines were reported by Araki and coworkers¹⁹. Mixtures of ESIPT and non-ESIPT chromophores were used for generation of white light¹⁹. Prior to this report based on ESIPT, Park S. Y. and coworker⁸⁷ have reported white light generation using two ESIPT chromophores having different Stokes shift and Chou et al.¹⁷ also reported white light generation in solution using ESIPT and normal luminophores.

In the design of white-light emitters, hydroxy and methoxy derivatives of 2-phenylimidazo[1,2-a]pyridine (PIP) chromophores (**Scheme 18**) having similar absorption properties and different emission properties were used¹⁹. Authors claimed that use of compounds of similar molecular structures is more advantageous, because these compounds may have similar physical properties. Before this ESIPT based white light emitters strategies, generation of white light has been reported by mixing blue- and yellow-emitting species having proper combination of donor and acceptors^{16,19}. In this case, no donor-acceptor relationship exists for white light generation. 2-Hydroxy derivatives **H1** ($\lambda_{\text{ex}} = 335$, $\lambda_{\text{em}} = 529 \text{ nm}$, $\Phi_{\text{FL}} = 37\%$, $(x, y) = (0.36, 0.55)$) and **H2** ($\lambda_{\text{ex}} = 330$, $\lambda_{\text{em}} = 536 \text{ nm}$, $\Phi_{\text{FL}} = 31\%$, $(x, y) = (0.41, 0.50)$) exhibiting ESIPT and 2-methoxy derivatives **M1** ($\lambda_{\text{ex}} = 312$, $\lambda_{\text{em}} = 382 \text{ nm}$, $\Phi_{\text{FL}} = 24\%$, $(x, y) = (0.23, 0.22)$) and **M2** ($\lambda_{\text{ex}} = 348$, $\lambda_{\text{em}} = 422 \text{ nm}$, $\Phi_{\text{FL}} = 15\%$, $(x, y) = (0.17, 0.09)$) having no intramolecular hydrogen bond were used for white light generation in solution and solid film. All compounds showed identical absorption spectra in UV region, while emission patterns were different for ESIPT and non-ESIPT chromophores. Hydroxy derivatives **H1** and **H2** emit with large Stokes shift (ESIPT process) and methoxy derivatives **M1** and **M2** emit with normal Stokes shift (normal emission).



Scheme 18 Hydroxy and methoxy derivatives of 2-phenylimidazo[1,2-a]pyridines.



Scheme 19 Substituted imidazo[1,2-a]pyridines

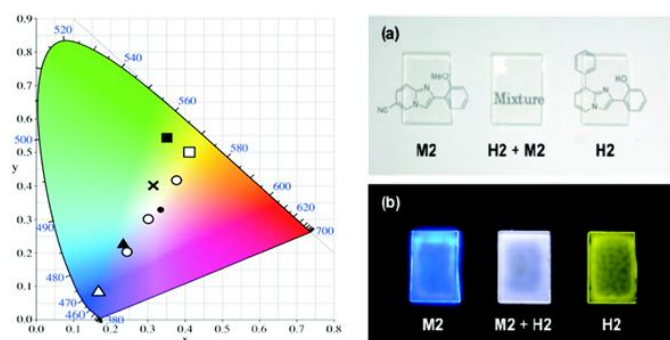
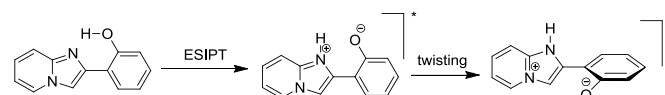


Figure 17 (Left) A CIE chromaticity diagram of **H1** (filled square), **H2** (open square), **M1** (filled triangle), **M2** (open triangle), a mixture of **H1 + M1** (1:100; cross), and **H2 + M2** (1:10, 3:10, and 10:10; open circle; from left to right). A black dot indicates the ideal white ($x, y = 0.33, 0.33$). (Right) Images of PMMA films containing **M2**, **H2+M2** (11:7), and **H2** (from left to right) under (a) room light and (b) a UV lamp (365 nm). Reproduced with permission [19]. Copyright 2011 American Chemical Society.

The absorption band should not trail into visible region to achieve pure white light emission in solid state. The same excitation wavelength was used to achieve yellow and blue luminescence in present study. Mixture of various ratios of hydroxy: methoxy were tested to achieve white–light luminescence in the solid state. At ratio of 1:100 by weight (**H1:M1**), bright whitish luminescence (prominent $\lambda_{em} = 386$ nm, and broad $\lambda_{em} = 470$ – 650 nm) with CIE coordinates (x, y) = (0.32, 0.40) was observed. The mixture of **H2:M2** (3:10 by weight) displayed a bright white luminescence at CIE (x, y) = (0.30, 0.31), which is almost pure white light **Figure 17**. The combination of ES IPT–**H2** and non ES IPT–**M2** in polymer matrix [poly(methyl methacrylate) (PMAA)] generates white light emissive film **Figure 17**. Araki et al. has concluded that whitish luminescence is a summation of the luminescence of ES IPT and non–ES IPT chromophores and both types of chromophores emit independently. The white light generated from mixture of **H2** and **M2** on vapor deposited film ($\Phi_{FL} = 18\%$, (x, y) = (0.30, 0.31) as well as in PMAA matrix ($\Phi_{FL} = 22\%$, (x, y) = (0.36, 0.33) showed similar luminescent properties at optimized **H2:M2** ratio and remained unchanged for long time.

Simultaneously, effect of substitution on ES IPT emission of imidazo [1,2-a] pyridine in rigid media was studied by Araki et al.⁵⁴ Various electron donor and acceptor groups on phenyl and imidazopyridine (**Scheme 19**) core were studied in solution as well as in polymer matrix (PMAA).



Scheme 20 Formation of zwitterionic ES IPT species

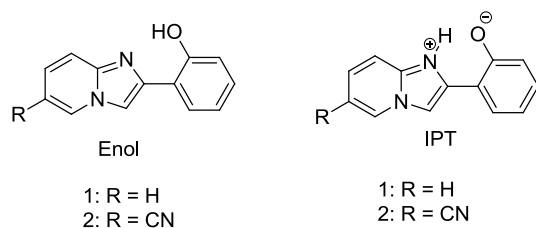
All compounds showed absorption in UV region ($\lambda_{abs} = 333$ – 341 nm) in THF and ($\lambda_{abs} = 331$ – 351 nm) in a PMMA film. This result concludes that substitution has little influence on the absorption spectra. Except few compounds (**2**, **10**, **13**–**14**), all the compounds showed dual emission (normal and ES IPT emission) in THF with significant change in emission pattern. The emission pattern depends on nature as well as position of substituents present in the molecules. The absorption and emission properties of the compounds were also studied in frozen THF. In frozen media the absorption spectra were similar to THF solution.

However blue shifted emissions (50 – 90 nm) were observed for compounds in frozen THF. The blue shift was assigned to effect of rigid medium. In THF solution, the fluorescence quantum efficiencies of the compounds was less than 2%, but was very high in a PMMA matrix ($\Phi_{FL} = 10$ – 60% , $\tau = 2.1$ – 4.9 ns). The average lifetime of compounds indicates that emission is a singlet emission originated from zwitterionic ES IPT species (**Scheme 20**). Douhal et al. reported¹³⁴ that zwitterionic ES IPT species further undergo twisted conformation along with rearrangement of surrounding medium which may be the reason for red shifted emission with large Stokes shift in THF solvent.

In rigid media, zwitterionic ES IPT species retain their planarity, which causes the blue shifted ES IPT emission. In summary, authors concluded that introduction of electron donor and acceptor groups on phenyl ring causes blue and red shift respectively, while reverse observations were observed for same groups on imidazopyridine core. The experimental results i.e. effect of substitution on fluorescence properties were well supported by theoretical results.

In addition to two–colors polymorph dependent ES IPT study of imidazo[1,2-a]pyridine **1**, three–colors polymorph dependent luminescence study of ES IPT imidazo[1,2-a]pyridine derivative **2** was reported by Araki et al. recently⁵⁵. Three (yellow–orange–red) colors were achieved by controlling the molecular packing of 6–cyano–2–(2–hydroxyphenyl)imidazo[1,2-a]pyridine (**Scheme 21**).

Three polymorphs namely 2–yellow (**2–Y**), 2–orange (**2–O**) and 2–red (**2–R**) were obtained by different crystallization methods from hexane, benzene, chloroform and THF solvents. All polymorphic crystals are luminescent under UV lamp (365 nm) **Figure 18**.



Scheme 21 6-Substituted-2-(2-hydroxyphenyl)imidazo[1,2-a]pyridines

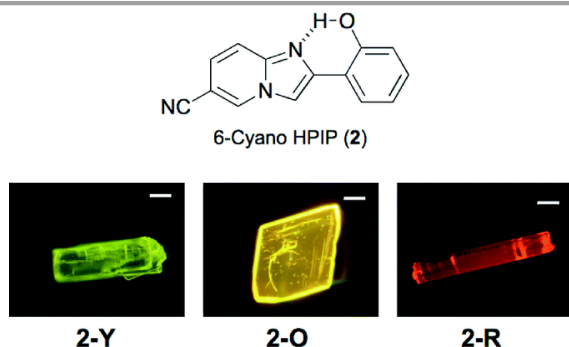


Figure 18 Luminescent images of polymorphic crystals, 2-Y, 2-O, and 2-R. Reproduced with permission [55]. Copyright 2014 The Royal Society of Chemistry.

Single emissions were observed for polymorphic crystals (2-Y: $\lambda_{em} = 548$ nm, $\Phi_{FL} = 49\%$, $\tau = 5.48$ ns; 2-O: $\lambda_{em} = 570$ nm, $\Phi_{FL} = 25\%$, $\tau = 5.51$ ns, and 2-R: $\lambda_{em} = 585$ nm, $\Phi_{FL} = 10\%$, $\tau = 2.26$ ns) upon excitation at 330 nm. The absorption spectra of three polymorphic crystals were almost identical in terms of shape and absorption maxima wavelength, which indicates that absorption properties of the compound 2 are not sensitive towards polymorph packing. Similar observation was reported⁵⁶ for two-color polymorph dependent ESIPT study of imidazo[1,2-a]pyridine 1.

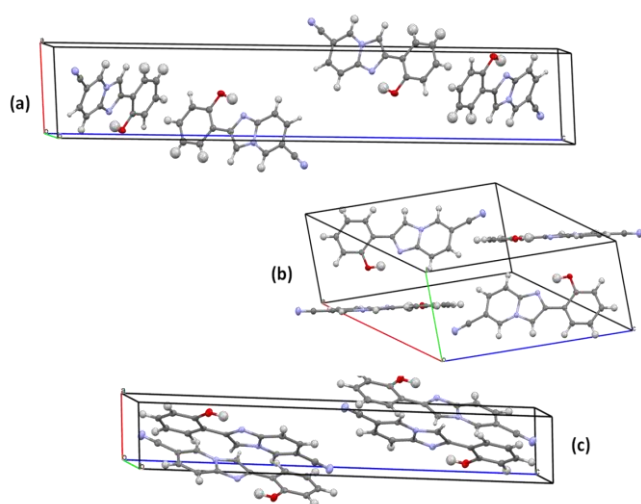
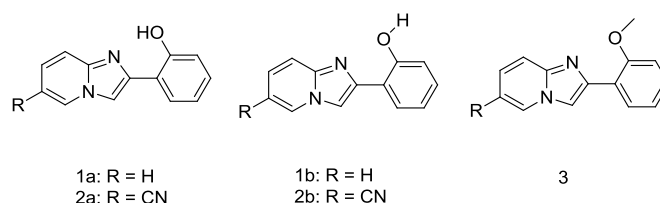


Figure 19 Molecular packing of (a) 2-Y (b) 2-O and (c) 2-R. Reproduced from CIF file [55]

Three polymorphs emit at different wavelength (yellow–orange–red region) with significant difference in quantum efficiencies ($\Phi_{FL} = 10$ –49%). This difference in luminescence properties of compound 2 was well studied by authors from X-ray single crystal data and theoretical calculations. All polymorphic crystals were monoclinic and had the same space group. The distances between basic nitrogen and acidic hydrogen were 2.582, 2.625, and 2.622 Å, for 2-Y 2-O and 2-R respectively indicating favorable geometry for intramolecular hydrogen bonding. The dihedral angle between two aromatic rings is close to zero ($\theta = 1.4$, 2.5 and 1.4° for 2-Y 2-O and 2-R respectively) which confirms the planar nature of polymorphic crystal.

However the molecular packing was different for different polymorphs **Figure 19**. 2-Y and 2-R crystals have slip-packed packing, while 2-O crystal had antiparallel π - π stacking with interplanar distance 3.35 Å. In crystal 2-Y, the interplanar distance between two parallel rings was 3.38 Å and distance between an oxygen atom and the nearest nitrogen atom of the neighboring molecules was 3.64 Å, which prohibits the formation of intermolecular hydrogen bond. Similar observations were reported for 2-R crystal. In 2-Y and 2-R crystal, the fused the imidazole part overlapped with phenyl-part of the stacked molecule. However, in 2-O crystal the imidazole part overlapped with phenyl andazole part of imidazole. This different intermolecular interaction may be the key factor for polymorph dependent luminescence. Different structural packing was supported by DSC and DFT computations and all results are well in agreement with experimental results.

Tunable luminescence properties of 2-(2'-hydroxyphenyl)imidazo[1,2-a]pyridines (**Scheme 22**) with surrounding medium were also studied by Araki group⁵⁷. Two derivatives 1 and 2 were studied for influence of matrices on luminescence properties. Polystyrene (PS), poly(vinyl acetate)(PVAC), poly(bisphenol A carbonate) (PC), poly(methyl methacrylate) (PMAA), poly(vinyl alcohol) (PVA) and poly(ethylene glycol) (PEG) were used as matrices for matrix dependent luminescence study. Spin coated samples were used for absorption and luminescence measurements. Compound 1 showed green to yellow–green luminescence, while compound 2 showed variety of colors such as purple, yellow and orange. It was reported that compounds 1 and 2 showed single emission in different polymorphic form with large Stokes shift. This emission was assigned to ESIPT from intramolecular proton transfer (IPT*) generated from 1a and 2a. In polymer matrices compounds showed dual emission, normal emission (1b* and 2b*) and ESIPT emission (1a* and 2a*).



Scheme 22 2-(2'-Hydroxyphenyl)imidazo[1,2-a]pyridines

However, in polar solvents the emission was single emission because in polar solvent the dissociation of the intramolecular hydrogen bond between imidazole nitrogen and phenolic hydrogen (**1a** and **2a**) to produce **1b** and **2b** is more favorable. This may be the reason for dual emission in polymer matrices. The luminescence properties of the compounds were dependent on polarity of polymer matrices due to mode of hydrogen bonding between polymers and ESIPT unit. The luminescence properties of compound **1** were not strongly dependent on polarity of matrices **Figure 20**, while significant change in luminescence properties was observed for compound **2** in PS, PVAC, PC, PMMA, PVA and PEG polymer matrices **Figure 20**. Further, authors also concluded that the relative intensity of normal and ESIPT emission depends on polymer matrices. The luminescence properties were tuned by varying the concentration of PS, PVAC, PC, PMMA, PVA and PEG polymer matrices. In case of compound **2**, as the concentration of **2** increased, the intensity of normal emission gradually decreased with enhancement of ESIPT emission intensity. In short, polarity of the surrounding polymer matrices tunes the relative intensities as well as emission bands produced by normal and ESIPT emission. Increasing concentration of compound **2** in polymer matrices changes the emission color from purple–white–green **Figure 20**.

Photophysical properties of compounds **1** ($\lambda_{\text{ex}} = 331\text{--}336$, $\lambda_{\text{Nem}} = 373\text{--}381$ nm, $\lambda_{\text{ESIPTem}} = 517\text{--}540$ nm, $\Phi_{\text{FL}} = 23\text{--}40\%$) and **2** ($\lambda_{\text{ex}} = 347\text{--}359$, $\lambda_{\text{Nem}} = 402\text{--}414$ nm, $\lambda_{\text{ESIPTem}} = 540\text{--}585$ nm, $\Phi_{\text{FL}} = 4\text{--}10\%$) in different polymer matrices concluded that compound **2** is more susceptible to surrounding medium.

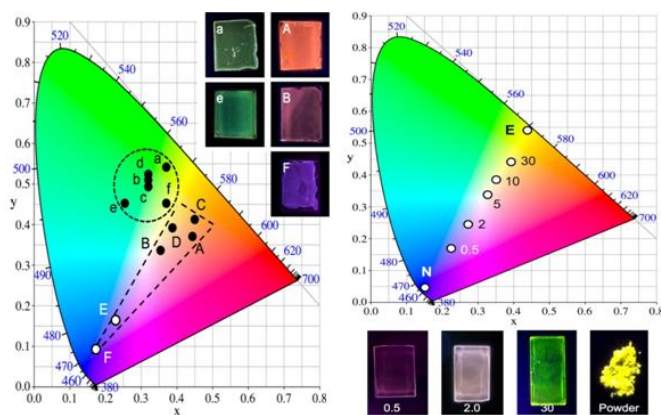
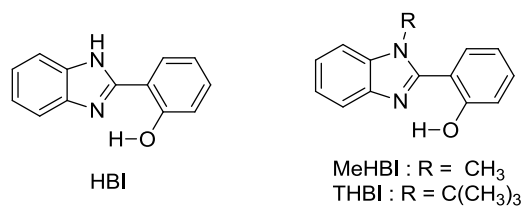


Figure 20 (Left) CIE 1931 chromaticity diagram of the luminescence ($\lambda_{\text{ex}} = 330$ nm) of spin-coated films containing 0.5 w/w% of **1** (a–f) and **2** (A–F) in PS (a, A) PVAC (b, B), PC (c, C), PMMA (d, D), PVA (e, E), and PEG (f, F). Images in the upper right corner show polymer films luminescing under a UV lamp (365 nm). (Right) CIE 1931 chromaticity diagram of the luminescence ($\lambda_{\text{ex}} = 333$ nm) of spin-coated PVA films containing 0.5–30 w/w% of **2**. “N” and “E” represent the color indices of the normal and ESIPT emission bands, respectively. The images below show luminescence of the polymer films and the powder of **2** under a UV lamp (365 nm). Reproduced with permission [57]. Copyright 2014 American Chemical Society.

Based on DFT computations and FT–IR analysis results, authors concluded that hydrogen bonding between imidazole –N= and phenolic –H is weaker due to electron withdrawing cyano group present in compound **2**. This could be the reason for more susceptibility of compound **2** with different polymer matrices.

After the experimental finding for tuning/enhancement of luminescence properties of 2–(2′-hydroxyphenyl)imidazo [1,2–a]pyridines by different means^{54–57}, theoretical calculations were also performed by Araki et al. to support all observations^{94,95}. They used different computational strategies for this study. Density functional theory (DFT), time-dependent density functional theory (TD–DFT), equation-of-motion coupled-cluster singles and doubles (EOM–CCSD), and our own N-layered integrated molecular orbital and molecular mechanics (ONIOM) calculations were performed on Gaussian 09; Complete active space multiconfiguration–SCF (CASSCF), multistate–CASPT2 (MS–CASPT2) calculation on MOLCAS 7.4 and fragment molecular orbital–TDDFT (FMO–TDDFT) calculation using GAMESS ver. 2012. Potential energy surface (PESs), geometry optimization, dipole moments, vertical excitations, electronic distribution and energies of different forms were studied for 2–(2′-hydroxyphenyl)imidazo[1,2–a]pyridines in the ground and excited state. The experimental results are well in accordance with theoretical results.

In addition to imidazo[1,2–a]pyridine ESIPT emitters, polymorph dependent ON–OFF luminescence study of hydroxy benzimidazoles type of ESIPT were also studied by Araki group¹⁰². *N*-Alkyl substituted hydroxybenzimidazole (**BHI**) were (**Scheme 23**) used for this study. The luminescence properties of sterically hindered imidazole were compared with reported luminescent HBI. Methyl and *tert*-butyl groups were introduced to cause steric hindrance with hydrogen atom of phenol ring. 2–(1–Methyl–1*H*–benzo[d]imidazol–2–yl)phenol (**MeBHI**) exhibits bright ESIPT luminescence in polymorphic form. The emission spectra of **MeBHI** were different in different solvents. In polar methanol, **MeBHI** showed single blue emission (E* emission: $\lambda_{\text{ex}} = 288$, $\lambda_{\text{em}} = 352$ nm, $\Phi_{\text{FL}} = 30\%$), while red shifted single emission was observed in cyclohexane (K* emission: $\lambda_{\text{ex}} = 291$ and 322, $\lambda_{\text{em}} = 484$ nm, $\Phi_{\text{FL}} = 4\%$). In THF, **MeBHI** showed dual emission (E* and K* emission: $\lambda_{\text{ex}} = 292$ and 321, $\lambda_{\text{E*em}} = 355$, $\Phi_{\text{FL}} = 2\%$ and $\lambda_{\text{K*em}} = 483$ nm, $\Phi_{\text{FL}} = 1\%$). Two polymorphic crystals of **MeBHI** were developed from ethanol **NL** (non-luminescent) and from benzene **L** (luminescent) by crystallization techniques. The polymorph obtained from benzene is highly luminescent ($\lambda_{\text{ex}} = 286$, $\lambda_{\text{em}} = 458$ nm, $\Phi_{\text{FL}} = 74\%$, $\tau = 4.4$ ns) in solid state in comparison to non-luminescent polymorph obtained from ethanol ($\lambda_{\text{ex}} = 291$, $\lambda_{\text{em}} = 470$ nm, $\Phi_{\text{FL}} = 0.7\%$). The 100 fold enhancement of quantum efficiency for polymorph **L** was described by hydrogen bonding, planarity and molecular packing of polymorphs. The crystal structure data showed that in polymorph **L**, the torsion angle between two rings is 15°, while in polymorph **NL** the torsion angle is 127°. This clearly indicates that intramolecular hydrogen bonding in polymorph **L** is more favorable as compared to that in polymorph **NL**. The red emission for polymorph **L** is assigned to ESIPT emission due to planarity and favorable geometry **Figure 21**.



Scheme 23 Structures of BHI derivatives

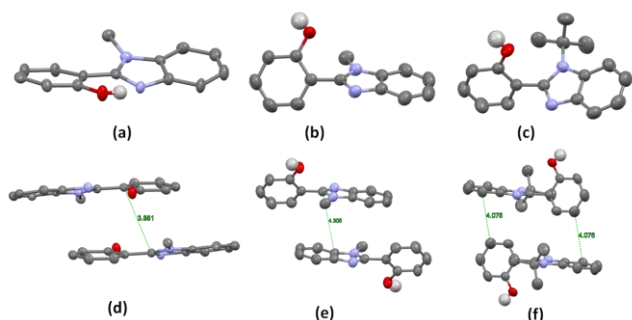


Figure 21 molecular structure (a) MeBHI-L (b) MeBHI-NL (c) THBI and packing (d) MeBHI-L (e) MeBHI-NL (f) THBI, Except –OH hydrogen other hydrogen atoms are omitted for clarity. Reproduced from CIF file [102]

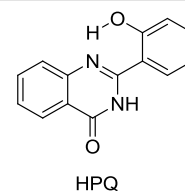
In polymorph **NL** intermolecular hydrogen bonding occurs instead of intra-molecular hydrogen bonding because of twisted conformation which resulted in non-ESIPT process. Similar to polymorph **NL**, 2-(1-*tert*.butyl-1*H*-benzo[d]imidazol-2-yl)phenol (**THBI**) is also non-luminescent because of twisted molecular structure ($\theta = 104^\circ$) which favors intermolecular hydrogen bonding instead of intramolecular hydrogen bonding. These results conclude that methyl group in **MeBHI** decreases the planarity of HBI which creates two different modes of molecular packing. Authors also studied the effect of temperature on luminescence properties of **MeBHI**. DSC data of **NL** showed only melting point peak, while peak at 75 °C was observed for **L** in addition to melting point peak. The spin coated sample from benzene on quartz showed bright luminescence, indicating that spin coated sample is in **L** form. Upon heating, luminescence decreased dramatically up to 75 °C and vanished completely at 90 °C. The XRD pattern of this spin coated heated samples matched with XRD pattern of **NL**. This concludes that highly luminescent ON luminescence state of **MeBHI** can be transferred to OFF state upon heating. The reverse process OFF-ON is also possible by dissolution in benzene and rapid crystallization. Further, authors also concluded that luminescence properties of **MeBHI** were mechanically tunable.

ESIPT inspired HBT, HBI, BHO, and imidazo[1,2-*a*]pyridine are well known as solid state luminescent chromophores and studied extensively in past decade. Recently Savarimuthu Anthony has reported quinazolinone based (**Scheme 24**) polymorph-dependent solid state emitter¹⁰⁴. 2-(2'-Hydroxyphenyl)-4-(3H)-quinazolinone (**HPQ**) exhibits solid state fluorescence in two different polymorphs through ESIPT process. Recrystallized **HPQ** from ethyl acetate, ethanol, methanol, acetone, DMF, DMSO and chloroform and solid powder obtained from reaction mixture showed blue-solid state fluorescence. Crystallization of **HPQ** from THF produced two types of crystals; needle shaped and plate shaped. Needle

type crystal showed blue emission (**HPQ-B**) while plate-like crystal showed blue-green emission in solid state (**HPQ-BG**). The different colors in two polymorphs were explained on the basis of molecular packing by single crystal analysis. The analysis showed that both crystal (**HPQ-B** and **HPQ-BG**) lattices contain intermolecular (amide-amide) as well as intramolecular interaction (=N-OH), however the interaction is rather strong in **HPQ-BG** **Figure 22**.

In addition to common interaction, unusual intermolecular interactions such as –C=O⋯C=O dipolar and OH⋯H=C– were observed between phenolic oxygen atom and hydrogen atoms of the adjacent aromatic ring for **HPQ-BG** **Figure 23**.

The dihedral angle between quinazolinone and phenyl ring determines the fluorescence properties of **HPQ**. In **HPQ-B** the dihedral angle is 3.68°, while more twisting was observed in **HPQ-BG** ($\theta = 9.9^\circ$). Polymorphic ability of **HPQ** leads to tuning of fluorescence properties in solid state. **HPQ-B** showed blue shifted emission ($\lambda_{em} = 497$ nm) in comparison to **HPQ-BG** ($\lambda_{em} = 511$ nm). The red shifted emission for **HPQ-BG** was assigned to additional intermolecular interaction which stabilizes the molecular twisting. The emission properties of **HPQ** were solvent dependent and also reported to have metal chelation ability. The applicability as sensors for Zn²⁺ and Cd²⁺ were examined by authors and concluded that the emission is highly selective and sensitive in **HPQ** towards Zn²⁺ and Cd²⁺.



Scheme 24: Structure of HPQ

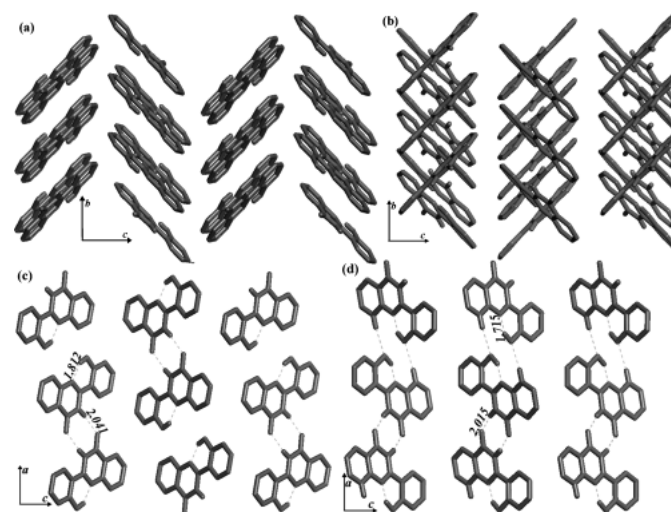


Figure 22 Molecular packing and selected H-bond interactions in the crystal lattice (a, c) **HPQ-B** and (b, d) **HPQ-BG**. Reproduced with permission [104]. Copyright 2012 Wiley-VCH Verlag GmbH & Co. KGaA, Weinheim

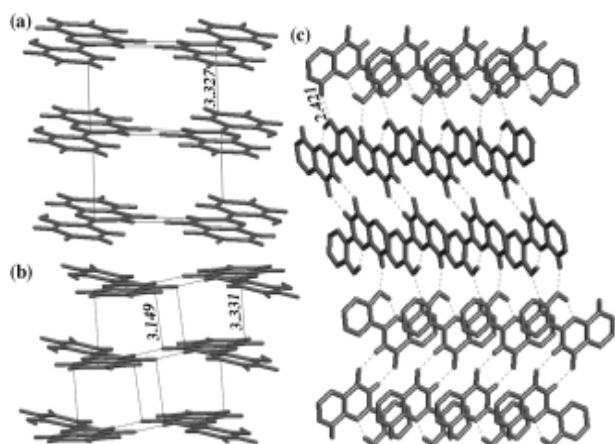
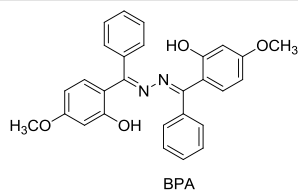


Figure 23 a) $\pi\cdots\pi$ interactions in **HPQ-B**, (b, c) $\pi\cdots\pi$, $C=O\cdots C=O$ dipolar and $OH\cdots H=C$ interactions in **HPQ-BG** crystal lattices. In (c), only H atoms involved in H-bond interactions are shown. Weak interactions are given as broken lines. Reproduced with permission [104]. Copyright 2012 Wiley-VCH Verlag GmbH & Co. KGaA, Weinheim

Benzophenone azine (BPA) (**Scheme 25**) based polymorph dependent ESIPT chromophore exhibiting AIE was reported by Tong et al.⁹⁹. BPA showed switchable solid state fluorescence upon annealing / melting treatment with large Stokes shift and high fluorescence quantum efficiency. High fluorescence in the solid state was assigned to aggregation. This conclusion was supported by red shifted absorption spectra in the aggregated state which is characteristic of compounds showing AIE process.

BPA forms two polymorphs namely **BPA-1G** and **BPA-1YG** upon crystallization from ethyl acetate. **BPA-1G** emits in green ($\lambda_{em} = 540$ nm, $\Phi_{FL} = 17\%$, $\tau = 1.24$ ns) region and **BPA-1YG** emits in yellowish-green ($\lambda_{em} = 521$ nm, $\Phi_{FL} = 13\%$, $\tau = 1.15$ ns) region as shown in **Figure 24**. This polymorph-dependent fluorescence was explained by mode of molecular packing of **BPA-1** in polymorph. X-Ray crystal analysis of **BPA-1** showed (**Figure 25**) presence of intramolecular hydrogen bonding (**YG** and **G**) for ESIPT process. Two polymorphs were structurally identical, but they were asymmetric in crystalline form. The torsion angle between phenyl and its attached Schiff base ring part were different for two polymorphs. The torsion is more in polymorph **G** ($\theta = 89.3^\circ$ and 80.4°) in comparison to polymorph **YG** ($\theta = 87.5^\circ$ and 74.7°). The distance between two adjacent layers in polymorph **G** is higher than that in **YG**. The difference in molecular packing is a responsible factor for fluorescence change in two polymorphs. The fluorescence properties of **BPA** are switchable in polymorphs and powder form after heating or annealing for multiple cycles.

A short summary of solid-state ESIPT emitters (color tuning) based on polymorph packing; substituents effect and type of polymer matrices as dopant are summarized in **Table 7**.



Scheme 25: Structure of BPA

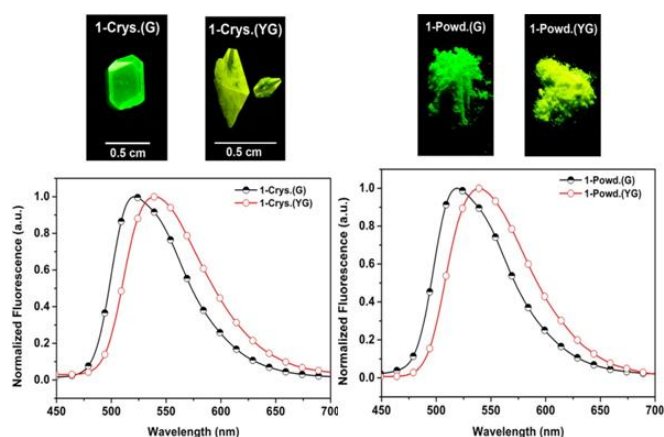


Figure 24 (Left) Polymorphic single crystals of **BPA-1 (G and YG)** under the illumination at 365 nm and their corresponding normalized fluorescence spectra, (Right) Solid powders of **BPA-1 (Powd-G)**, treated with THF; (**Powd-YG**), as prepared) illuminated at 365 nm and their corresponding normalized fluorescence spectra. Reproduced with permission [99]. Copyright 2013 American Chemical Society.

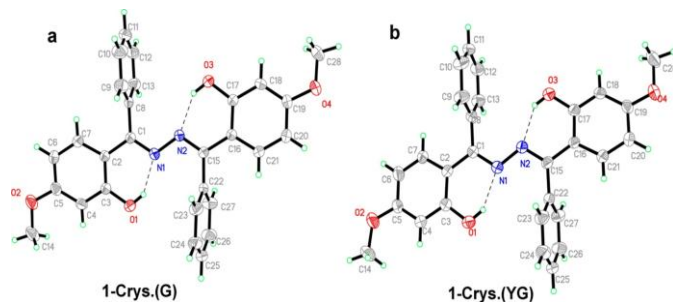


Figure 25 ORTEP drawing with 50% probability ellipsoids (295 K): (a) **BPA-1G**; (b) **BPA-1YG** Reproduced with permission [99]. Copyright 2013 American Chemical Society

7. Solid state ESIPT emitters through AIE / AIEE Mechanism

In 2001, first report describing enhancement of fluorescence emission in aggregated state was reported by Tang and coworkers¹³⁶. AIE chromophores are highly emissive in aggregated state and weakly or non-emissive in solution⁷⁰. In recent years, AIE or AIEE process has been utilized for generations of tunable solid state luminescent materials^{65,105,137}. In AIE process, molecules pack efficiently through $\pi\cdots\pi$ stack interaction, which blocks the non-radiative deactivation pathways through restriction of intramolecular rotation effect (RIR)⁷⁰. This helps in improving the luminescence properties in the aggregated state. It was reported that, *H*-aggregates causes fluorescence quenching^{3,138}, while *J*-aggregates of conjugated molecules enhances the luminescence properties (AIEE)⁹¹. AIE and AIEE responsive materials also exhibit multiple color emission due

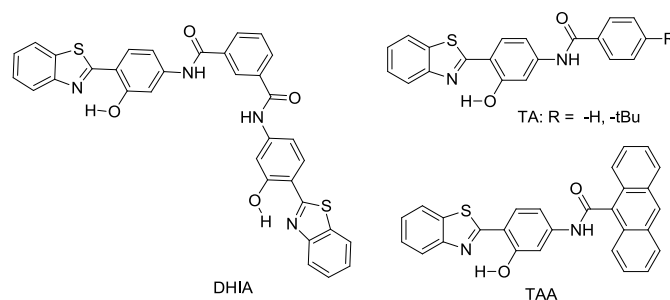
Review Article

Chem Soc Rev

to mode of packing or different conformation of molecules in the aggregated state. Since 2001 till date many research groups have reported the design, synthesis and mechanism of solid state chromophores by AIE/AIEE processes for optoelectronic devices⁷⁰. However, the AIE and AIEE processes for ESIPT chromophores are rare. The structures of ESIPT solid state chromophores with AIE mechanism reported till 2011^{91,96,139–145} have been summarized below **Table 8** and their photophysical properties have been summarized by Park et al.³. This section considers the subsequent report on solid state ESIPT fluorophores with AIE or AIEE properties.

AIE/AIEE characteristics of the reported chromophores are due to restriction of intramolecular rotation effect (RIR) through organic ion formation or hydrogen bond formation. Recently, AIE processes through restriction of charge transfer (RCT)¹⁴⁶ or restriction of twisted intramolecular charge transfer (RTICT)⁸⁵ and restriction of *cis-trans* isomerization have been reported⁸⁴. Huang and colleagues synthesized HBT based chromophores⁸⁴ *N*-(3-(benzo[*d*]thiazol-2-yl)-4-hydroxyphenyl)phenyl-carboxamide (**TA**) and *N*-(3-(benzo[*d*]thiazol-2-yl)-4-hydroxyphenyl)anthracene-9-carboxamide (**TAA**) (**Scheme 26**), which are analogues of **DHIA** have been reported by Yang and coworkers⁹¹.

TA and **TAA** showed very weak fluorescence in solvents of different polarities, but the fluorescence intensity were significantly enhanced upon aggregation as demonstrated in **Figure 26**. The absorption maxima for **TA** and **TAA** aggregates were red shifted compared to dilute solution (THF). This red shift can be assigned to rigid crystalline packing of molecules in aggregated state. It was reported that AIEE mechanism is more efficient in non-planar structures⁷⁰. In crystalline **TAA**, the dihedral angle between HBT and anthracene unit is 80.7° which prevents quenching by blocking face-to-face interaction in the aggregate state. In **TAA**, molecular packing is head-to-tail between two units which can be stabilized by N- π stacking between nitrogen atoms of two thiazole units **Figure 27**. The bathochromic shift in absorption indicates the formation of *J*-type aggregates which were supported by π - π interaction between two adjacent anthracene units and Ar-H...O=C- hydrogen bond between two adjacent **TAA**. Yang and coworkers also reported that AIEE for **DHIA** type of chromophores was due to *J*- or *H*-types aggregation which restricts the non-radiative TICT of the enol excited state. Similar process occurs in **TA** for AIEE processes. In HBT derivatives, *cis-trans* isomerization of the keto form can effectively deactivate the excited state which causes quenching of fluorescence emission in solution. In aggregate state, *cis-trans* isomerization is effectively blocked through tight molecular packing. This conformational change significantly suppresses the deactivation pathways and populates the radiative decay. The fluorescence lifetime of **TAA** in THF is less than 100ps, indicating significant nonradiative decay. In the aggregate state, the fluorescence lifetime is significantly enhanced to 2.55 ns. Based on these results Huang et al. concluded that, AIEE mechanism for **TAA** chromophore is not only because of restricted TICT, but also from effective restriction of *cis-trans* isomerization in the keto excited state. **TAA** showed bright fluorescence in solid state ($\Phi_{FL} = 78.1\%$, $\tau = 2.55$ ns) which was 27 fold higher than **DHIA**.



Scheme 26: Structure of **TAA** and **DHIA**

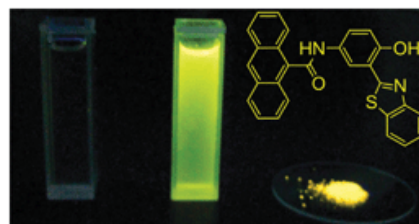


Figure 26 Photographs of **TAA** under UV illumination at 365 nm in THF, water and powder state from left to right, respectively. Reproduced with permission [84]. Copyright 2012 PCCP Owner Societies.

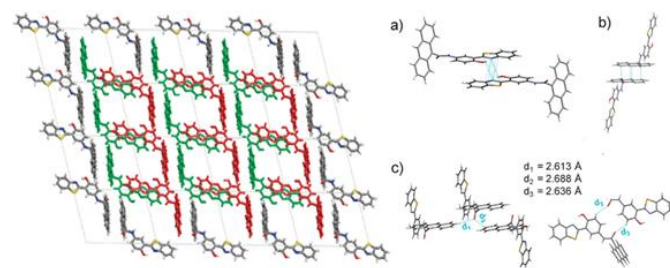
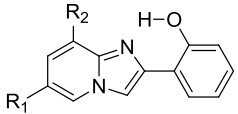
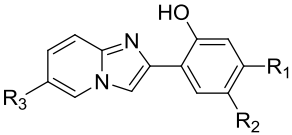
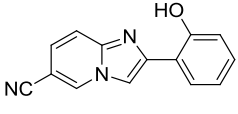
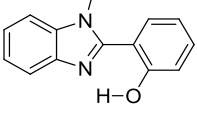
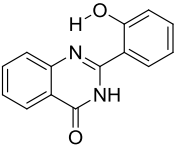
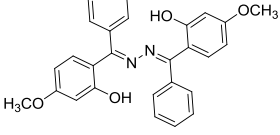


Figure 27 (Left) Molecular packing of **TAA** in single crystals viewed along the *b*-*c* plane (**Right**) (a) *N*... π interaction of HBT subunits. (b) π - π interaction of anthracene subunits. (c) Multiple aromatic Ar-H...O=C hydrogen bonds. Reproduced with permission [84]. Copyright 2012 PCCP Owner Societies

The OLED device was fabricated using **TAA** as the emissive layer, with a device configuration [ITO / NPB (60 nm) / **TAA** (10 nm) / TPBI (50 nm) / LiF (1 nm) / Al (80 nm)]. NPB and TPBI were used as hole and electron transport layers. The device showed maximum luminescence of 5616 cd m⁻² at 11.85 V. Device offers an external quantum efficiency of 0.46 % with a current density of 0.50 mA cm⁻², equivalent to current efficiency of 1.18 cd A⁻¹. The red shifted electroluminescence ($\lambda_{el} = 560$ nm) peak was observed in comparison to fluorescence emission ($\lambda_{em} = 552$ nm). This red shift may caused by a more ordered molecular arrangement¹⁴⁷.

Table 7 Solid state ESIPT chromophores: color tuning based on polymorphs packing

ESIPTs Structure	Spectral and Photophysical data	Ref
 <p>$R_1, R_2 = H, C_6H_5, CN$</p>	White luminescence; $\Phi_{FLS} = 31 - 37\%$; $\lambda_{em} = 529 - 536$ nm; CIE (0.36–0.41, 0.50–0.55); combination of ESIPT and non-ESIPT generates white light; White luminescence is a summation of luminescence of ESIPT and Non-ESIPT.	19
	Dual emission; $\Phi_{FLpm} = 10 - 60\%$, $\tau = 2.1-4.9$ ns; $\lambda_{em} = 378 - 571$ nm, Singlet emission from zwitterionic ESIPT species; single as well as dual emission in PMMA; Fl. depends on nature and position of substitution; Electron donor and acceptor groups on hydroxy phenyl ring causes blue and red shift respectively.	54
	Three solid-state luminescence colors; yellow–orange–red; $\Phi_{FLp} = 10 - 49\%$; $\lambda_{em} = 548 - 585$ nm; $\tau = 2.26 - 5.48$ ns; slip and $\pi-\pi$ stacking; polymorph dependent ESIPT emission; different molecular packing for three polymorph.	55 57
	Polymorph dependence emission; $\Phi_{FLS} = 74\%$; $\lambda_{em} = 458$ nm; $\tau = 4.4$ ns; coplanar conformation; Fl. depends on H–bonding, planarity and molecular packing; two polymorphs, Luminescent and non-luminescent; ON–OFF type of luminescent ESIPT; Fl. mechanically tuneable.	102
	Polymorph dependence emission; $\lambda_{em} = 497 - 511$ nm; amide–amide interaction; unusual interactions (C=O...C=O dipolar and OH...H=C–); two polymorphs (blue and blue-green).	104
	Polymorph dependence emission; $\Phi_{FLag} = 13-17\%$; $\lambda_{em} = 521 - 540$ nm; $\tau = 1.15 - 1.24$ ns; non-planar conformation; thermochromism; two polymorph (green and yellow-green); polymorph dependence ESIPT; reversible Fl. tuning by heating/annealing; thermally stable ~ 236 °C.	99

Φ_{FLS} : Fluorescence quantum efficiency in solid state, Φ_{FLpm} : Fluorescence quantum efficiency in polymorph, Φ_{FLp} : Fluorescence quantum efficiency in polymer matrices, Fl : Fluorescence, τ : Fluorescence lifetime, CIE: CIE 1931 chromaticity diagram.

Table 8 Solid state ESIPT chromophores with AIE/AIEE processes reported before 2011

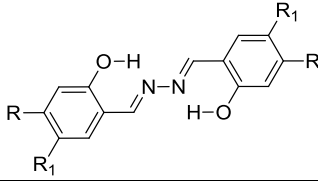
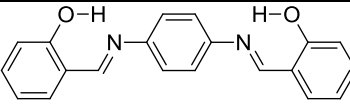
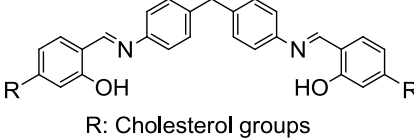
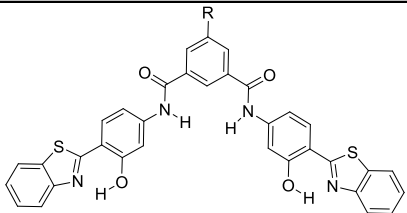
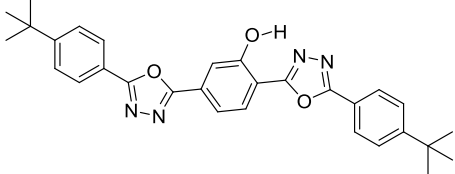
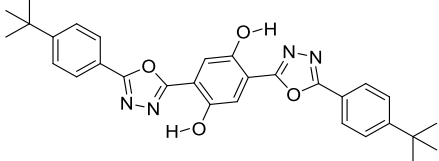
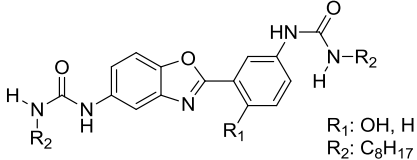
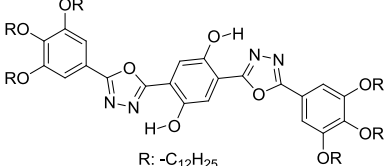
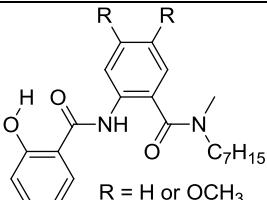
ESIPTs Structure	Spectral and Photophysical data	Ref
	AIEE; $\Phi_{FL} = \sim 13\%$; $\lambda_{em} = \sim 513-570$ nm; $\tau = 2.32-3.09$ ns; green to red emission depending on nature of substituents; <i>J</i> - & <i>H</i> -aggregation; intramolecular rotation allowed only for N–N bond; AIEE pH dependent.	145
	AIE; $\Phi_{FL} = \sim 6\%$; $\lambda_{em} = \sim 546$ nm; $\tau = 2.1$ ns; 60 fold enhancement of quantum efficiency in aggregate state; <i>J</i> -aggregates; orange crystal in aggregate state.	140
 <p>R: Cholesterol groups</p>	Gelation –induced enhanced emission; $\Phi_{FL} = \sim 3\%$; $\lambda_{em} = 520$ nm; helical <i>J</i> -type packing; cholesterol groups as a gelator moieties; photochromism; photoinduced isomerization.	141 142

Table 8 (continue) Solid state ESIPT chromophores with AIE/AIEE processes reported before 2011

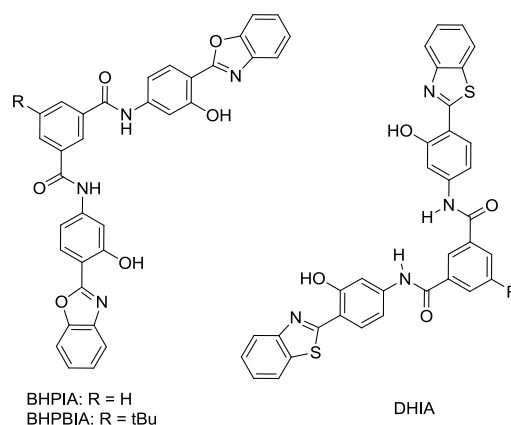
ESIPTs Structure	Spectral and Photophysical data	Ref
	<p>AIEE; $\Phi_{FL} = \sim 29\%$; $\lambda_{em} = \sim 510$ nm; <i>J</i>- & <i>H</i>-aggregation; restricted intramolecular/intermolecular motion in aggregated state; 21 fold enhancement of quantum efficiency in aggregated state; red shifted emission in aggregate state; <i>J</i>-aggregates causes enhanced emission; <i>H</i>-aggregates would induce a decreased emission; molecular packing depended on nature of alkyl group.</p>	91
	<p>Blue – green K* emission; $\Phi_{FL} = \sim 47\%$; $\lambda_{em} = \sim 486$ nm; $\tau = 3900$ ps; slip-stacking; planar; intramolecular H–interaction; dual emission in solvents.</p>	139
	<p>Orange K* emission; $\Phi_{FL} = \sim 13\%$; $\lambda_{em} = \sim 573$ nm; $\tau = 650$ ps; slip-stacking; dual emission in solvents.</p>	139
 <p>R₁: OH, H R₂: C₈H₁₇</p>	<p>Gelation-induced enhanced emission; $\Phi_{FL} = \sim 35\%$; $\lambda_{em} = \sim 402$ and 519 nm; $\tau = 0.5$–7.2ns; π–π stacking; planar conformation; H–bonding interaction; abnormal AIE; AIE causes blue shifted emission.</p>	143
 <p>R: -C₁₂H₂₅</p>	<p>Liquid crystals; $\Phi_{FL} = \sim 34\%$; $\lambda_{em} = \sim 422$ and 576 nm; <i>J</i>-stacking; two mesophases (columnar hexagonal and rectangular); temperature dependent emission.</p>	144
 <p>R = H or OCH₃</p>	<p>Gelation-induced enhanced emission; $\Phi_{FL} = \sim 13\%$; $\lambda_{em} = \sim 470$ nm; rigidochromism; π–stacking/columnar hexagonal packing; 10-50 folds fluorescence enhancement in gel state; gelation due to intramolecular H–interaction; restriction of TICT.</p>	96

Φ_{FLs} : Fluorescence quantum efficiency in solid state, FL : Fluorescence, τ : Fluorescence lifetime.

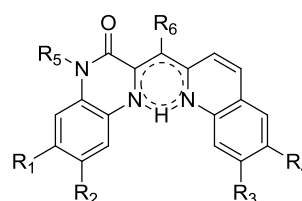
Gelators functionalized by ESIPT unit are known for solid state emission for use in photoelectrical and nano-electrical devices. Few reports based on ESIPT organogelators (**Table 8**) which contain long alkyl chain or dendrimeric units have been reported in the past^{96,142,143}. Recently, Yang and coworkers¹⁴⁸ synthesized highly emissive ESIPT organogelators based on 2-hydroxybenzoxazole (HBO). *N,N*-Bis(4-benzo[*d*]oxazol-2-yl)-3-hydroxyphenyl)isophthalamide (**BHPIA**) and *N,N*-bis(4-benzo[*d*]oxazol-2-yl)-3-hydroxyphenyl)-5-*tert*-butylisophthalamide (**BHPBIA**) contain small alkyl chain (**Scheme 27**). These gelators are structural analogues of **DHIA**, reported by same group⁹¹. The gelators **BHPIA** and **BHPBIA** are highly emissive in solid state with large Stokes shift of 137 nm. This characteristic was assigned to AIEE due to *J*-aggregation and ESIPT process. Hydrogen and *tert*-butyl groups at the central ring were incorporated purposefully to study the effect of slip-stacking on the ESIPT process as well as to study the substituent effect for organogel formation. **BHPBIA** forms organogel effectively in comparison to **BHPIA** because of *tert*-butyl group reducing tight molecular stacking and intermolecular interaction. Optical properties, molecular stacking, and FT-IR studies indicate that four types of interactions (N- π , O- π stacking of the oxazole rings, π - π stacking of phenol rings and consecutive H-bonding) interplayed in **BHPBIA**. These interactions help in formation of long-range-1-D nanostructures.

Xia et al. synthesized novel class of ESIPT fluorophores based on quinoxaline core which showed aggregation induced emission¹⁰⁰. Various substituted (*Z*)-3-quinolin-2-ylmethylene)-3,4-dihydroquinoxaline-2(1*H*)-one (**Q1-Q5**) derivatives (**Scheme 28**) were synthesized and their photophysical properties studied in solid state and in solution. Compounds showed intense orange-red fluorescence in solid state with large Stokes shift similar to emission spectra in THF. In aggregated state, compounds showed ~ 50 fold enhancement of fluorescence quantum efficiencies in comparison to that in solution. In both solid state and solution, the compounds had been predicted to take planar geometry from DFT computations. Although bathochromic shift in absorption or appearances of new band in red region with respect to original bands are well known characteristics of *J*-aggregated chromophores. These observations were not seen at various THF-water ratios. As a consequence, Xia et al. concluded that AIE for **Q1-Q5** was not due to planarity or RIR effect in the solid state. However AIE is due to restraint TICT process in the aggregated molecules in the excited state which was predicated by theoretical calculations.

Subsequently, Xia group reported combined RTICT and RIR processes for AIE in ESIPT system⁹² (**Scheme 29**). They synthesized two chromophores containing ESIPT unit. Tetraphenylethene (TPE) group was introduced on N atom (**Q6**) of dihydroquinoxaline one and on phenyl ring of quinoline core (**Q7**). The AIE process due to RIR and RTICT units or RIR and multiple RTICT units have been reported in past for π -conjugated chromophores¹⁴⁹⁻¹⁵². However, the AIE mechanism for ESIPT **Q6** and **Q7** were different in comparison to reported AIE systems. The absorption and emission properties of **Q** ($\lambda_{\text{abs}} = 430, 452 \text{ nm}$, $\lambda_{\text{em}} = 486, 544, 583 \text{ nm}$), **Q6** ($\lambda_{\text{abs}} = 432, 455 \text{ nm}$, $\lambda_{\text{em}} = 543, 585 \text{ nm}$), and **Q7** ($\lambda_{\text{abs}} = 444, 460 \text{ nm}$, $\lambda_{\text{em}} = 555, 595 \text{ nm}$) suggest that introduction of TPE unit on parent core will not change the ESIPT characteristics. However it affects AIE mechanism.



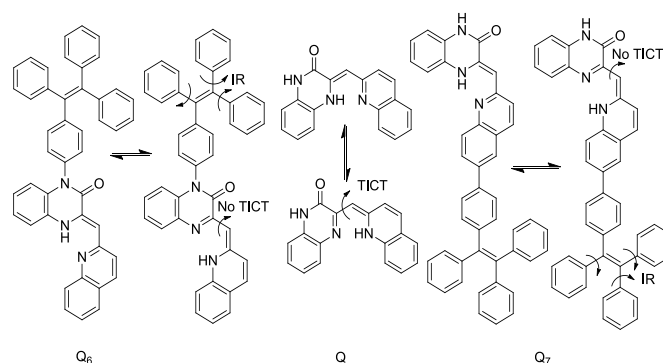
Scheme 27 ESIPT organogelators based on hydroxy benzimidazoles (**BHPIA** and **BHPBIA**), and their analogue **DHIA**.



- Q1: R₁=OCH₃, R₂=OCH₃, R₃=H, R₄=H, R₅=H, R₆=H
 Q2: R₁=H, R₂=H, R₃=OH, R₄=OH, R₅=H, R₆=H
 Q3: R₁=H, R₂=H, R₃=H, R₄=H, R₅=H, R₆=H
 Q4: R₁=H, R₂=H, R₃=H, R₄=H, R₅=3,4-(CH₃O)₂C₆H₃, R₆=H
 Q5: R₁=H, R₂=H, R₃=H, R₄=H, R₅=H, R₆=CH₃

Scheme 28 Substituted (*Z*)-3-quinolin-2-ylmethylene)-3,4-dihydroquinoxaline-2(1*H*)-one derivatives

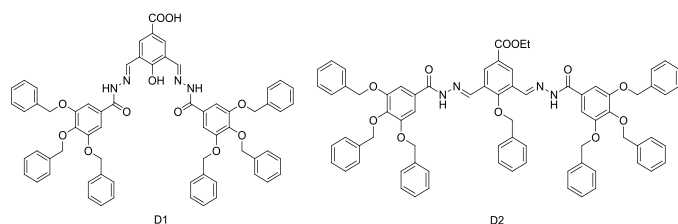
In aggregate state, fluorescence intensity increases significantly with red shifted emission and enhancement of 2.7 and 11.5-fold emission intensity in **Q6** and **Q7** respectively due to introduction of TPE unit. The higher emission intensity for **Q7** was assigned to crystallization induced emission enhancement (CIEE) which was supported by molecular morphology. Based on theoretical calculation, Xia et al. concluded that AIE mechanism in parent **Q** was due to RTICT around exocyclic bond, while AIE in **Q6** and **Q7** was due to RIR of TPE phenyl rings (**Scheme 29**). Authors also claimed that this is the first report for such type of AIE.



Scheme 29 TICT and IR mechanism of **Q**, **Q6** and **Q7**

Recently, tunable luminescence and white-light emission from single gelator molecule through ESIPT coupled AIEE process was reported by Das et al.¹⁰⁵. In this article, authors claim that this is the first report describing ESIPT coupled AIEE process for single molecule in generation of tunable luminescence. Two poly(aryl ether) dendron based gelators **D1** and **D2** were synthesized (Scheme 30) by Das group.

Compound **D1** contains basic flexible imine group and acidic phenolic hydrogen suitable for ESIPT. To understand the role of ESIPT process in the luminescence enhancement, dendron **D2** was synthesized for comparison study. The absorption and fluorescence properties of **D1** were studied in pure THF as well as in various ratio of THF/water mixture. In pure THF, **D1** showed two absorption bands ($\lambda_{\text{abs}} = 306$ and 355 nm), however, the intensity of absorption bands decreases upon addition of water due to formation of aggregates. Dendron **D1** (–OH group) has one hydroxyl group which can undergo ESIPT and showed dual emission in THF ($\lambda_{\text{ex}} = 365$ nm; $\lambda_{\text{em}} = 454$ and 487 nm). In THF–water mixture (1:1) along with dual emission, new emission band ($\lambda_{\text{em}} = 551$ nm) was observed for **D1**. In higher percentage of water, the emission band at 487 nm was shifted to blue region. This emission band ($\lambda_{\text{em}} = 551$ nm) with a large Stokes shift of 186 nm was assigned to AIEE band. After various combinations of water/THF, both ESIPT and AIEE processes were concluded to be operational at 1:1 water/THF ratio with dual emission ($\lambda_{\text{em}} = 468$ and 551 nm). At higher concentration of water the intensity of 551 nm band increases, which indicates that AIEE process dominates over ESIPT process. The simultaneous ESIPT and AIEE processes in **D1** are due to lock conformer Figure 28.



Scheme 30: Poly(arylether) dendron based gelators **D1** and **D2**

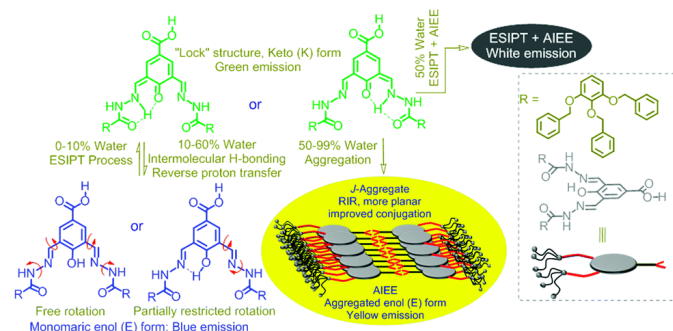


Figure 28 Changes in the configuration of **D1** from the twisted ground state to a more planar excited state, and finally J-aggregated rigid structure through ESIPT coupled AIEE processes with the variation of the water fraction to its THF solution. Reproduced with permission [105]. Copyright 2015 The Royal Society of Chemistry

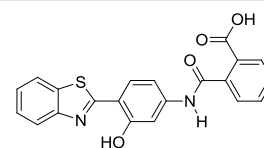
In case of **D2** single broad emission band ($\lambda_{\text{em}} = 481$ nm) was observed under similar conditions, this was assigned to AIE process. This clearly indicates that **D1** undergoes ESIPT as well as AIEE processes, while **D2** is only susceptible to AIE. The fluorescence properties of the **D1** depend on the ratio of THF/water, at 1:1 ratio **D1** covered the entire visible spectrum (400 – 700 nm) resulting in white-light emission with CIE coordinates (x, y) = ($0.31, 0.37$). Field emission scanning electron microscopy (FESEM) study results clearly indicate that conformational changes occur after varying the amount of water. The aggregation was J-type one confirmed by electronic properties and X-ray powder diffraction (XPRD). Fourier transform infrared spectroscopy (FT-IR) study also supported the observation of locked structure of **D1** over **D2**. The compound **D1** is highly emissive in powder form and on thin film, while **D2** is unable to form gel under similar condition.

Recently, AIE phenomenon has been demonstrated to be efficient tool for monitoring activities of various biomolecules. Huang et al. prepared small ESIPT molecule 2-((4-(benzo[d]thiazol-2-yl)-3-hydroxyphenyl)carbonyl)benzoic acid (**TIA**) (Scheme 31) exhibiting AIE for fast and photostable turn-on bioimaging⁹⁸. **TIA** is an analogue of **TA**, **TAA** and **DHIA** and is soluble in organic solvents like THF, DMF and DMSO and also poorly soluble in water. **TIA** showed weak dual emission in THF. However it is strongly emissive in aggregate form and in solid state. 52 fold enhancement of fluorescence quantum efficiency ($\Phi_{\text{FL}} = 4\%$) was observed in solid state in comparison to dilute solution. The emission bands between 320 – 420 nm and 470 – 600 nm were assigned to enol and keto emission respectively. This chromophore was used for sensing of HeLa cells and it was concluded that **TIA** is very sensitive to HeLa cells.

Short summary of solid state ESIPT emitters based on AIE–AIEE is summarized in Table 9.

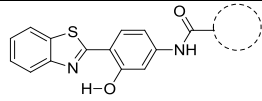
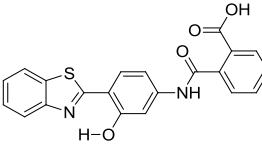
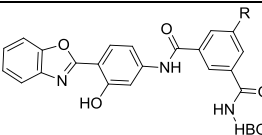
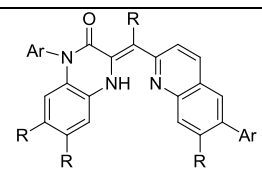
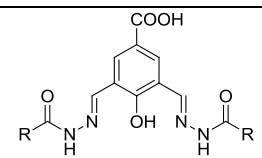
In addition to above solid-state ESIPT emitters caused by AIE/AIEE process, ESIPT chromophores exhibiting AIE/AIEE mechanism in aqueous/solution were also reported in last few years^{52,153–157}. These types of chromophores were used for biosensing applications, but solid-state properties of these fluorophores were not explored in detail by respective groups. Different types of ESIPT chromophores^{52,153–157} enhancing the fluorescence by AIE or AIEE mechanisms are summarized in Table 10

Chromophores containing ESIPT unit with enhancement of fluorescence properties in solid state or aggregated state through AIE/AIEE have also been reported in recent years^{158–160}. The solid state properties of these chromophores were also studied for different applications. However, the role of ESIPT unit in enhancement of fluorescence efficiency was not considered for these fluorophores. The reported representative examples^{158–160} are summarized in Table 11.



Scheme 31 Structure of **TIA**

Table 9 Solid state ESIPT emitters based on AIE/AIEE mechanism

ESIPT Chromophore Structure	Spectral and Photophysical data	Ref
	AIEE; $\Phi_{\text{FLag}} = \sim 78.1\%$; $\tau = 2.55$ ns; <i>J</i> -type aggregation; N- π stacking; AIEE due to RTICT and restriction of <i>cis-trans</i> isomerization; non-planer conformation.	84 91
	AIE; $\Phi_{\text{FLs}} = 4\%$; $\lambda_{\text{em}} = 470 - 600$ nm; 52 Fold enhancement FI. intensity after aggregation.	98
	AIEE; $\lambda_{\text{em}} = \sim 360 - 420$ and ~ 477 nm; $\Delta\lambda = \sim 137$ nm; slip-stacking; <i>J</i> -aggregation; RIR; thermo-reversible gel; alkyl group prohibits tight molecular packing and intermolecular interaction. low-molecular-weight-mass organogelators with AIEE and ESIPT properties.	148
	AIE; AIEE; $\lambda_{\text{em}} = \sim 500$ and ~ 600 nm; Many fold (~ 36) enhancement of FI. intensity upon aggregation; <i>J</i> -aggregation; AIE/AIEE due to RIR, RTICT and CIEE effects; morphology dependent emission; first report for solid state emission due to RIR and CIEE in one molecule.	92 100
	AIEE; blue-green-white-yellow emission; $\lambda_{\text{em}} = \sim 487$ and ~ 551 nm; <i>J</i> -aggregation; RIR; intramolecular H-interaction; AIEE coupled with ESIPT; first report for AIEE-ESIPT for single molecule for tuneable color.	105

Φ_{FLag} : Quantum efficiencies in aggregated state, τ : Fluorescence lifetime, Φ_{FLs} : Quantum efficiencies in solid state, B: Maximum brightness, η_{ext} : Maximum external quantum efficiency, η_{c} : Maximum current efficiency, CIE: CIE 1931 chromaticity diagram.

Table 10 ESIPT chromophores with AIE/AIEE properties in solution

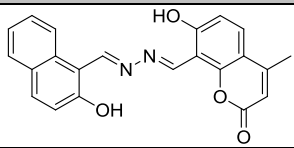
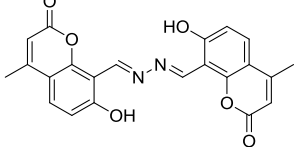
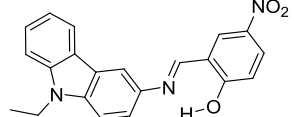
ESIPT Chromophore Structure	Spectral and Photophysical data	Ref
	AIE; $\Phi_{\text{FLag}} = 54\%$; $\lambda_{\text{em}} = \sim 531$ nm; <i>J</i> -aggregation; reddish-orange emission; AIE due to RIR; fluorescence enhancement is due to aggregation induced planarization and <i>J</i> -aggregate formation; thermally stable ~ 300 °C.	52
	AIE; $\Phi_{\text{FLag}} = 82\%$; $\lambda_{\text{em}} = \sim 570$ nm; <i>J</i> -aggregation; yellow emission; AIE due to RIR; thermally stable ~ 300 °C.	52
	AIEE; $\Phi_{\text{FLag}} = 45\%$; $\lambda_{\text{emag}} = 441$ nm; <i>J</i> -aggregation.	153

Table 10 (continue) ESIPT chromophores with AIE/AIEE properties in solution

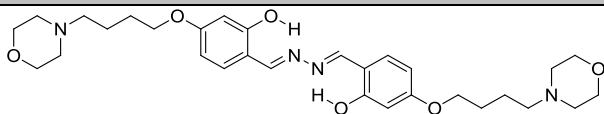
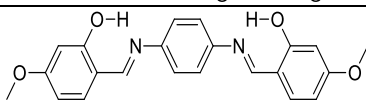
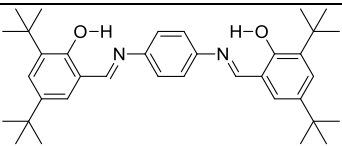
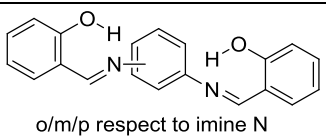
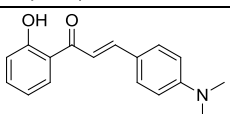
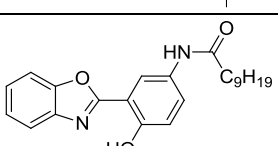
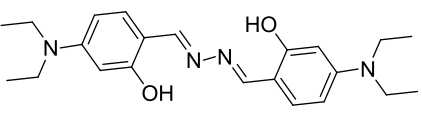
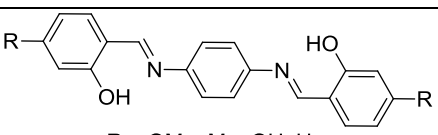
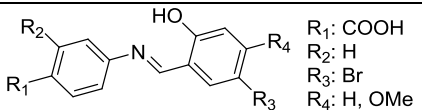
ESIPT Chromophore Structure	Spectral and Photophysical data	Ref
	AIE; $\lambda_{em_{ag}} = 532$ nm; planar, rigid, intramolecular <i>H</i> -bonding; 14 fold enhancement of emission in aggregated state.	154
	AIE; $\Phi_{FLag} = 10\%$; $\lambda_{em_{ag}} = 517$ nm, <i>H</i> -aggregation; two-photon absorption.	155
	AIE; $\Phi_{FLag} = 6\%$; $\lambda_{em_{ag}} = 575$ nm, <i>J</i> -aggregation; two-photon absorption.	155
 o/m/p respect to imine N	AIE; $\Phi_{FLag} = \sim 26\%$; $\lambda_{em_{ag}} = \sim 547$ nm, <i>J</i> - or <i>H</i> -aggregation; co-planar.	155
	AIE; $\Phi_{FL} = 18\%$; $\lambda_{em} = 640$ nm; 60 fold enhancement of fluorescence intensity in aggregate state; absence of π - π stacking.	156
	AIEE; $\lambda_{em} = 500$ nm.	157

Table 11. Chromophores having ESIPT unit with solid state emission

ESIPT Chromophore Structure	Spectral and Photophysical data	Ref
	Donor-acceptor chromophore; $\Phi_{FL} = 8 - 30\%$; $\lambda_{em} = 529-553$ nm; π - π interaction; planar conformation; intramolecular <i>H</i> - interaction; piezo/thermo responsive emission.	158
 R = OMe, Me, OH, H	AIE; $\Phi_{FL} = 9 - 33\%$; $\lambda_{em} = 503 - 543$ nm; morphology controlled emission; tuneable three color emission (green, yellow, orange); thermally stable ~ 319 °C.	159
 R ₁ : COOH R ₂ : H R ₃ : Br R ₄ : H, OMe	AIEE; $\Phi_{FL} = 0.6 - 14\%$; $\lambda_{em} = 512 - 552$ nm; AIEE due to restriction of intramolecular rotation of C-N bond; thermochromism.	160

9. Summary and Outlooks

This article summarizes the progress towards the development of solid state ESIPT emitters mainly focusing on photophysical properties in the solid state. The summarized solid state ESIPT fluorophores are derivatives of carbazole, benzothiazole, imidazole, indanone, phenanthroimidazoles, benzofuranbenzoxazoles, julidine, bis-benzothiazole, imidazopyridine, indolizines, quinazolinone, polyimide, benzophenoneazines, quinoxalines and azine having red/white-light emission. As summarized, ESIPT fluorophores are emissive (i) in polymorphic forms (ii) in gel (iii) in polymer matrices (v) in KBr matrix (vi) in aggregated state and (vii) in solution.

Most of them are white-light emitters in solid state and in solution. A short summary of various approaches for generation of white-light emission from ESIPT chromophores are listed below.

- White-light-emission through single molecule dyad.
- Single ESIPT system by fine-tuning the energetics in the excited state.
- Based on solvatochromism properties.
- Mixture of proton-transfer and nonproton-transfer fluorophores.
- Mixture of two ESIPT luminophores having different Stokes shift.
- Mixture of two complementary, blue- and orange- emitting chromophores exhibiting ESIPT process.
- Panchromatic emission via modulating substitution pattern of ESIPT chromophores.
- Tuning of acidic and basic centers of ESIPT chromophores.
- Altering the surrounding medium (e.g. polymer matrices or rigid media) of ESIPT chromophores.
- Controlling molecular packing of ESIPT chromophores (e.g. polymorphs dependence emission).
- AIE and AIEE processes generate white light emission of ESIPT chromophores.
- Based on halochromism property of ESIPT chromophores.

In reported ESIPT systems, the fluorescence properties are superior (high fluorescence quantum efficiencies, red emission etc.) in solid/ rigid media in comparison to solution. Enhancement of fluorescence quantum efficiencies in solid state has been realized by many approaches such as restricted intramolecular rotation (RIR), hydrogen bonding, restriction of twisted intramolecular charge transfer (RTICT), flipping of flexible alicyclic components, J-aggregations, cross packing, and dimer/excimer stacking.

Based on different design strategies and photophysical data of the summarized ESIPT fluorophores in solid state/ polymer matrices/ rigid media/ in solution, here we have summarized few points which suppress the other deactivation pathways occurring in the excited state resulting in the enhancement of fluorescence quantum yields and red shifted emission.

- Planar geometry in the excited state helps to enhance the fluorescence properties over non-planar geometry.
- Strong intra-molecular hydrogen bonding favors ESIPT process over weak H-bonding.
- RIR, RTICT and RCT enhance the fluorescence properties.
- J-aggregation with a head-to-tail arrangement greatly blocks the nonradiative pathways and effectively suppresses

the self quenching which helps in enhancement of fluorescence properties over H-type of aggregation (face-to-face arrangement).

- Intramolecular stacking interaction in a crystal (face-to-face intermolecular interaction between π -conjugated chromophores) quenches the fluorescence except in few cases causing fluorescence enhancement via restricted intramolecular rotation (RIR) effect.
- Introduction of steric groups on the ESIPT chromophores could improve the fluorescence properties by limiting the non-radiative pathways via vibronic and rotational relaxation.
- Two molecular freely rotatable joints in solution (free state) can be locked in aggregate state by the formation of strong intramolecular H-bond with basic atom (locked state i.e. RIR effect) which causes enhancement of quantum efficiency.
- In polar/ protic solvents generally quenching of keto emission is caused because of intermolecular hydrogen bonding between solvents and acidic hydrogen instead of intramolecular hydrogen bonding.
- pH of medium determines the red/ blue shift of ESIPT chromophores (generally basic media-red shift and acidic media-blue shift).
- Restricted cis-trans isomerization of the excited keto form causes enhancement of fluorescence quantum efficiencies by suppressing deactivation pathway (Restricted cis-trans isomerization is more effective in rigid media).
- π - π Interplanar distance between two units determines the fluorescence behavior of ESIPT chromophores.
- Dendrimer units on ESIPT core help to enhance fluorescence quantum efficiencies via inhibition of fluorescence quenching due to intermolecular interaction (Bulky dendrimeric units enhance the fluorescence quantum efficiencies by suppressing isomerization process).
- Twisted intramolecular charge transfer (TICT) pathway in the excited state keto form quenches the fluorescence. 5-Membered (generally) ring ESIPT fluorophores exhibit higher fluorescence quantum efficiencies than 6-membered ESIPT fluorophores (planar conformation is more stable in 5-membered ring ESIPT molecules)
- Fluorescence quantum efficiencies depend on nature and position of substituted groups.
- Tuning/ enhancement of fluorescence depend on extension of conjugation, nature of heterocyclic rings, nature of electron donor/acceptor groups and supported matrices.
- In polymer matrices, the polarity of the surrounding matrix controls the fluorescence emission as well as fluorescence quantum efficiencies.
- Mode of molecular packing helps to tune the color of ESIPT chromophores (ESIPT chromophores give varying emissions in different polymorphic forms).
- AIE and AIEE processes enhance the quantum efficiencies of the ESIPT fluorophores in solid state (generally).
- In imidazopyridine, extensions of π -conjugation cause red shift in emission but lowering in the fluorescence quantum efficiencies.
- Energy-level mismatch between the LUMOs of the enol and keto tautomer is key factor for suppression of non-radiative pathways (large mismatch of their molecular orbital's energy levels) which cause fluorescence enhancement.

- Nodal plane model is a simple but informative tool for prediction of fluorescence properties of known fluorophores as well as in helping in designing fluorophores as per emission requirement.

The above mentioned strategies will guide in designing or tuning the properties of solid state ESIPT emitters.

The reported ESIPT inspired fluorescent materials were used for fabrication of organic light emitting diodes (OLEDs), field-effect transistors, white-light emitters for optoelectronic devices, metal sensing and bioimaging. Tremendous interdisciplinary research efforts over the last five years have made significant progress in the designing; synthesis and applications of ESIPT chromophores. We believe that the innovative design, efficient synthesis and improved fluorescence properties will be one of the prime challenges on the path of developing highly emissive solid state ESIPT chromophores. We hope this review will provide sufficient information to design new strategies for the development of ESIPT materials which will emit in red region with very high fluorescence quantum efficiencies.

10. Acknowledgment

The authors acknowledge KAKENHI and NEXT grants from the Ministry of Education, Culture, Sports, Science and Technology (MEXT) of Japan (No. 26102011, 26249145, and 26620104.). V. S. P. thanks Japan Society for the Promotion of Science (JSPS) for research fellowship (No. 2604063).

11. Abbreviations

ESIPT	Excited state intramolecular proton transfer
λ_{abs}	Absorption maxima wavelength
λ_{em}	Emission maxima wavelength
λ_{ex}	Excitation wavelength
Φ_{FL}	Fluorescence quantum efficiency
E^*	Enol emission
K^*	Keto emission (ESIPT emission)
τ	Fluorescence lifetime
$\Delta\lambda$	Stokes shift
EL	Electroluminescence
B	Maximum brightness
WLE	White light emission
EQE	External quantum efficiency
ACQ	Aggregation caused quenching
AIE	Aggregation induced emission
AIEE	Aggregation induced enhanced emission
RIR	Restricted intramolecular rotation
TICT	Twisted intramolecular charge transfer
RTICT	Restriction of twisted intramolecular charge transfer
IPT	Intramolecular proton transfer
ICT	Intramolecular charge transfer
RCT	Restriction of charge transfer
CIEE	Crystallization induced emission enhancement
OLED	Organic light emitting diodes
WOLEDs	White organic light emitting diodes
GFP	Green fluorescent protein
CIE	International Commission on Illumination
HBI	2-(2'-Hydroxyphenyl)benzimidazole
HBO	2-(2'-Hydroxyphenyl)benzoxazole

HBT	2-(2'-Hydroxyphenyl)benzothiazole
PIP	2-Phenylimidazo[1,2-a]pyridine
BTZ	2-(2'-Hydroxyphenyl)benzothiazole
TPBI	1,3,5-Tri(1-phenyl-1H-benzo[d]imidazol-2-yl)phenyl
NPD	4,4'-Bis[N-(1-naphthyl)-N-phenylamino]biphenyl
CPB	4,4'-N,N-Dicarbonyl-1,1-biphenyl
NPB	4,4'-Bis[N-(1-naphthyl)-N-phenylamino]biphenyl
TCTA	4,4',4''-Tri(N-carbazolyl)triphenylamine
CBP	4,4'-Bis-(9-carbazolyl) biphenyl
PMAA	Poly(methyl methacrylate)
PS	Polystyrene
PVAC	Poly(vinyl acetate)
PC	Poly(bisphenol A carbonate)
PVA	Poly(vinyl alcohol)
PEG	Poly(ethylene glycol)
PE-DOT	Poly(ethylene dioxythiophene)
PSS	Poly(styrene sulfonate)
HPhI	2-(1H-Phenanthro[9,10-d]imidazol-2-yl)phenol
HPPHI	2-(1-Phenyl-1H-phenanthro[9,10-d]imidazol-2-yl)phenol
TsPPhI	4-Methyl-N-(2-(1-phenyl-1H-phenanthro[9,10-d]imidazol-2-yl)phenyl)benzenesulfonamide
HBDI	(Z)-4-(4-Hydroxybenzylidene)-1,2-dimethyl-1H-imidazol-5(4H)-one (HBDI)
HBBO	2-2'-(Hydroxybenzofuran)benzoxazole
TA	N-(3-(Benzo[d]thiazol-2-yl)-4-hydroxyphenyl)phenyl-carboxamide
TAA	N-(3-(Benzo[d]thiazol-2-yl)-4-hydroxyphenyl)anthracene-9-carboxamide
TIA	2-((4-(Benzo[d]thiazol-2-yl)-3-hydroxyphenyl)carbamoyl)benzoic acid
2,4-DBTP	2,4-Dibenzothiazolylphenols
2,6-DBTP	2,6-Dibenzothiazolylphenols
MeBHI	2-(1-Methyl-1H-benzo[d]imidazol-2-yl)phenol
TBHI	2-(1-Tert.butyl-1H-benzo[d]imidazol-2-yl)phenol
HPQ	2-(2'-Hydroxyphenyl)-4-(3H)-quinazolinone
BPA	Benzophenone azine
BHPIA	N,N-Bis(4-benzo[d]oxazol-2-yl)-3-hydroxyphenylisophthalamide
BHPBIA	N,N-Bis(4-benzo[d]oxazol-2-yl)-3-hydroxyphenyl)-5-tert-butylisophthalamide
TPE	Tetraphenylethene
NHPI	1-(1,4,5-Triphenyl-1H-imidazo-2-yl)phenol
HPIC	2-(1-Phenyl-1H-phenanthro[9,10-d]imidazol-2-yl)phenol
HBPI	3-(1,4,5-Triphenyl-1H-imidazol-2-yl)-[1,1'-biphenyl]-4-ol
HBPIC	3-(1-Phenyl-1H-phenanthro[9,10-d]imidazol-2-yl)-[1,1'-biphenyl]-4-ol
HPO	2-(4,5-Diphenyloxazol-2-yl)phenol
HPNI	3-(1,4,5-Triphenyl-1H-imidazol-2-yl)naphthalene-2-ol
HPNIC	3-(1-Phenyl-1H-phenanthro[9,10-d]imidazol-2-yl)-naphthalene-2-ol
HPNO	3-(4,5-Diphenyloxazol-2-yl)naphthalene-2-ol
DFT	Density functional theory
TD-DFT	Time dependent density functional theory
HOMO	Highest occupied molecular orbital
LUMO	Lowest unoccupied molecular orbital
EOM-CCSD	Equation-of-motion coupled-cluster singles and doubles

ONIOM	Our own <i>N</i> -layered integrated molecular orbital and molecular mechanics
CASSCF	Complete active space multiconfiguration–SCF
MS–CASPT2	Multistate–CASPT2
FMO–TDDFT	Fragment molecular orbital–TDDFT
DMF	Dimethylformamide
KBr	Potassium bromide
THF	Tetrahydrofuran
DMSO	Dimethyl sulfoxide
DMF	Dimethylformamide
XPRD	X-ray powder diffraction
DSC	Differential scanning calorimetry
FESEM	Field emission scanning electron microscopy
FT–IR	Fourier transform infrared spectroscopy
UV	Ultraviolet

12. Notes and References

- J. Goodman and L. E. Brus, *J. Am. Chem. Soc.*, 1978, **100**, 7472–7474.
- J. Zhao, S. Ji, Y. Chen, H. Guo and P. Yang, *Phys. Chem. Chem. Phys.*, 2012, **14**, 8803–8817.
- J. E. Kwon and S. Y. Park, *Adv. Mater.*, 2011, **23**, 3615–3642.
- A. Weller, *Elektrochemie*, 1952, **56**, 662–668.
- L. G. Arnaut and S. J. Formosinho, *J. Photochem. Photobiol. A Chem.*, 1993, **75**, 1–20.
- P. F. Barbara and P. K. Walsh, *J. Phys. Chem.*, 1989, **93**, 29–34.
- A. Douhal, F. Lahmani and A. H. Zewail, *Chem. Phys.*, 1996, **207**, 477–498.
- C.-C. Hsieh, C.-M. Jiang and P.-T. Chou, *Acc. Chem. Res.*, 2010, **43**, 1364–1374.
- J. Wu, W. Liu, J. Ge, H. Zhang and P. Wang, *Chem. Soc. Rev.*, 2011, **40**, 3483–3495.
- A. P. Demchenko, K.-C. Tang and P.-T. Chou, *Chem. Soc. Rev.*, 2013, **42**, 1379–408.
- B. Dick and N. P. Ernsting, *J. Phys. Chem.*, 1987, **91**, 4261–4265.
- T. Iijima, A. Momotake, Y. Shinohara, T. Sato, Y. Nishimura and T. Arai, *J. Phys. Chem. A*, 2010, **5**, 1603–1609.
- J. Cheng, D. Liu, L. Bao, K. Xu, Y. Yang and K. Han, *Chem. - An Asian J.*, 2014, **9**, 3215–3220.
- G.-J. Zhao and K.-L. Han, *Acc. Chem. Res.*, 2012, **45**, 404–413.
- S. J. Formosinho and L. G. Arnaut, *J. Photochem. Photobiol. A Chem.*, 1993, **75**, 21–48.
- F. Laquai, Y.-S. Park, J.-J. Kim and T. Basché, *Macromol. Rapid Commun.*, 2009, **30**, 1203–1231.
- K.-Y. Chen, C.-C. Hsieh, Y.-M. Cheng, C.-H. Lai and P.-T. Chou, *Chem. Commun. (Camb.)*, 2006, **1**, 4395–4397.
- K.-C. Tang, M.-J. Chang, T.-Y. Lin, H.-A. Pan, T.-C. Fang, K.-Y. Chen, W.-Y. Hung, Y.-H. Hsu and P.-T. Chou, *J. Am. Chem. Soc.*, 2011, **133**, 17738–17745.
- H. Shono, T. Ohkawa, H. Tomoda, T. Mutai and K. Araki, *ACS Appl. Mater. Interfaces*, 2011, **3**, 654–657.
- J. Cheng, D. Liu, W. Li, L. Bao and K. Han, *J. Phys. Chem. C*, 2015, **119**, 4242–4251.
- K. Benelhadj, J. Massue, P. Retailleau, G. Ulrich and R. Ziessel, *Org. Lett.*, 2013, **15**, 2918–2921.
- K. Furukawa, N. Yamamoto, T. Nakabayashi, N. Ohta, K. Amimoto and H. Sekiya, *Chem. Phys. Lett.*, 2012, **539–540**, 45–49.
- H. Konoshima, S. Nagao, I. Kiyota, K. Amimoto, N. Yamamoto, M. Sekine, M. Nakata, K. Furukawa and H. Sekiya, *Phys. Chem. Chem. Phys.*, 2012, **14**, 16448–16457.
- V. S. Padalkar, P. Ramasami and N. Sekar, *J. Fluoresc.*, 2013, **23**, 839–851.
- S. Park, J. E. Kwon and S. Y. Park, *Phys. Chem. Chem. Phys.*, 2012, **14**, 8878–8884.
- S. Park, O.-H. Kwon, S. Kim, S. Park, M.-G. Choi, M. Cha, S. Y. Park and D.-J. Jang, *J. Am. Chem. Soc.*, 2005, **127**, 10070–10074.
- V. S. Padalkar, P. Ramasami and N. Sekar, *J. Lumin.*, 2014, **146**, 527–538.
- V. Padalkar, A. Tathe, V. Gupta, V. Patil, K. Phatangare and N. Sekar, *J. Fluoresc.*, 2012, **22**, 311–322.
- W. Chen, E. B. Twum, L. Li, B. D. Wright, P. L. Rinaldi and Y. Pang, *J. Org. Chem.*, 2012, **77**, 285–290.
- A. Ohshima, A. Momotake, R. Nagahata and T. Arai, *J. Phys. Chem. A*, 2005, **109**, 9731–9736.
- V. Padalkar, P. Ramasami and N. Sekar, *Procedia Comput. Sci.*, 2013, **18**, 797–805.
- V. S. Patil, V. S. Padalkar, A. B. Tathe and N. Sekar, *Dyes Pigments*, 2013, **98**, 507–657.
- D. Yao, S. Zhao, J. Guo, Z. Zhang, H. Zhang, Y. Liu and Y. Wang, *J. Mater. Chem.*, 2011, **21**, 3568–3570.
- J. Ma, J. Zhao, P. Yang, D. Huang, C. Zhang and Q. Li, *Chem. Commun.*, 2012, **48**, 9720–9722.
- F. S. Rodembusch, L. F. Campo, V. Stefani and A. Rigacci, *J. Mater. Chem.*, 2005, **15**, 1537–1541.
- P. Majumdar and J. Zhao, *J. Phys. Chem. B*, 2014, **119**, 2384–2394.
- V. S. Padalkar and N. Sekar, *J. Lumin.*, 2014, **155**, 58–64.
- P. Chou, Y. Chen, W. Yu, Y. Chou and C. Wei, 2001, **105**, 1731–1740.
- M. W. Chung, T. Y. Lin, C. C. Hsieh, K. C. Tang, H. Fu, P. T. Chou, S. H. Yang and Y. Chi, *J. Phys. Chem. A*, 2010, **114**, 7886–7891.
- M. T. Ignasiak, C. Houée-Levin, G. Kciuk, B. Marciniak and T. Pedzinski, *ChemPhysChem*, 2015, **16**, 628–633.
- P.-T. Chou and M. L. Martinez, *Radiat. Phys. Chem.*, 1993, **41**, 373–378.
- D. Ghosh, S. Batuta, S. Das, N. A. Begum and D. Mandal, *J. Phys. Chem. B*, 2015, **119**, 5650–5661.
- X. Jin, C. Liu, X. Wang, H. Huang, X. Zhang and H. Zhu, *Sensors Actuators B Chem.*, 2015, **216**, 141–149.
- S. Nagaoka, H. Endo and K. Ohara, *J. Phys. Chem. B*, 2015, **119**, 2225–2232.
- S. J. Schmidtke, D. F. Underwood and D. A. Blank, *J. Am. Chem. Soc.*, 2004, **126**, 8620–8621.
- M. J. Paterson, M. A. Robb, L. Blancafort and A. D. DeBellis, *J. Am. Chem. Soc.*, 2004, **126**, 2912–2922.
- C. T. Liao, Y. J. Wang, C. S. Huang, H. S. Sheu, G. H. Lee and C. K. Lai, *Tetrahedron*, 2007, **63**, 12437–12445.
- E. Hadjoudis and I. M. Mavridis, *Chem. Soc. Rev.*, 2004, **33**, 579–588.
- Y. Nakane, T. Takeda, N. Hoshino, K. Sakai and T. Akutagawa, *J. Phys. Chem. A*, 2015, **119**, 6223–6231.
- R. Das, G. Duportail, A. Ghose, L. Richert, A. Klymchenko, S. Chakraborty, S. Yesylevskyy and Y. Mely, *Phys. Chem. Chem. Phys.*, 2014, **16**, 776–84.
- S. Barman, S. K. Mukhopadhyay, M. Gangopadhyay, S. Biswas, S. Dey and N. D. P. Singh, *J. Mater. Chem. B*, 2015, **3**, 3490–3497.

- 52 H. Xiao, K. Chen, D. Cui, N. Jiang, G. Yin, J. Wang and R. Wang, *New J. Chem.*, 2014, **38**, 2386–2393.
- 53 L. Wilbraham, M. Savarese, N. Rega, C. Adamo, I. Cio, S. Chimiche, N. Federico, C. Universitario and M. S. Angelo, *J. Phys. Chem. B*, 2015, **119**, 2459–2466.
- 54 T. Mutai, H. Sawatani, T. Shida, H. Shono and K. Araki, *J. Org. Chem.*, 2013, **78**, 2482–2489.
- 55 T. Mutai, H. Shono, Y. Shigemitsu and K. Araki, *CrystEngComm*, 2014, **16**, 3890–3895.
- 56 T. Mutai, H. Tomoda, T. Ohkawa, Y. Yabe and K. Araki, *Angew. Chemie - Int. Ed.*, 2008, **47**, 9522–9524.
- 57 S. Furukawa, H. Shono, T. Mutai and K. Araki, *ACS Appl. Mater. Interface*, 2014, **6**, 16065–16070.
- 58 V. Bhalla, Roopa and M. Kumar, *Org. Lett.*, 2012, **14**, 2802–2805.
- 59 M. K. Bera, C. Chakraborty, P. K. Singh, C. Sahu, K. Sen, S. Maji, A. K. Das and S. Malik, *J. Mater. Chem. B*, 2014, **2**, 4733–4739.
- 60 L. Geng, X.-F. Yang, Y. Zhong, Z. Li and H. Li, *Dye. Pigment.*, 2015, **120**, 213–219.
- 61 H.-M. Lv, Y. Chen, J. Lei, C. Au and S.-F. Yin, *Anal. Methods*, 2015, **7**, 3883–3887.
- 62 M. L. Martinez, W. C. Cooper and P.-T. Chou, *Chem. Phys. Lett.*, 1992, **193**, 151–154.
- 63 D. Santa María, R. M. Claramunt, V. Bobosik, M. C. Torralba, M. R. Torres, I. Alkorta and J. Elguero, *Tetrahedron*, 2013, **69**, 3027–3038.
- 64 V. I. Tomin, A. P. Demchenko and P.-T. Chou, *J. Photochem. Photobiol. C Photochem. Rev.*, 2015, **22**, 1–18.
- 65 K. T. Kamtekar, A. P. Monkman and M. R. Bryce, *Adv. Mater.*, 2010, **22**, 572–582.
- 66 K. Sakai, T. Ishikawa and T. Akutagawa, *J. Mater. Chem. C*, 2013, **1**, 7866–7871.
- 67 I. D. W. Samuel and G. A. Turnbull, *Chem. Rev.*, 2007, **107**, 1272–1295.
- 68 H. Sasabe and J. Kido, *Chem. Mater.*, 2011, **23**, 621–630.
- 69 F. Liang, L. Wang, D. Ma, X. Jing and F. Wang, *Appl. Phys. Lett.*, 2002, **81**, 4–6.
- 70 Y. Hong, J. W. Y. Lam and B. Z. Tang, *Chem. Soc. Rev.*, 2011, **40**, 5361.
- 71 T. Mutai, and K. Araki, *Kokagaku*, 2009, **40** (3), 184–187.
- 72 V. S. Padalkar, S. B. Chemate, S. K. Lanke and N. Sekar, *J. Lumin.*, 2015, **168**, 114–123.
- 73 V. S. Patil, V. S. Padalkar, K. R. Phatangare, V. D. Gupta, P. G. Umape and N. Sekar, *J. Phys. Chem. A*, 2012, **116**, 536–545.
- 74 V. Patil, V. Padalkar and N. Sekar, *J. Lumin.*, 2015, **158**, 243–251.
- 75 K. R. Phatangare, V. D. Gupta, A. B. Tathe, V. S. Padalkar, V. S. Patil, P. Ramasami and N. Sekar, *Tetrahedron*, 2013, **69**, 1767–1777.
- 76 R. Rao M, C.-W. Liao, W.-L. Su and S.-S. Sun, *J. Mater. Chem. C*, 2013, **1**, 5491–5501.
- 77 Y. Liu, X. Tao, F. Wang, J. Shi, J. Sun, W. Yu, Y. Ren, D. Zou and M. Jiang, *J. Phys. Chem. C*, 2007, **111**, 6544–6549.
- 78 B. Li, J. Lan, D. Wu and J. You, *Angew. Chemie Int. Ed.*, 2015, doi.org/10.1002/anie.201507272.
- 79 T. Zhou, F. Li, Y. Fan, W. Song, X. Mu, H. Zhang and Y. Wang, *Chem. Commun. (Camb)*, 2009, **1**, 3199–3201.
- 80 A. Douvali, G. S. Papaefstathiou, M. P. Gullo, A. Barbieri, A. C. Tsipis, C. D. Malliakas, M. G. Kanatzidis, I. Papadas, G. S. Armatas, A. G. Hatzidimitriou, T. Lazarides and M. J. Manos, *Inorg. Chem.*, 2015, **54**, 5813–5826.
- 81 M. Kasha, *J. Chem. Soc. Faraday Trans 2*, 1986, **82**, 2379–2392.
- 82 S. Kim, J. Seo and S. Y. Park, *J. Photochem. Photobiol. A Chem.*, 2007, **191**, 19–24.
- 83 M. I. Knyazhansky, A. V. Metelista, A. J. Bushkov, S. M. Aldoshin, *J. Photochem. Photobiol. A: Chem.*, 1996, **97**, 121–126.
- 84 M. Cai, Z. Gao, X. Zhou, X. Wang, S. Chen, Y. Zhao, Y. Qian, N. Shi, B. Mi, L. Xie and W. Huang, *Phys. Chem. Chem. Phys.*, 2012, **14**, 5289–5296.
- 85 Y. Qian, M. M. Cai, L. H. Xie, G. Q. Yang, S. K. Wu and W. Huang, *ChemPhysChem*, 2011, **12**, 397–404.
- 86 S. H. Kim, S. Park, J. E. Kwon and S. Y. Park, *Adv. Funct. Mater.*, 2011, **21**, 644–651.
- 87 S. Park, E. K. Ji, H. K. Se, J. Seo, K. Chung, S. Y. Park, D. J. Jang, B. M. Medina, J. Gierschner and Y. P. Soo, *J. Am. Chem. Soc.*, 2009, **131**, 14043–14049.
- 88 C. C. Hsieh, P. T. Chou, C. W. Shih, W. T. Chuang, M. W. Chung, J. Lee and T. Joo, *J. Am. Chem. Soc.*, 2011, **133**, 2932–2943.
- 89 M. Ikegami and T. Arai, *J. Chem. Soc. Perkin Trans. 2*, 2002, 1296–1301.
- 90 W.-T. Chuang, C.-C. Hsieh, C.-H. Lai, C.-H. Lai, C.-W. Shih, K.-Y. Chen, W.-Y. Hung, Y.-H. Hsu and P.-T. Chou, *J. Org. Chem.*, 2011, **76**, 8189–8202.
- 91 Y. Qian, S. Li, G. Zhang, Q. Wang, S. Wang, H. Xu, C. Li, Y. Li and G. Yang, *J. Phys. Chem. B*, 2007, **111**, 5861–5868.
- 92 D.-E. Wu, Q.-C. Yao and M. Xia, *Phys. Chem. Chem. Phys.*, 2015, **17**, 3287–3294.
- 93 Q. Wu, Q. Peng, Y. Niu, X. Gao and Z. Shuai, *J. Phys. Chem. A*, 2012, **116**, 3881–3888.
- 94 Y. Shigemitsu, T. Mutai, H. Houjou and K. Araki, *J. Phys. Chem. A*, 2012, **116**, 12041–12048.
- 95 Y. Shigemitsu, T. Mutai, H. Houjou and K. Araki, *Phys. Chem. Chem. Phys.*, 2014, **16**, 14388–14395.
- 96 M. K. Nayak, B. H. Kim, J. E. Kwon, S. Park, J. Seo, J. W. Chung and S. Y. Park, *Chem. - A Eur. J.*, 2010, **16**, 7437–7447.
- 97 A. Nano, M. P. Gullo, B. Ventura, N. Armaroli, A. Barbieri and R. Ziessel, *Chem. Commun.*, 2015, **51**, 3351–3354.
- 98 Z. Tu, M. Liu, Y. Qian, G. Yang, M. Cai, L. Wang and W. Huang, *RSC Adv.*, 2015, **5**, 7789–7793.
- 99 R. Wei, P. Song and A. Tong, *J. Phys. Chem. C*, 2013, **117**, 3467–3474.
- 100 Q.-C. Yao, X.-L. Lu and M. Xia, *New J. Chem.*, 2014, **38**, 2693–2700.
- 101 K. Kanosue, T. Shimosaka, J. Wakita and S. Ando, *Macromolecules*, 2015, **48**, 1777–1778.
- 102 T. Shida, T. Mutai and K. Araki, *CrystEngComm*, 2013, **15**, 10179–10182.
- 103 K. Sakai, H. Kawamura, N. Kobayashi, T. Ishikawa, C. Ikeda, T. Kikuchi and T. Akutagawa, *CrystEngComm*, 2014, **16**, 3180–3185.
- 104 S. P. Anthony, *Chem. - An Asian J.*, 2012, **7**, 374–379.
- 105 A. Maity, F. Ali, H. Agarwalla, B. Anothumakkool and A. Das, *Chem. Commun.*, 2015, **51**, 2130–2133.
- 106 W. Sun, S. Li, R. Hu, Y. Qian, S. Wang and G. Yang, *J. Phys. Chem. A*, 2009, **113**, 5888–5895.
- 107 H. C. Peng, C. C. Kang, M. R. Liang, C. Y. Chen, A. Demchenko, C. T. Chen and P. T. Chou, *ACS Appl. Mater. Interfaces*, 2011, **3**, 1713–1720.
- 108 K. Benelhadj, W. Muzuzu, J. Massue, P. Retailleau, A. Charaf-Eddin, A. D. Laurent, D. Jacquemin, G. Ulrich and R. Ziessel, *Chem. - A Eur. J.*, 2014, **20**, 12843–12857.
- 109 S. Kim, J. Seo, H. K. Jung, J. J. Kim and S. Y. Park, *Adv. Mater.*, 2005, **17**, 2077–2082.

- 110 P. Coppo, M. Duati, V. N. Kozhevnikov, J. W. Hofstraat and L. De Cola, *Angew. Chemie - Int. Ed.*, 2005, **44**, 1806–1810.
- 111 A. H. Shelton, I. V. Sazanovich, J. A. Weinstein and M. D. Ward, *Chem. Commun.*, 2012, **48**, 2749–2751.
- 112 M. Mazzeo, V. Vitale, F. Della Sala, M. Anni, G. Barbarella, L. Favaretto, G. Sotgiu, R. Cingolani and G. Gigli, *Adv. Mater.*, 2005, **17**, 34–39.
- 113 Y. Liu, M. Nishiura, Y. Wang and Z. Hou, *J. Am. Chem. Soc.*, 2006, **128**, 5592–5593.
- 114 M. K. Nayak, *J. Photochem. Photobiol. A Chem.*, 2012, **241**, 26–37.
- 115 V. Thanikachalam, J. Jayabharathi, A. Arunpandiyam and P. Ramanathan, *J. Fluoresc.*, 2014, **24**, 377–387.
- 116 K.-I. Sakai, S. Takahashi, A. Kobayashi, T. Akutagawa, T. Nakamura, M. Dosen, M. Kato and U. Nagashima, *Dalton Trans.*, 2010, **39**, 1989–1995.
- 117 J. Huang, Q. Liu, J. H. Zou, X. H. Zhu, A. Y. Li, J. W. Li, S. Wu, J. Peng, Y. Cao, R. Xia, D. D. C. Bradley and J. Roncali, *Adv. Funct. Mater.*, 2009, **19**, 2978–2986.
- 118 S. Nakazono, Y. Imazaki, H. Yoo, J. Yang, T. Sasamori, N. Tokitoh, T. Cédric, H. Kageyama, D. Kim, H. Shinokubo and A. Osuka, *Chem. - A Eur. J.*, 2009, **15**, 7530–7533.
- 119 Y.-T. Lee, C.-L. Chiang and C.-T. Chen, *Chem. Commun. (Camb.)*, 2008, **2**, 217–219.
- 120 M. Shimizu, Y. Takeda, M. Higashi and T. Hiyama, *Angew. Chemie - Int. Ed.*, 2009, **48**, 3653–3656.
- 121 A. Wakamiya, K. Mori and S. Yamaguchi, *Angew. Chemie - Int. Ed.*, 2007, **46**, 4273–4276.
- 122 A. J. Stasyuk, M. Banasiewicz, B. Ventura, M. K. Cyrański and D. T. Gryko, *New J. Chem.*, 2014, **38**, 189–197.
- 123 S. Nagaoka, U. Nagashima, N. Ohta, M. Fujita and T. Takemura, *J. Phys. Chem.*, 1988, **92**, 166–171.
- 124 H. Ma, B. Chen, T. Sassa, L. R. Dalton and A. K. Y. Jen, *J. Am. Chem. Soc.*, 2001, **123**, 986–987.
- 125 V. S. Padalkar, D. Sakamaki, N. Tohnai, T. Akutagawa, K. Sakai and S. Seki, *RSC Adv.*, 2015, **5**, 80283–80296.
- 126 M. Tasior, V. Hugues, M. Blanchard-Desce and D. T. Gryko, *Chem. - An Asian J.*, 2012, **7**, 2656–2661.
- 127 L. Xie, Y. Chen, W. Wu, H. Guo, J. Zhao and X. Yu, *Dye. Pigment.*, 2012, **92**, 1361–1369.
- 128 L. Cui, W. Zhu, Y. Xu and X. Qian, *Anal. Chim. Acta*, 2013, **786**, 139–145.
- 129 M. A. Satam, R. D. Telore, A. B. Tathe, V. D. Gupta and N. Sekar, *Spectrochim. Acta Part A Mol. Biomol. Spectrosc.*, 2014, **127**, 16–24.
- 130 M. A. Satam, R. D. Telore and N. Sekar, *Dye. Pigment.*, 2015, **123**, 274–284.
- 131 M. Avadanei, V. Cozan, S. Shova and J. A. Paixão, *Chem. Phys.*, 2014, **444**, 43–51.
- 132 K. F. Byth, J. D. Culshaw, S. Green, S. E. Oakes and A. P. Thomas, *Bioorganic Med. Chem. Lett.*, 2004, **14**, 2245–2248.
- 133 C. J. R. Fookes, T. Q. Pham, F. Mattner, I. Greguric, C. Loc, X. Liu, P. Berghofer, R. Shepherd, M. Gregoire and A. Katsifis, *J. Med. Chem.*, 2008, **51**, 3700–3712.
- 134 A. Douhal, F. Amat-Guerri and A. U. Acuna, *J. Phys. Chem.*, 1995, **99**, 76–80.
- 135 A. Douhal, F. Amat-Guerri and A. U. Acuna, *Angew. Chem. Int. Ed.*, 1997, **36**, 1514–1516.
- 136 J. Luo, Z. Xie, J. W. Lam, L. Cheng, H. Chen, C. Qiu, H. S. Kwok, X. Zhan, Y. Liu, D. Zhu and B. Z. Tang, *Chem. Commun. (Camb.)*, 2001, **381**, 1740–1741.
- 137 C. Y. K. Chan, Z. Zhao, J. W. Y. Lam, J. Liu, S. Chen, P. Lu, F. Mahtab, X. Chen, H. H. Y. Sung, H. S. Kwok, Y. Ma, I. D. Williams, K. S. Wong and B. Z. Tang, *Adv. Funct. Mater.*, 2012, **22**, 378–389.
- 138 B. K. An, S. K. Kwon, S. D. Jung and S. Y. Park, *J. Am. Chem. Soc.*, 2002, **124**, 14410–14415.
- 139 J. Seo, S. Kim, Y. S. Lee, O. H. Kwon, K. H. Park, S. Y. Choi, Y. K. Chung, D. J. Jang and S. Y. Park, *J. Photochem. Photobiol. A Chem.*, 2007, **191**, 51–58.
- 140 S. Li, L. He, F. Xiong, Y. Li and G. Yang, *J. Phys. Chem. B*, 2004, **108**, 10887–10892.
- 141 P. Chen, R. Lu, P. Xue, T. Xu, G. Chen and Y. Zhao, *Langmuir*, 2009, **25**, 8395–8399.
- 142 P. Xue, R. Lu, G. Chen, Y. Zhang, H. Nomoto, M. Takafuji and H. Ihara, *Chem. - A Eur. J.*, 2007, **13**, 8231–8239.
- 143 T. H. Kim, M. S. Choi, B.-H. Sohn, S.-Y. Park, W. S. Lyoo and T. S. Lee, *Chem. Commun. (Camb.)*, 2008, **1**, 2364–2366.
- 144 J. Seo, S. Kim, S. H. Gihm, C. R. Park and S. Y. Park, *J. Mater. Chem.*, 2007, **17**, 5052–5057.
- 145 W. Tang, Y. Xiang and A. Tong, *J. Organic Chem.*, 2009, **74**, 2163–2166.
- 146 B.-R. Gao, H.-Y. Wang, Y.-W. Hao, L.-M. Fu, H.-H. Fang, Y. Jiang, L. Wang, Q.-D. Chen, H. Xia, L.-Y. Pan, Y.-G. Ma and H.-B. Sun, *J. Phys. Chem. B*, 2010, **114**, 128–134.
- 147 J. Chen, B. Xu, K. Yang, Y. Cao, H. H. Y. Sung, I. D. Williams and B. Z. Tang, *J. Phys. Chem. B*, 2005, **109**, 17086–17093.
- 148 Y. Qian, S. Li, Q. Wang, X. Sheng, S. Wu, S. Wang, J. Li and G. Yang, *Soft Matter*, 2012, **8**, 757–764.
- 149 E. Wang, J. W. Y. Lam, R. Hu, C. Zhang, Y. S. Zhao and B. Z. Tang, *J. Mater. Chem. C*, 2014, **2**, 1801–1807.
- 150 J. Zhang, B. Xu, J. Chen, L. Wang and W. Tian, *J. Phys. Chem. C*, 2013, **117**, 23117–23125.
- 151 E. Lager, J. Liu, A. Aguilar-Aguilar, B. Z. Tang and E. Peña-Cabrera, *J. Org. Chem.*, 2009, **74**, 2053–2058.
- 152 M. Yang, D. Xu, W. Xi, L. Wang, J. Zheng, J. Huang, J. Zhang, H. Zhou, J. Wu and Y. Tian, *J. Org. Chem.*, 2013, **78**, 10344–10359.
- 153 S. Sharma, A. Dhir and C. P. Pradeep, *Sensors Actuators, B Chem.*, 2014, **191**, 445–449.
- 154 M. Gao, Q. Hu, G. Feng, B. Z. Tang and B. Liu, *J. Mater. Chem. B*, 2014, **2**, 3438–3442.
- 155 H. Deng, B. Liu, C. Yang, G. Li, Y. Zhuang, B. Li and X. Zhu, *RSC Adv.*, 2014, **4**, 62021–62029.
- 156 Z. Song, R. T. K. Kwok, E. Zhao, Z. He, Y. Hong, J. W. Y. Lam, B. Liu and B. Z. Tang, *ACS Appl. Mater. Interfaces*, 2014, **6**, 17245–17254.
- 157 G. Li, D. Zhu, Q. Liu, L. Xue and H. Jiang, *Org. Lett.*, 2013, **15**, 924–927.
- 158 X. Chen, R. Wei, Y. Xiang, Z. Zhou, K. Li, P. Song and A. Tong, *J. Phys. Chem. C*, 2011, **115**, 14353–14359.
- 159 C. Niu, L. Zhao, T. Fang, X. Deng, H. Ma, J. Zhang, N. Na, J. Han and J. Ouyang, *Langmuir*, 2014, **30**, 2351–2359.
- 160 X. T. Chen, Y. Xiang, P. S. Song, R. R. Wei, Z. J. Zhou, K. Li and A. J. Tong, *J. Lumin.*, 2011, **131**, 1453–1459.